INFORMATION TO USERS

This manuscript has been reproduced from the microfilm master. UMI films the text directly from the original or copy submitted. Thus, some thesis and dissertation copies are in typewriter face, while others may be from any type of computer printer.

The quality of this reproduction is dependent upon the quality of the copy submitted. Broken or indistinct print, colored or poor quality illustrations and photographs, print bleedthrough, substandard margins, and improper alignment can adversely affect reproduction.

In the unlikely event that the author did not send UMI a complete manuscript and there are missing pages, these will be noted. Also, if unauthorized copyright material had to be removed, a note will indicate the deletion.

Oversize materials (e.g., maps, drawings, charts) are reproduced by sectioning the original, beginning at the upper left-hand corner and continuing from left to right in equal sections with small overlaps.

Photographs included in the original manuscript have been reproduced xerographically in this copy. Higher quality 6" x 9" black and white photographic prints are available for any photographs or illustrations appearing in this copy for an additional charge. Contact UMI directly to order.

ProQuest Information and Learning
300 North Zeeb Road, Ann Arbor, MI 48106-1346 USA
800-521-0600

UMI®

University of Alberta

Chemical Weathering in a Glaciated Carbonate Catchment, Canadian High Arctic: Implications for Subglacial Hydrology

by

Karen Elizabeth Heppenstall

©

A thesis submitted to the Faculty of Graduate Studies and Research in partial fulfillment of the requirements for the degree of Master of Science

Department of Earth and Atmospheric Sciences

Edmonton, Alberta

Spring 2002

National Library of Canada
Bibliothèque nationale du Canada

Acquisitions and Bibliographic Services
Acquisitions et services bibliographiques

395 Wellington Street
Ottawa ON K1A 0N4
Canada

395, rue Wellington
Ottawa ON K1A 0N4
Canada

Your file Votre référence

Our file Notre référence

The author has granted a non-exclusive licence allowing the National Library of Canada to reproduce, loan, distribute or sell copies of this thesis in microform, paper or electronic formats.

L'auteur a accordé une licence non exclusive permettant à la Bibliothèque nationale du Canada de reproduire, prêter, distribuer ou vendre des copies de cette thèse sous la forme de microfiche/film, de reproduction sur papier ou sur format électronique.

The author retains ownership of the copyright in this thesis. Neither the thesis nor substantial extracts from it may be printed or otherwise reproduced without the author's permission.

L'auteur conserve la propriété du droit d'auteur qui protège cette thèse. Ni la thèse ni des extraits substantiels de celle-ci ne doivent être imprimés ou autrement reproduits sans son autorisation.

0-612-69716-9

Canada

University of Alberta

Library Release Form

Name of Author: Karen E. Heppenstall

Title of Thesis: Chemical weathering of a glaciated carbonate basin, Canadian High Arctic: Implications for subglacial hydrology

Degree: Master of Science

Year this Degree Granted: 2002

Permission is hereby granted to the University of Alberta Library to reproduce single copies of this thesis and to lend and sell such copies for private, scholarly or scientific research purposes only.

The author reserves all other publication and other rights in association with the copyright in the thesis, ans except as herein before provided, neither the thesis nor any substantial portion thereof may be printed or otherwise reproduced in any material form whatever without the author's prior written permission.

Karen Heppenstall
Flat 2, Maple Court,
262 Ledbury Road,
Hereford
HR1 1QD.
England

15 NOVEMBER 2001

University of Alberta

Faculty of Graduate Studies and Research

The undersigned certify that they have read, and recommended to the Faculty of Graduate Studies and Research for acceptance, a thesis entitled Chemical Weathering in a Glaciated Carbonate Catchment, Canadian High Arctic: Implications for Subglacial Hydrology submitted by Karen Elizabeth Heppenstall in partial fulfillment of the requirements for the degree of Master of Science.

Martin Sharp, Supervisor

Brian Jones, Committee Member

Kevin Devito, Committee Member

15 NOVEMBER 2001

Abstract:

Hydrochemical analysis of waters draining polythermal John Evans Glacier, Ellesmere Island, during the summer of 2000 indicated significant chemical weathering of gypsum, calcite, dolomite and feldspars within the subglacial environment. Geochemical modeling using data collected in the field indicated that the balance of weathering rates was different in different hydrological settings. Calcite and gypsum dissolution were important in high discharge waters, and dolomite and feldspar dissolution were important in low discharge waters. A two-component drainage system was thus implied. At high discharge, the subglacial drainage system is at high pressure, and SSC is high. At low discharge, a drop in water pressure in subglacial channels allows stored water from the surrounding distributed system to enter the channels and exit the subglacial environment. This degree of subglacial channel development on an Arctic glacier is unusual, and is attributed to an unusually high rate of meltwater input to the subglacial environment.

Acknowledgements:

Financial support for this thesis was provided in the form of a University of Alberta Graduate Teaching Assistantship in the Department of Earth and Atmospheric Sciences for the duration of my degree program. Extra financial support was provided by an NSERC grant awarded to Dr. Martin Sharp. This grant, along with a grant awarded to myself from the Canadian Circumpolar Institute provided funding for field and laboratory research. Thanks to Polar Continental Shelf Project, who provided logistical support for the 2000 field season, and to the Nunavut Research Institute and the communities of Resolute Bay and Grise Fiord for allowing field research on John Evans Glacier. Finally, I acknowledge a Mary-Louise Imrie scholarship that enabled me to attend the 2001 Eastern Snow Conference, where some of my work was presented.

Thanks to Dr. Nick Spedding (University of Aberdeen) and Dr. Peter Nienow (University of Glasgow) who triggered my interests in glacier hydrology, and gave me the initial suggestion of working with Dr. Martin Sharp at the University of Alberta. And thanks, of course, to Martin, who had the faith and the courage to take me on, and has subsequently developed my interest and knowledge of glacier hydrology, and in particular hydrochemistry. Special thanks also go to Martin and Pete, for providing guidance in the field, and to Rob Bingham and Sarah Boon who also provided field assistance. Melissa Lafreniere and Candice Stuart were responsible for turning me into a lab-rat, and helping me master the Dionex.. My mum, Angela, shed a lot of light on chemical thermodynamics, and made useful comments on parts of this manuscript (not to mention the emotional and financial support whenever I needed it!)

To my close friends Catriona Morrison and Asuka Forest, who in their own ways have a great outlook on life that helped to keep me sane (and fit) throughout my time in Canada, and in particular to my boyfriend Sean Peats, who never lost faith in me, even when I had lost faith in myself.

Finally, thanks to intra-mural sport, the 2000 varsity cross-country team, and the Edmonton Overlanders Orienteering Club, and all the friends I made and fun I had whilst taking part in these diverse activities. Without all this, I wouldn't have survived!

Table of Contents:

CHAPTER 1 – INTRODUCTION 1

Rationale 1

Temperate Glacier Hydrology – Theory 2

Thermal Regime and Hydrology of Arctic Glaciers 3

Ionic provenance and solute acquisition in a glacier basin 5

Atmospheric Sources 5

Subglacial (crustal) sources 6

Thesis Outline 8

CHAPTER 2 – QUALITATIVE ANALYSIS OF SEASONAL VARIATIONS IN SOLUTE CONCENTRATION OF MELTWATER, JOHN EVANS GLACIER, ELLESMERE ISLAND 10

Introduction 10

Field Site 13

Sampling Methods 15

Analytical Methods for Chemical Data 17

Principal Components Analysis 17

Ratios, Saturation Indices and pCO_2 calculations 18

Discharge Measurements 20

Temporal and spatial variation in snowpack and supraglacial water chemistry 21

Supraglacial – Subglacial Comparisons 22

Temporal variation of solute concentrations in subglacial water 23

Changes in composition of runoff as an indicator of chemical weathering regime 24

Phase 1: Days 174 – 179 24

Phase 2: Days 180 – 204 25

Phase 3: Days 205 – 215 26

Inferences about drainage system structure and development 27

CHAPTER 3 – QUANTIFICATION OF CHEMICAL WEATHERING REACTIONS USING PHREEQC 50

An introduction to PHREEQC 50

Supraglacial water evolution 53

Introduction 53

Lake water evolution 53

Lake water dilution 55

Developing mean supraglacial input using proportional mixing of 5 streams 55

Subglacial water evolution 56

Introduction 56

Outburst water evolution 57

Outburst water dilution 58

Post-mixing reactions 59

Phase 2b 60

Phase 3 evolution 61

Interpretation of modeling results 63

Subglacial water evolution from supraglacial meltwater input 63

Late stages of subglacial water evolution from previously evolved subglacial waters 65

Precipitation of calcite in model results 65

Precipitation of gypsum in model results 67

Post-mixing reactions 67

Synthesis 68

Implications of chemical weathering environments for subglacial hydrology 68

CHAPTER 4 – SUMMARY AND CONCLUSIONS 89
Summary 89
Comparison of results with previous work 91
John Evans Glacier 91
Other Arctic glaciers 93
An Alpine glacier (Haut Glacier d'Arolla) 94
Implications for Arctic glacier hydrology 95
Conclusions 96

REFERENCES 103
APPENDICES 110

List of Tables:

Table 2:1 – Major hydrometeorological events observed during the 2000 melt season 29

Table 2:2 – Seasonal mean and standard deviation CBE for each sampling site 30

Table 2:3 – Equilibrium constants for common dissolution reactions 30

Table 2:4 – Supraglacial discharge calculations 31

Table 2:5 – Principal components analysis results for snowpack and supraglacial channels 31

Table 2:6 – Seasonal mean solute concentrations in snowpack, supraglacial and subglacial streams 32

Table 2:7 – Seasonal mean subglacial : supraglacial ratios 33

Table 2:8 – Mean concentrations of solutes in each subglacial phase and sub-phase 34

Table 3:1 – Results from lake water evolution inverse modeling simulations 72

Table 3:2 – Results from lake water dilution experiments 73

Table 3:3 – Results from supraglacial mixing simulations 74

Table 3:4 - (a) Results from inverse modeling of outburst water evolution 75

(b)Phase mole transfer ratios, outburst water evolution 76

Table 3:5 – Results from outburst water dilution experiments 76

Table 3:6 - (a) Results from post-mixing inverse modeling simulations 77

(b) Phase mole transfer ratios, Day 180 evolution 78

(c) Proportions of solutes derived from post-mixing reactions, Day 180 78

Table 3:7 – Results from inverse modeling of Phase 2b waters 79

Table 3:8 – Phase mole transfer ratios for all simulations from snowmelt 81

Table 3:9 - (a) Results from inverse modeling, Phase 2c to Day 205 82

(b) Results from inverse modeling, Day 209 simulations 82

(c) Results from inverse modeling, Day 208 simulations 83

(d) Results from inverse modeling of Day 209 from Day 208 85

Table 3:10 – Selected ion concentrations from speciation calculations for Days 205 and 208 85

Table 3:11 – Classification of water types 86

Table 4:1 – Seasonal mean solute concentrations from John Evans Glacier subglacial outflow, 1994 – 2000 98

Table 4:2 – Comparison of meteorological conditions between melt seasons, John Evans Glacier 99

Table 4:3 – Comparison of hydrological studies on Cold, Polythermal and Temperate Glaciers 100

List of Figures:

Figure 1:1 – Polythermal structures in Arctic Glaciers 9

Figure 2:1 – Location map of John Evans Glacier 35

Figure 2:2 – Bedrock geology in the John Evans Glacier area 36

Figure 2:3 – John Evans Glacier, showing water and snow sampling sites 38

Figure 2:4 – Daily mean temperatures and net radiation, 2000 melt season 39

Figure 2:5 – Suspended sediment concentration regressed on OBS 39

Figure 2:6 – Mean air temperature and subglacial discharge 40

Figure 2:7 – Seasonal variations in (a) HCO_3^-, (b) Ca^{2+} and (c) Mg^{2+} in supraglacial streams, snowpack and lakes 41

Figure 2:8 – Seasonal variations in (a) Cl^- and (b) Na^+ in supraglacial streams, snowpack and lakes 42

Figure 2:9 – Seasonal subglacial : supraglacial ratios (a) carbonate ions (b) sea-salt ions (c) SO_4^{2-} 43

Figure 2:10 – PCA Factor scores against time for subglacial samples 44

Figure 2:11 – Seasonal variations in subglacial (a) HCO_3^-, SO_4^{2-} and Ca^{2+}, and (b) Sr^{2+} 45

Figure 2:12 – Seasonal variations in subglacial (a) K^+ and Cl^-, and (b) Na^+ and Mg^{2+} 46

Figure 2:13 - (a) Seasonal Ca^{2+} : SO_4^{2-} in subglacial waters 47

(b) Seasonal Ca^{2+} : Mg^{2+} in subglacial waters 47

Figure 2:14 - (a) Seasonal log (pCO_2) of subglacial waters 48

(b) Seasonal saturation indices for calcite, dolomite and gypsum 48

Figure 2:15 – Seasonal variations in subglacial EC and SSC 49

Figure 3:1 – Flow-chart of water types on John Evans Glacier, Summer 2000 87

Figure 3:2 – Time series plot of EC with subglacial drainage phases 88

Chapter 1 – Introduction

This thesis presents results from a study of solutes contained in glacial meltwaters draining polythermal John Evans Glacier, Ellesmere Island in the Canadian High Arctic during the summer of 2000. Meteorological conditions leading up to the summer of 2000 led to unusual behaviour during the melt season. 1998 and 1999 were both very warm summers, and during the winter of 1999-2000, a thin snowpack was developed, due to wind removal of snow in January and low spring snowfall. Very warm temperatures were seen early in the summer, and a Chinook-type event was observed at the end of July. Thus in comparison to previous documented work on John Evans Glacier (Skidmore, 1995; 2001), observations made in 2000 showed unprecedented drainage system development.

The spatial and temporal variations in solute concentrations are examined both qualitatively (Chapter 2) and quantitatively using an aqueous geochemical modeling program (Chapter 3). Possible sources of solutes are discussed, and inferences are made on the structure and evolution of the subglacial drainage system over the course of the melt season. These inferences are then compared with results from other studies of temperate, polythermal and cold-based glaciers, to place these findings in a wider context. The importance of thermal regime in controlling glacier hydrology is discussed, along with the implications of this study for Arctic glacier hydrology.

Rationale for study:

The structure and seasonal evolution of a subglacial drainage system is directly related to seasonal variations in glacier motion (Iken and Bindschadler, 1986; Kamb, 1987), as the presence of water at the bed acts as a lubricant that enhances basal sliding (Paterson, 1994). This in turn affects the glacier long profile and the proportion of the ice mass above and below the equilibrium altitude. Thus, the nature and evolution of the subglacial drainage system, and the controls upon how this varies between years, will affect the response of the glacier to global warming in terms of melt rates. As glaciers are so widespread in Arctic areas (Dowdeswell, 1995), understanding how these glaciers may respond to global changes in temperature is crucial for predictions of sea-level change and possible feedbacks, both positive and negative, on the global system linked to temperature and precipitation.

Alpine Glacier Hydrology – Theory:

Most water enters the glacier hydrological system as it falls as precipitation (rain- or snow-fall) onto the surface of the glacier. The most important input to the system is the accumulation of snow during the winter months, although in some areas of high elevation or high latitude, summer accumulation may also play a key role in the hydrological cycle. During the summer months, and depending on the location on the glacier relative to the equilibrium line, the snowpack will either melt to become runoff, or will become glacier ice through the processes of compaction by new snow layers, and melting and refreezing within the firn layer (Fountain, 1989). Snowmelt may also be temporarily stored in the firn layer, which acts as an unconfined aquifer, until it is able to find a more efficient route by which to run-off.

Water in the subglacial component of the glacier hydrological system is derived from two sources. Internal and basal frictional melt of glacier ice layers and melting of channel walls by flowing water contribute only a small proportion of the total subglacial water volume. A more important water source is meltwater entering the subglacial system through crevasses and moulins at the ice surface. Crevasses are formed by differential strain rates within an ice mass, and therefore require the glacier to be in motion. On Arctic glaciers, where ice is cold and viscous, and mass balance gradients are low, longitudinal strain rates are also low, and crevasses are rare (Sugden and John, 1976).

Theoretical studies (e.g. Röthlisberger, 1972; Walder and Fowler, 1994) and observations in the field, both direct (Sharp et al., 1989) and indirect (e.g Collins, 1979 – solute characteristics; Hubbard et al., 1995 – borehole investigations; Nienow et al., 1998 – dye tracer studies) have allowed the identification of 6 modes of drainage that fall into two distinct categories of drainage structure. Distributed systems (Darcian porewater flow, advection in deforming permeable sediments, subglacial water film, linked cavities, canals incised into till) cover wide areas of the glacier bed, but are inefficient at evacuating water, and therefore store water for extended periods of time at high pressure. These systems are stable for small fluctuations in meltwater input. However, when large meltwater fluxes are forced onto the system, unstable orifice growth may ensue, and the distributed system can become unstable (Kamb, 1987). At high discharge, therefore, channelised systems (Nye-channels incised into bedrock, or R-channels incised into ice) provide a stable configuration, particularly under conditions of high surface slope (Walder and Fowler, 1994). They allow for rapid evacuation of large volumes of water at low pressure.

It is now believed that these two structures may co-exist beneath many Alpine glaciers (Fountain and Walder, 1998). Seasonal evolution in the form of subglacial drainage systems is

proposed based on dye-tracing tests (Hock and Hooke, 1993; Nienow et al., 1998). A predominantly distributed system exists during the early part of the melt season, while the glacier is snow-covered. Snow cover allows for storage of water on the glacier surface, and therefore dampens the diurnal runoff cycle by releasing water at a steady rate. As the snowline retreats upglacier, runoff from the ice surface is no longer delayed, and the decreased albedo leads to greater melt rates. Subglacial discharge increases and develops a diurnal cycle, causing instability and subsequent collapse of the distributed system under areas experiencing surface icemelt. Therefore the upglacier limit of the subglacial channelised system closely follows the location of the snowline (Nienow et al., 1998). Results of hydrochemical and dye-tracing studies, however, suggest that at periods of low discharge due to decreased incoming solar radiation, the contribution to bulk-flow (the mix of waters from both distributed and channelised systems) from the distributed system increases relative to that from the channelised system (Brown et al., 1996a). This is sometimes defined as recession flow (Collins, 1982).

Thermal Regime and Hydrology of Arctic Glaciers:

The High Arctic has been defined as the area north of 75°N (Dowdeswell, 1995), and therefore includes the glaciers and ice sheets of Greenland, Arctic Canada, Svalbard and Arctic Russia. This region of the globe has very low levels of incoming solar radiation, and as a result, has very low mean annual temperatures (-18°C at Alert, Northern Ellesmere Island; Arendt, 1995). It is also effectively a polar desert, with mean annual precipitation of 136mm (Alert; Rouse, 1993), although the eastern Canadian Arctic Islands (Ellesmere, Devon and Baffin Islands) see significantly more precipitation due to proximity to the Baffin Bay moisture source (Koerner, 1979).

Climatic conditions may account for differences in geometry and thermal regime between temperate (Alpine) and Arctic glaciers. Whereas Alpine glaciers have a high mass balance gradient (1.24m $100m^{-1}$; North Cascade Range, Washington State, USA; Pelto et al., 1990) and a fairly steep profile, Arctic glaciers generally have a much gentler profile due to the lower mass balance gradient (0.41m $100m^{-1}$; Svalbard mean from 8 ice masses; Pelto et al., 1990). Mass balance gradient is one factor that controls crevassing on a glacier surface (Hodgkins, 1997), and will therefore control penetration of meltwater to the bed of the glacier. Low mean annual air temperatures result in parts of Arctic ice masses that do not reach pressure melting point (PMP), whereas Alpine glaciers are composed predominantly of warm ice. Cold ice ($T < 0°C$) has high viscosity, so will deform more slowly than warm ice for a given applied stress, and is

impermeable on the intergranular scale (Paterson, 1994). The presence of cold ice will therefore also inhibit penetration of meltwater to the glacier bed.

The thermal regime of Arctic ice masses is therefore very important in determining the nature of the glacier hydrological system. Entirely cold glaciers that are frozen to their beds (e.g. Scott Turnerbreen, Hodgkins et al., 1998) are unlikely to possess a subglacial drainage system. Instead, surface meltwater runs off in supraglacial and ice marginal channels, although storage of water occurs both in the snowpack, depending upon the depth of the snowpack, and on the glacier surface in supraglacial lakes. This surface storage of meltwater seems to be characteristic of many Arctic glaciers, and has been observed on Austre Brøggerbreen (Hagen et al., 1991) and Erikbreen (Vatne et al., 1995). It is attributed to the layer of impermeable superimposed ice on the glacier surface (Hagen et al., 1991), as well as to the blockage of drainage channels (supraglacial and englacial) by snow and ice (Hodgkins, 1997).

Polythermal glaciers are comprised of regions of both cold ice, and ice at local PMP (Blatter and Hutter, 1991). Several polythermal structures are proposed (Blatter and Hutter, 1991; figure 1:1), given two potential causes for the formation of temperate ice (Hodgkins, 1997). Firstly, it is thought that ice thickness must be large in order for basal ice to reach PMP (Hodgkins, 1997). Heat is generated at the base of an ice mass though frictional heat and strain heating (Blatter and Hutter, 1991). This heat, along with any heat derived from the geothermal heat flux will diffuse through the ice mass, at a rate dictated by the temperature gradient and the thermal conductivity of the ice mass. Assuming constant boundary conditions (air temperature and basal heat source), temperature gradient will be smaller when ice depth is greater. Therefore, more heat will remain near the base of the glacier, allowing it to reach pressure melting point. This explanation accounts for structure *a* (Fig.1:1) and characterizes the thermal regime of White Glacier, Axel Heiberg Island (Blatter, 1987), Austre Brøggerbreen (Hagen et al., 1991) and McCall Glacier, Alaska (Rabus and Echelmeyer, 1997).

To account for structure *b* (Fig.1:1), Blatter and Hutter (1991) invoke heat generated through the percolation and refreezing of meltwater in the firn and superimposed ice layers (Hooke at al., 1983) in the accumulation zone. Heat from this source is then transported into the glacier by the processes of advection and diffusion. Erikbreen (Etzelmüller et al., 1993) and Storglaciären (Holmlund and Eriksson, 1989) (structure c, figure 1:1) both consist predominantly of warm ice, with a cold surface layer in the ablation area, caused by low annual air temperatures.

All the glaciers listed above exhibit some characteristics indicating the presence of a subglacial drainage system. These characteristics include drainage of supraglacial lakes and

channels into moulins or crevasses, turbid upwellings in the proglacial area that often have high concentrations of solutes such as HCO_3^-, SO_4^{2-} and Ca^{2+} and low pCO_2 values (believed to be indicative of rapid chemical weathering in a closed or partially closed system) and increases in glacier velocity at times when subglacial storage of water is predicted.

However, these observations have not yet been synthesized into a comprehensive model for the character and behaviour of Arctic subglacial drainage systems. An intensive study of Arctic subglacial drainage is required using one or more of the above indirect methods in order to establish the nature and seasonal evolution of a subglacial drainage system. Although subglacial hydrochemical data have been collected and analysed since 1994 at John Evans Glacier (Skidmore, 1995; 2001), this thesis presents results from the first seasonal study of subglacial waters where significant drainage system evolution has been inferred.

Ionic provenance and solute acquisition in a glacier basin:

Solutes in glacial meltwater are derived from two sources. Most solutes in supraglacial runoff are atmospherically derived, and additional solutes are derived from chemical weathering of rocks and dust in supraglacial, ice-marginal and subglacial environments.

Atmospheric sources

Atmospherically derived solute includes natural aerosols derived from sea salt (Na^+, Cl^-, K^+, Mg^{2+}, SO_4^{2-}) and aeolian dust (K^+, Ca^{2+}, Mg^{2+}, HCO_3^-) and anthropogenically derived acid aerosols (NO_3^-, SO_4^{2-}), as well as other neutral species (e.g. O_2, N_2, CO_2). These solutes are transferred to the earth's surface in precipitation, through dry deposition directly onto the surface, and by diffusion for gases. Barrie (1985) describes the processes by which aerosols are incorporated into rain and snow. Larger particles (>0.05μm), such as sea-salt aerosols, are generally considered to have high hygroscopicity, and therefore act as condensation nuclei. Finer particles (e.g. SO_4^{2-}) are more commonly scavenged from the atmosphere as water droplets are falling. In the Arctic, the majority of precipitation falls as snow, and ions are stored in the snowpack following deposition until melting starts to occur. As snowmelt begins, an ionic pulse is observed in runoff, due to preferential leaching of ions from the snowpack. Johannessen and Henriksen (1978) and Tranter et al. (1993) observed differential rates of leaching, with NO_3^- and SO_4^{2-} peaking before Cl^-, although the leaching sequence may vary between sites. Fountain (1996) suggests, though, that this is not a result of atmospheric processes as discussed by Barrie (1985), but instead is due to less soluble ions such as SO_4^{2-} being more efficiently excluded by vapour transfer processes within the snowpack.

Subglacial (crustal) sources

Meltwaters draining the surface of glaciers are generally dilute in comparison to waters that have been involved in chemical weathering. These dilute supraglacial waters are chemically aggressive, and readily acquire more solute when placed in contact with reactive rock material, especially if they contain high levels of dissolved gases (e.g. O_2, CO_2). Subglacial erosion (abrasion and crushing) produces large quantities of glacial rock flour with a large reactive surface area (Brown et al., 1996b) that may exist either as subglacial till, or as suspended sediment. Thus, the degree of rock-water contact is high. Carbonates (calcite, dolomite) and evaporites (anhydrite, gypsum, halite) are generally more vulnerable to chemical weathering than other minerals such as quartz, feldspars and pyrite, due to their rapid dissolution kinetics (Morse and MacKenzie, 1988). In most catchments, even those where only trace carbonates are present (e.g. Haut Glacier d'Arolla; Tranter et al., 1998), subglacial chemical weathering is dominated by carbonate dissolution (Holland, 1978; Tranter et al., 1998).

The most rapid chemical weathering reactions within the glacial environment are those where dissociation occurs in the presence of water. Dissolution of all evaporites follows this behaviour, although anhydrite must hydrate into gypsum prior to dissociation.

(1-1) $$CaSO_4.\,2H_2O \Leftrightarrow Ca^{2+} + SO_4^{2-} + 2H_2O$$

(1-2) $$NaCl \Leftrightarrow Na^{+} + Cl^{-}$$

In catchments where evaporites are present, they are likely to dominate the chemical signature of runoff.

Other chemical weathering reactions require a proton supply. In carbonate systems, this is mostly provided by the diffusion (1-3) and dissociation (1-4) of $CO_2(g)$ in water.

(1-3) $$CO_2(g) \Leftrightarrow CO_2(aq)$$

(1-4) $$CO_2(aq) + H_2O \Leftrightarrow HCO_3^{-} + H^{+}$$

HCO_3^- may also dissociate (1-5), depending upon the balance of ions in solution.

(1-5) $$HCO_3^{-} \Leftrightarrow CO_3^{2-} + H^{+}$$

Hydrolysis is often the initial reaction between water and carbonates (1-6; Tranter et al, 1993), and does not consume protons. Dissolution of calcite (1-7), dolomite (1-8) or feldspar (K (1-9) or Na (1-10) rich) dissolution may also occur following (1-4).

(1-6) $$CaCO_3 + H_2O \Leftrightarrow Ca^{2+} + OH^{-} + HCO_3^{-}$$

(1-7) $$CaCO_3 + H^{+} \Leftrightarrow Ca^{2+} + HCO_3^{-}$$

(1-8) $$CaMg(CO_3)_2 + 2H^{+} \Leftrightarrow Ca^{2+} + Mg^{2+} + 2HCO_3^{-}$$

(1-9) $$KAlSi_3O_8 + H^{+} \Leftrightarrow K^{+} + HAlSi_3O_8$$

(1-10) $NaAlSi_3O_8 + H^+ \Leftrightarrow Na^+ + HAlSi_3O_8$

Combining the sequence of CO_2 reactions with mineral dissolution and phase alteration reactions gives:

(1-11) $CaCO_3 + CO_2 + H_2O \Leftrightarrow Ca^{2+} + 2HCO_3^-$

(1-12) $CaMg(CO_3)_2 + 2CO_2 + 2H_2O \Leftrightarrow Ca^{2+} + Mg^{2+} + 4HCO_3^-$

(1-13) $KAlSi_3O_8 + CO_2 + 11/2H_2O \Leftrightarrow K^+ + HCO_3^- + 2Si(OH)_4 + 1/2Al_2Si_2O_5(OH)_4$ (kaolinite)

(1-14) $NaAlSi_3O_8 + CO_2 + 11/2H_2O \Leftrightarrow Na^+ + HCO_3^- + 2Si(OH)_4 + 1/2Al_2Si_2O_5(OH)_4$ (kaolinite)

Excluding evaporite dissolution, calcite dissolution is the most simple of these reactions, and therefore has the most rapid dissolution kinetics. It will hence play a dominant role in the chemical signature of all waters with short periods of rock-water contact. Dolomite dissolution is a two-stage process, as $CaCO_3$ dissolves first, followed by the slower dissolution of $MgCO_3$ (Ford and Williams, 1989). Feldspar dissolution is an incongruent reaction that requires the breaking down of the alumino-silicate lattice prior to release and replacement of ions (Stumm and Morgan, 1981). This process requires much time, and therefore feldspar dissolution is only important in long residence time waters.

Redox reactions that generate protons, such as that of sulphide oxidation (1-15), are often seen as important reactions in the subglacial environment.

(1-15) $4FeS_2$ (pyrite) $+ 15O_2 + 14H_2O \Leftrightarrow 16H^+ + 8SO_4^{2-} + 4Fe(OH)_3$

Brown et al. (1994) show that this reaction requires extended rock-water contact time, and therefore suggests that it is likely to occur over winter, at the beginning of the melt season, and within a distributed ("delayed-flow") part of the drainage network. Many authors (e.g. Tranter et al., 1993; Brown et al., 1996a) suggest that the carbonate dissolution and sulphide oxidation reactions are coupled, such that the H^+ derived as a by-product of sulphide oxidation is the proton used in the carbonate dissolution reactions (1-16).

(1-16) $4FeS_2 + 16CaCO_3 + 15O_2 + 14H_2O \Leftrightarrow 16Ca^{2+} + 16HCO_3^- + 8SO_4^{2-} + 4Fe(OH)_3$

Based on changing water chemistry throughout the course of a melt season, in relation to the weathering reactions listed above, it is possible to derive information on the degree of rock-water contact a solution has experienced. As modes of subglacial drainage are distinctive in terms of residence times, the degree of rock-water contact and access to atmospheric gases (CO_2

and O_2), hydrochemical data provide a useful tool upon which to base conclusions about the nature and evolution of a subglacial drainage system over the course of a melt season.

Thesis Outline:

Chapter 1 has presented the necessary background material for the work carried out in the rest of the thesis, as well as introducing the rationale for the study. Chapter 2 describes the field site, monitoring and analytical procedures for water samples, as well as presenting and interpreting hydrochemical variations in supraglacial and subglacial runoff in a qualitative manner. A distinct 3-phase evolution of the drainage system is identified, that provides a structure for the modeling procedure presented in Chapter 3. Mixing and inverse modeling simulations are performed in PHREEQC. Results of these simulations are presented in Chapter 3, along with an in-depth analysis of mineral (phase) transfers, especially $CO_2(g)$, in relation to their implications on drainage system structure and evolution. Chapter 4 presents a summary of the main findings of the thesis, and compares results with those from previous studies on John Evans Glacier, other Arctic glaciers, and Haut Glacier d'Arolla in the Swiss Alps.

Figure 1:1 Polythermal structures in Arctic glaciers (from Blatter and Hutter, 1991)

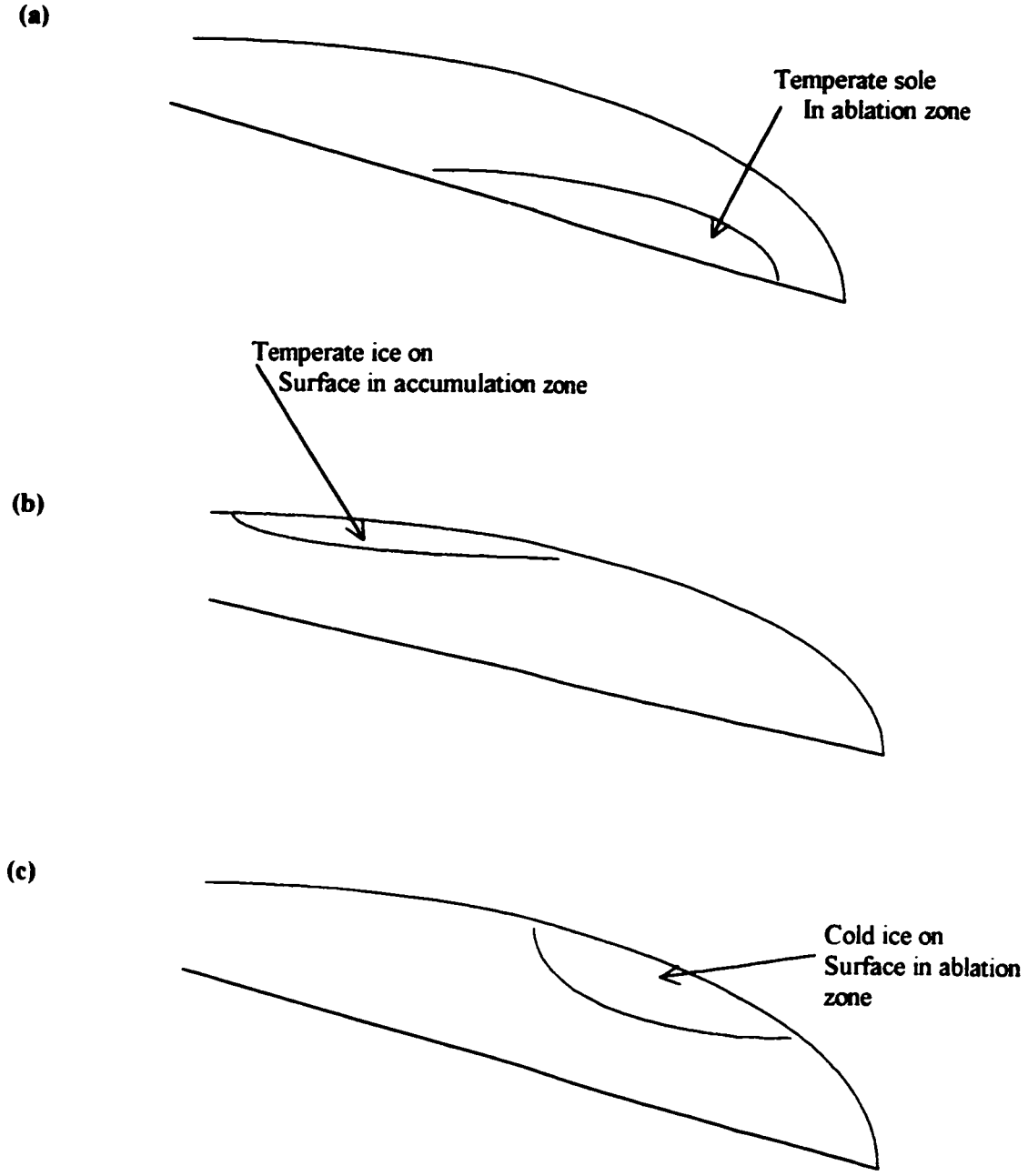

Chapter 2 – Qualitative analysis of seasonal variations in solute concentration of meltwater, John Evans Glacier, Ellesmere Island

Introduction

This chapter will examine the chemical composition of meltwaters draining John Evans Glacier, a polythermal glacier in the Canadian High Arctic (figure 2:1). Various components of the hydrological system, including the snowpack, supraglacial and subglacial runoff will be compared and contrasted in terms of their chemical composition, and seasonal variation in each of these subsystems will be examined. Possible sources of each solute in each system component will be considered, and hydrological inferences will be made on the basis of solute sources and weathering regimes.

Many hydrochemical studies have been carried out on Alpine glaciers (e.g. Collins, 1979), where the varying chemical composition of runoff throughout the melt season has been used to infer the characteristics of the subglacial drainage system and their changes over time. Early in the melt season, runoff is comprised predominantly of "delayed flow" which has passed through a widespread distributed system, whereas later on, it is comprised mainly of "quick flow" draining through an efficient channelised system, although at times of low flow, "delayed flow" may still be observed (Brown et al., 1994). Each of these water types displays a distinct chemical signature, imparted on the waters by differences in the duration and degree of rock-water contact.

Similar studies on Arctic glaciers are more limited (e.g. Hodgkins et al., 1998; Wadham et al., 1998; Hodson et al., 2000). These have often been undertaken on cold-based glaciers in Svalbard where there is little or no subglacial drainage (e.g. Scott Turnerbreen; Hodgkins et al., 1998). Therefore, the chemical composition of meltwaters is dictated much more by the chemical composition of the snowpack, or by rapid chemical weathering in an open ice-marginal channel system (e.g. Hodgkins et al., 1998). Observations of polythermal glaciers (Finsterwalderbreen; Wadham et al., 1998; Erdmannbreen, Erikbreen, Midre Lovénbreen, Hannabreen; Hodson et al., 2000) suggest that subglacial drainage does occur where temperate ice at the sole in much of the ablation area and the accumulation area is surrounded by cold ice at the margins and surface, assuming a route by which supraglacial runoff may access the bed. However, the dynamics of such drainage systems are as yet poorly understood.

Previous work on John Evans Glacier suggests that a subglacial drainage system also exists here. Skidmore (1995) carried out an evaluation of the hydrochemistry of various streams flowing from the glacier in the proglacial area. Distinct differences in chemistry were detected

between supraglacial and ice marginal channels, and an inferred subglacially -fed channel. The inferred subglacial outflow was not present at the beginning of the melt season. However, following an extended period of warm weather and rapid melting of the snowpack, an upwelling of turbid water was observed in the proglacial area in conjunction with an artesian fountain on the glacier surface, located a short distance from the terminus. Waters from the upwelling and the fountain had similar chemistry, and detailed analysis suggested that they were likely to be subglacial in nature, due to high concentrations of Ca^{2+} and SO_4^{2-} and silicate weathering products (Skidmore and Sharp, 1999) that were not observed in supraglacial runoff. Similar outburst and upwelling phenomena have been observed on several other High Arctic polythermal glaciers (Erdmannbreen, Midre Lovénbreen, Hannabreen; Hodson et al, 2000; Finsterwalderbreen; Wadham et al, 1998; Werenskioldbreen; Baranowski, 1973).

The outburst mechanism has been outlined in Skidmore and Sharp (1999). It is suggested that meltwater that initially entered the subglacial system from surface melt is trapped within the subglacial environment by a marginal dam of cold ice or frozen sediment, forming a reservoir. Some of this water may be trapped at freeze-up at the end of the summer melt season and stored over winter. As surface water input augments this reservoir, water pressure builds up over time. Once pressure is great enough, fracturing of the glacier occurs in association with enhanced horizontal motion (Copland, 2001), which allows outflow of meltwater via the artesian fountain. Meltwater also forces its way through or under frozen marginal sediment to appear in the proglacial area as a turbid upwelling. The mechanism involved here may be similar to that outlined by Shoemaker (1994), by which water is stored in an unfrozen confined aquifer near the glacier terminus. As overburden pressure is released in the proglacial area, stored water is forced to the surface as a turbid upwelling. This upwelling migrates headwards over time, until it reaches the ice margin, when it develops into a subglacial channel cut into the ice.

Further support for the occurrence of subglacial drainage is derived from radio-echo sounding data (Copland and Sharp, 2000; in press). High bed reflection powers (suggesting the presence of water at the bed) were found to coincide with a reconstruction of subglacial flowpaths based upon the calculated subglacial hydraulic potential distribution.

Observations of the drainage system since 1994 have suggested that the timing of the subglacial outburst at the terminus may be linked to the onset of input of supraglacial waters via moulins. At the beginning of the melt season, prior to the outburst, significant water storage occurs in the supraglacial channel network, and in two large ice marginal lakes that eventually connect to the supraglacial channels. In 1999, drainage of the ice marginal Nunatak Lake

coincided closely with the opening of moulins and the subglacial outburst, although the exact sequence of events was not recorded (M.Sharp, pers.comm..).

Although it is now established that polythermal glaciers can have a subglacial drainage system fed by surface-derived meltwaters, the nature of this system is not known. Polythermal glacier hydrology is expected to be different from that of both temperate and cold-based glaciers, due to the thermal regime of the glacier (Hodgkins, 1997). Cold ice on the glacier surface is impermeable; hence runoff may only access the bed via crevasses or moulins, which will deliver channelised runoff to the bed in a limited number of discrete locations. Where longitudinal velocity gradients are low, as is often the case on predominantly cold-based Arctic glaciers (Rabus and Echelmeyer, 1997; Copland, 2001), crevasses do not form, and meltwater cannot reach the bed at all. During the winter months, any drainage conduits that have been established are likely to be closed up by snow infill, plastic deformation and freezing, as water input cannot be maintained due to the very low air temperatures (Hock and Hooke, 1993). Cold ice or frozen sediment may also act as a dam to outflow of subglacial water, so that water may be stored in the subglacial system for long periods of time prior to the re-initiation of outflow in spring by a subglacial outburst (Skidmore and Sharp, 1999; Hodson et al, 2000). If water storage does occur by this mechanism, a distributed drainage system may be maintained throughout the winter months. As meltwater input during the summer months tends to be less than in temperate glaciers it may be unlikely that a channelised system of subglacial conduits will develop (Rabus and Echelmeyer, 1997). Instead, the drainage network is likely to maintain its distributed structure year round. If so, this would delay the export of water from the subglacial system, and allow for extended periods of rock-water contact.

Hydrochemical data may provide a useful mechanism for evaluating the validity of this hypothesis of polythermal glacier drainage system structure. Minerals in subglacial rocks have varying dissolution kinetics, and chemical weathering reactions take place at different rates, depending upon whether they are congruent or incongruent (Stumm and Morgan, 1981). In temperate glaciers, water residence times are typically short (1-3 hours; Nienow et al, 1998), especially when channels are present. Thus, the most rapid reactions dominate solute acquisition. However, if channels don't develop and residence times are longer (hours to days), as expected in polythermal glaciers, the importance of other, slower reactions may increase. Temporal variation in the chemical composition of meltwaters allows for an evaluation of changes in chemical weathering regime, and thus for the development of inferences about the structure and evolution of the hydrological system

This chapter will address five questions: (1) How do the composition of supraglacial waters (and the snowpack) vary in time and space? (2) How do supraglacial and subglacial waters compare, in terms of varying solute concentrations and compositions, and what does this tell us about potential linkages between the systems? (3) How does the composition of subglacial waters vary over time? (4) How can temporal changes in solute composition be interpreted in terms of changing subglacial chemical weathering regime? (5) What does the changing subglacial chemical weathering regime tell us about the structure and evolution of the subglacial drainage system?

Field site:

The study was undertaken on John Evans Glacier, Ellesmere Island, Nunavut, in Arctic Canada (80°N, 78°W; figure 2:1), during the summer (June – August) of 2000. John Evans Glacier is a large valley glacier that lies between 100m - 1350m a.s.l., and covers a total area of 165km^2. Based on radio-echo sounding data (Copland and Sharp, 2000; in press), the glacier is believed to be polythermal with a temperate sole in the ablation area surrounded by cold ice at the surface, margins and in the accumulation area. Mean annual air temperature since 1997 near the glacier terminus is -14.3°C (http://arctic.eas.ualberta.ca).

Bedrock underlying the glacier is a carbonate - evaporite sequence of Ordovician - Lower Devonian age (figure 2:2; from Kerr, 1972). The majority of the bedrock is limestone, although dolomite, anhydrite and gypsum are present, as are small amounts of quartzites and sandstones. Mineralogical analysis of sediments from two locations detected trace quantities of quartz, K-feldspar, illite and kaolinite, and it is likely that albite is also present. In the terminus area, there is a layer of unconsolidated sediment between the glacier and the bedrock. It is unknown how far this layer extends beneath the glacier, although given that the sole of the glacier is temperate in the ablation area, and that this leads to enhanced horizontal motion (Copland, 2001), subglacial erosion of bedrock is likely, and hence the till layer may be fairly extensive. The presence of such a till layer is likely to enhance dissolution rates of minerals, due to the increased reactive surface area relative to bedrock (Morse and Mackenzie, 1990).

John Evans Glacier has a very well developed supraglacial drainage network in its ablation area, with numerous deeply incised channels (10-20m depth). The 5 major channels flow into a series of moulins located in a crevasse field approximately 4km from the glacier terminus, just upstream of a significant subglacial bedrock bump (figure 2:3). Many smaller channels flow from the glacier surface into ice-marginal streams. Three main supraglacial

catchments were defined for this study. The first is the "Ridge Stream" catchment, which originates in an ice-marginal lake fed by two ice marginal channels flowing over lateral moraine. The "Nunatak Stream" catchment has a similar structure. These channels are comprised mostly of a series of supraglacial ponds (up to 10m diameter), linked by englacial channels. Significant storage takes place in these channels in the earlier part of the melt season. The third catchment ("Stream 4"), has its source high on the glacier, and flows through a channel that is partially snow-covered over much of its length, but which gradually deepens and widens into a major supraglacial channel. Each of these streams terminates at the crevasse field where runoff flows into moulins and enters the englacial - subglacial system.

The exact origin of these channels is not known, but examination of a 1959 air photo in comparison to channel form in 2000 suggests that the features are essentially permanent, although substantial downglacier extension has occurred during this period. The exact location of the moulins into which each of these channels drains varies from year to year, and sometimes changes during the course of the melt season (M.Sharp, pers.comm.).

The field season commenced on June 16 (Day 168), at which point the glacier was still predominantly snow-covered, but daily mean temperatures were above 0°C. Data from the Lower Weather Station indicated that the first Positive Degree Day (PDD) was June 7 (Day 159). The field season ended prior to the end of the melt season, on August 3 (Day 216), and the last PDD at the Lower Weather Station was August 25 (Day 238). On Day 216, the proglacial discharge was significantly reduced relative to peak discharge earlier in the melt season. Throughout the season, meteorological data were collected at 3 automatic weather stations (figure 2:3), located near the glacier terminus (250m), just above the Nunatak (850m) and near the top of the glacier (1180m). Readings were taken every 10 minutes, and averaged hourly and daily. As limited proglacial discharge readings are available, temperature (max, min and mean) and incoming solar radiation measurements from the Middle Weather Station will be used as a proxy for surface melt rates and discharge (figure 2:4). Warm temperatures and high incoming radiation were observed from Days 166 – 182, followed by a period of lower temperatures in association with low incoming radiation. Days 192 – 196 saw negative temperatures and low incoming radiation. Snowfall was observed on several of these days at various locations on the glacier (Table 2:1). From Day 200, temperatures and radiation started to increase once more, with peak values on Day 210, in association with strong warm winds and very high levels of melt (Boon and Sharp, submitted).

A number of important hydrological and hydrometeorological events were observed over the course of the melt season (Table 2:1). Many of these events will be seen to coincide with "events" in the hydrochemical record, and changes in the chemistry of meltwaters may be influenced by these hydrological or meteorological events.

As part of the 2000 monitoring program, a series of dye tracing tests was carried out (R.Bingham, University of Glasgow). Rhodamine WT fluorescent dye was injected into all major moulins several times over the course of the melt season in order to verify the connection between the supraglacial and subglacial systems, and to investigate variability in residence times. All injections were detected in the proglacial area, indicating that all moulins were connected to the subglacial drainage network. Analysis of dye return curves from the Nunatak and Ridge Stream moulins suggested that residence times (c.10 hours) and dispersivities were high at the beginning of the melt season (Day 177), and decreased as the melt season progressed to < 2 hours when discharge was at its peak during the chinook (Day 210; R.Bingham, pers.comm.). However, during the cold spell (JD190-196), an increase in residence times was observed (Day 193 – 9.83 hours; Day 196 – 11.5 hours). It should be noted that dye tracing provides a minimum estimate of residence times, as the dye is likely to remain in the channelised part of the system. Residence times in the distributed system are likely to be significantly longer, possibly in the order of days.

Sampling Methods:

Water sampling was carried out at several different sites across the ablation area of the glacier, and included 1 snow sampling location, 5 supraglacial streams, 2 ice marginal lakes, a lake formed in a large crevasse, and the subglacial channel at its point of emergence from the glacier (figure 2:3). Snow samples were collected from the glacier surface. For the majority of the melt season, this involved scraping remnants of snow off the ice surface using a clean Ziploc™ bag turned inside out over the samplers' hand. Once a sufficient quantity of snow had been collected, air was squeezed out of the bag, and it was sealed, double bagged, and returned to camp, where it was allowed to melt and processed no later than 3 days after collection. Stream samples were collected using Nalgene™ 500ml sample bottles, which were triple-rinsed in the stream and then filled with water sample. These, too, were returned to camp and processed no later than 3 days after collection. After processing, the sample collection bottles were rinsed with de-ionized water prior to their next use.

All samples were analysed for electrical conductivity (EC) using an ORION 128 EC probe, and were then filtered using Whatman™ 0.45μm cellulose nitrate filter papers and a Nalgene™ handpump and 500ml filter chamber. Filter papers and chamber were rinsed 3 times using sample water prior to filtration. Following filtration, sample pH was measured using an ORION 290A pH meter calibrated using low ionic strength buffers of pH 4.1, 7.01 and 9.27. 100ml of sample was then used to test for total alkalinity, using a Hach digital titrator, 0.16N sulphuric acid and Bromcresol red-green powder pillows. The end point for titration was determined colorimetrically.

Most subglacial samples were analysed for suspended sediment concentration (SSC). Samples were filtered through pre-weighed and bagged Whatman™ 45μm cellulose nitrate filter papers, and filter papers were folded and re-bagged, ready for return to the laboratory.

Procedures in the laboratory were as follows: Filter papers were removed from their bags, and placed in pre-weighed ovenproof dishes. If sediment remained in the bag, it was rinsed into the dish using de-ionized water. The samples were dried in the oven overnight at 200°F, and then weighed. As well as 26 used filter papers, 4 blanks were tested. They had 500ml of DI water pumped through them, and were dried out and weighed following an identical procedure. The change in weight of the blanks was insignificant (0.0001g), so it can be assumed that all filter papers behave conservatively throughout the process. SSC in g/l was calculated using:

$$\mathbf{SSC = \frac{((weight\ of\ filter + sediment) - (initial\ weight\ of\ filter)) * 1000ml}{Volume\ of\ sample\ in\ ml}}$$

An Optical Backscatter Sensor (OBS) was used to measure suspended sediment concentrations in the proglacial channel for parts of the melt season. Readings were taken every 15 minutes. In order to obtain a fuller SSC series, readings from this sensor were compared with coincident measured SSC values. A close correlation was found between the two variables (Figure 2:5), and a linear regression equation was generated as follows:

$$\mathbf{S = 0.0011*OBS + 0.0535}$$

(S - suspended sediment concentration; $R^2 = 0.8148$; n=14).

This equation was used to interpolate SSC values for sampling times when SSC was not measured directly.

One 30ml vial of each filtered sample was stored in the shade and returned to the laboratory for major ion analysis. Once in the laboratory, samples were stored at 4°C prior to analysis. Major anion (Cl^-, NO_3^- and SO_4^{2-}) and cation (Li^+, Na^+, K^+, Mg^{2+}, Ca^{2+} and Sr^{2+}) concentrations were analysed using a Dionex DX500 ion chromatograph. Anion analysis was

carried out using an AS4 column and 1.7mM Sodium Carbonate/1.8mM Sodium Bicarbonate eluent. Due to the very high concentrations of SO_4^{2-} in the subglacial samples, anion analyses were repeated at 10* dilution (0.5ml sample in 5ml DI water). Cl^- and NO_3^- concentrations in all samples, and SO_4^{2-} concentrations in all samples except subglacial water were very comparable in both runs when dilution was taken into consideration, so values from the initial run were used. Subglacial SO_4^{2-} values were significantly higher in the second run, because concentrations were within the calibrated range of the instrument when diluted. These values are therefore used, as they are likely to be more accurate. Cation analysis was carried out using a CS12 column and 20mM Methanesulphonic Acid (MSA) eluent. 10% of samples were repeated, including those seeming to have abnormal values. Calibration error of the instrument was found to be very small ($1.5 * 10^{-11}$ μeq/l), so was not included in further calculations of error. Precision error was calculated using the reproducibility error on known standards that gave concentrations similar to those in samples, following the procedure set out in Kretz (1985). Errors on supraglacial samples lay between 0.23% and 1.84%, and were lower for subglacial samples (maximum precision error of 0.45%).

As a check on the accuracy of the chemical analyses, the Charge Balance Error (CBE) was calculated as follows:

$$\mathbf{CBE = (SUM+ - SUM-)/(SUM+ + SUM-)*100}$$

The seasonal mean and standard deviation CBE for most of the monitoring sites is large (Table 2:2). As all major inorganic ionic species were analysed, and organic anions are likely to be negligible in an Arctic glacial environment, this suggests an error in chemical analysis. As Dionex results are calibrated against known standards, and errors are small (< 2% precision error), and no such checks exist on total alkalinity readings, it is these measurements that are suspected to be less accurate. Based on this assumption, HCO_3^- values were recalculated as CBE $HCO_3^- = (SUM+) - (Cl^- + NO_3^- + SO_4^{2-})$ in all instances except for a few samples where CBE HCO_3^- was negative. These calculated values are used in all subsequent analyses.

Analytical Methods for Chemical Data:

Principal Components Analysis:

In order to identify possible intercorrelation between components of the solute load, and to examine the dataset for variations in the importance of the different components over the course of the melt season, Principal Components Analysis (PCA) was performed on the Subglacial, Nunatak Stream, Ridge Stream, Stream 4 and Snowpack datasets. This is a statistical

method used to analyse large datasets given large numbers of correlated variables. It uses intercorrelation between variables as a basis for reducing the number of variables used in further analyses (Johnston, 1978). Each principal component represents several of the initial variables, and the loading for each variable must be greater than 0.7 for it to be used as an identifier for that component. Principal components are statistically independent. Factor scores may be calculated for each component for each sample collected in order to illustrate the variability of the importance of each factor over time.

Each dataset includes the variables of HCO_3^-, SO_4^{2-}, NO_3^-, Cl^-, Li^+, Na^+, K^+, Mg^{2+}, Ca^{2+} and Sr^{2+} for each sample collected from the given stream throughout the course of the melt season. Some of these variables are thought to be intercorrelated, based on solute source and weathering regime. Groupings of solutes and factor scores for each grouping plotted against time may highlight which solutes are likely to have similar sources, and which of these sources are important at different stages of the melt season.

Ratios, Saturation Indices and pCO_2 calculations:

Further calculations were performed on subglacial data. Simple ratios between two ion concentrations are used to provide information on the balance of weathering reactions (e.g. Ca^{2+}: SO_4^{2-} as an indication of the proportion of Ca^{2+} produced by gypsum dissolution; Ca^{2+}:Mg^{2+} as an indication of the balance between calcite and dolomite dissolution). Indices such as pCO_2 and saturation indices for calcite, dolomite and gypsum may provide insight into the state of the system. Chemical equilibrium is attained when all saturation indices are zero, and $pCO_2 = 10^{-3.5}$ (at sea level). Calculations are based upon equilibrium constants (K_{eq}) for each of the dissolution reactions involved (Table 2:3).

The value of K_{eq} provides an indication of the solubility of the reactant. Positive K values indicate a higher level of solubility than negative values, and as negative values increase, solubility decreases.

Simple calculations of K_{eq} and saturation indices use concentrations. For example, for calcite:

$$K_{calcite} = \frac{[Ca^{2+}][CO_3^{2-}]}{[CaCO_3(s)]}$$

where [ ] signifies concentration in mol/l. However, any solids in dissolution reactions are assigned a value of unity (=1), so may be removed from the equation. The saturation index may then be calculated as:

$$SI = \log \frac{K_{IAP}}{K_{eq}}$$

And for calcite:

$$SI_{cal} = \frac{\log [Ca^{2+}][CO_3^{2-}]}{K_{cal}}$$

This may be re-written using measurable parameters as:

$$SI_{cal} = \log [Ca^{2+}] + \log [HCO_3^-] + pH - pK_2 + pK_{cal}$$

where the prefix p indicates the negative logarithm, and pH is a substitute for the concentration (or activity) of H^+ (Ford and Williams, 1989).

The calculation of pCO_2 follows these same basic principles, and leads to the equation:

$$PCO_2 = \frac{[HCO_3^-][H^+]}{K_1 K_{CO2}}$$

Using concentrations, however, takes no account of ion pairs that form in solution, and therefore overestimates saturation indices (Ford and Williams, 1989). A better method is to calculate the activity of all ions in solution, and substitute these values for concentrations in the above equations. Activity (a_i) is derived using the Debye-Hückel Equation (Ford and Williams, 1989; pg.48; Parkhurst and Appelo, 1999). Manually, this would be a time-consuming process. However, many geochemical modeling programs have an application that calculates activities and fully speciates aqueous solutions. Saturation indices for calcite, dolomite and gypsum, and pCO_2 were thus derived using WEB-PHREEQC[1]. More detailed description of the equations and numerical method used by this program are presented in Chapter 3.

The pCO_2 of a sample provides an indication of the partial pressure of CO_2 in the atmosphere with which the sample would be in equilibrium (Ford and Williams, 1989). At sea level, atmospheric $pCO_2 = 10^{-3.5}$. This value decreases with increasing altitude. When pCO_2 of a sample exceeds this value, this is indicative of excess dissolved CO_2 in the sample. Situations that could lead to this in the subglacial environment include (a) early melt season acidic snowmelt mixing with subglacially stored water (Tranter et al, 1993); (b) freezing of a water body expelling CO_2 from the ice lattice, hence concentrating CO_2 in a smaller body of unfrozen water (Killawee et al, 1998); and (c) precipitation of carbonate minerals and production of CO_2(aq) which cannot degas in the subglacial system (Tranter et al, 1993). However, when pCO_2 of a sample is lower than atmospheric pCO_2, this is indicative of consumption of CO_2 in weathering reactions without

[1] WEB-PHREEQC may be found at
http://www.ndsu.nodak.edu/conference/sainieid/geochem/webphreeq/simplegeo.cgi

replacement of CO_2 by diffusion from the atmosphere. This situation is most likely to occur when there is a large amount of suspended sediment in glacial runoff (as often occurs in association with peak melt and peak discharge), providing a large surface area for dissolution of minerals. Using this knowledge, calculation of pCO_2 can provide information on the nature of the drainage system, and the chemical weathering reactions that are taking place within it.

Saturation indices are used as indicators of the aggressivity of a water sample in relation to a specific mineral; or, in other words, as a measure of the tendency for a water sample to dissolve or precipitate a specific mineral. Solutions with $SI < 0$ are undersaturated (aggressive), and hence have the ability to further dissolve a mineral. If $SI = 0$, the solution is in equilibrium with the mineral. When $SI > 0$, solutions are supersaturated with respect to a given mineral, and precipitation of the mineral may occur, given a suitable nucleation site (e.g. dust or sediment in the water column, glacier bed). However, it is suggested that precipitation is unlikely to occur until $SI \geq +0.3$ (Ford and Williams, 1989).

Discharge Measurements:

To support chemical analyses, discharge measurements were taken whenever possible. Supraglacial discharge was measured intermittently and mostly in conjunction with dye tracing tests, following a simplified version of the velocity-area method described by Gardiner and Dackombe (1983). The cross-sectional area of channels was measured using a tape measure and metre rule. Smooth ice-walled channels and proximity of monitoring locations to moulins meant that it was hazardous to enter the channels to measure velocity. Instead, surface velocity measurements were taken by repeatedly throwing small balls of paper into the thalweg of the channel. The time taken for the ball to travel 10m was recorded, and the mean of 5 times was used for velocity-area calculations.

In order to assess the proportional importance of each of the supraglacial channels, results from intensive studies of discharge carried out on JD196 and JD207 were used. Total supraglacial discharge was derived as the sum of discharge in all 5 channels. Proportional discharge from each channel was derived (Table 2:4). Although the method is not very accurate and assumes constant relative discharges throughout the melt season, it shows that the most important of the channels in terms of discharge was Stream 4 (> 30% of total supraglacial input), with the least important being the Nunatak Stream (c.15% of total supraglacial input).

Manual proglacial discharge readings in the proglacial channel were taken whenever possible, considering that at high discharge, it was not safe to enter the channel with the current

meter. The velocity-area method described by Gardiner and Dackcombe (1983) was employed, using a GURLEY current meter to measure velocity at 0.6depth. Measurements, where available, show a similar pattern of temporal variation to the temperature records (figure 2:6), hence supporting the use of these records as a discharge proxy.

Temporal and spatial variation in snowpack and supraglacial water chemistry

Principal Components Analysis (PCA) identified 3 components of the snowpack chemistry. Factor 1 accounted for 54% of the variance, and included sea-salt ions (Cl^-, Na^+, K^+ and SO_4^{2-}) as well as EC. Factor 2 accounted for another 28% of the variance, and included all parameters linked to the dissolution of carbonate dust (Ca^{2+}, Mg^{2+}, HCO_3^-), and Factor 3 (12% of variance) included the acid aerosol, NO_3^-. These results are similar to those found by Sharp et al. (in review) who carried out a detailed analysis of snow chemistry during the spring of 1995. This grouping of variables is repeated in all other analyses of supraglacial waters (Table 2:5), although loadings are different in different environments. The carbonate factor becomes the most important factor in supraglacial channels, particularly in the Ridge and Nunatak Streams.

The concentrations of HCO_3^-, Ca^{2+} and Mg^{2+} are higher in the Nunatak and Ridge Streams than in the snowpack or Stream 4 (Table 2:6; Figure 2:7). In the Nunatak and Ridge Streams, they approach those in the lakes feeding these channels (Figure 2:7a-c), although some dilution of lake water by snow and ice melt is apparent from the lower concentrations observed in the supraglacial channels. The concentrations in Stream 4 are directly comparable with snowpack values, which suggests that this meltwater is pure snowmelt. The high concentrations of carbonate-derived ions in the Ridge and Nunatak Lakes suggest that some chemical weathering of carbonates occurs in the moraine across which the streams feeding the ice-marginal lakes flow. At the beginning of the melt season, prior to drainage of the Ridge Lake on Day 175 (Table 2:1), HCO_3^-, Ca^{2+} and Mg^{2+} concentrations in the Ridge Stream were in the same range as snowmelt values. This indicates that at the beginning of the melt season, the Ridge Lake was not connected to the Ridge Stream. Similar behaviour is expected to have occurred in the Nunatak Stream because the Nunatak Lake also drained shortly after the subglacial outburst (Day 176; Table 2:1). There is however no direct evidence of this as samples were not collected from this stream during this period. Other smaller peaks of carbonate-derived ions are observed throughout the melt season, all of which may be associated with drainage events from the lake basins (e.g. Days 191-192, Ridge; Day 211-212, Nunatak).

Sea-salt ion (Na^+, Cl^-) concentrations however show a different pattern. Concentrations in all channels are similar, and peaks are approximately coincident, although they have different magnitude in different channels (figure 2:8). These peaks are observed late in the melt season (JD205 and 209). Similar peaks are seen in the snowpack series (collected in the vicinity of the Nunatak Stream), but there is a lag time of approximately two days. It is unusual that these peaks in sea-salt ions, usually associated with fresh precipitation, are at this time coincident with a period of warm and sunny weather. However, by this point in the melt season, only basal layers of the snowpack remained on the glacier surface at the sampling location. If solutes had been stored in these layers, these would have been flushed out at times of peak melt and runoff. The differences in magnitude of the sea-salt ion peaks between the streams may thus be related to the proportions of snowmelt from these basal layers in comparison to ice-melt and snowmelt from a deeper snowpack further up the glacier, hence explaining the lower magnitude peak in Stream 4 waters.

Supraglacial – Subglacial comparisons

Comparison of supraglacial and subglacial waters reveals a significant difference in solute concentration between the two hydrological environments (Table 2:6). As all dye injected into the supraglacial system was detected in the subglacial runoff, this suggests that ultimately, most subglacial water, except for a small amount that is melted from basal ice, is derived in the supraglacial environment. Therefore, a substantial amount of subglacial chemical weathering is apparent.

Mean supraglacial concentration was derived using concentrations from all supraglacial streams sampled on a specific day (Appendix 1), and the daily and seasonal mean subglacial - supraglacial ratio was calculated for all solutes. It is apparent that over the course of the melt season, the weathering of some ions in the subglacial environment is more important than others, and that there is seasonal variation in the contribution to total solute concentration from the two different environments (Table 2:7; Figure 2:9). The highest mean ratio is for SO_4^{2-} (>200), indicating that the contribution from the supraglacial environment is negligible. K^+ ratios are also high (>10), although very variable (Figure 2:9). The only ion that exhibits a ratio close to 1 is Cl^-. This suggests that Cl^- is mostly conservative in the subglacial environment. The mean HCO_3^- ratio is also small (~2, excluding outburst waters).

However, all ion ratios show significant seasonal variation, indicating that addition of solutes by weathering is not constant throughout the melt season. Ratios are at their highest at the

time of the subglacial outburst. Above average values, indicating an increase in the contribution from the subglacial environment, are also seen in the Cl^-, Na^+ and K^+ records from JD190-196 and on JD207, and in the Ca^{2+} and SO_4^{2-} records from JD205 onwards.

Temporal variation of solute concentrations in subglacial water

PCA of subglacial waters identified 2 factors explaining 89.5% of the variance of the dataset. Factor I (48.5%) loaded on Cl^-, NO_3^-, Li^+, Na^+, K^+ and Mg^{2+}. Factor II (41%) loaded on HCO_3^-, SO_4^{2-}, Ca^{2+} and Sr^{2+}. The variation of factor scores over time (Figure 2:10) shows that both factors have high loadings in outburst waters, although the loading on F1 is higher. Following this, the two factors appear to be inversely correlated, with F1 peaking from JD192-196, and on JD207 and JD208, and F2 peaking at the end of the melt season, particularly from JD209-211. These results suggest that there may be significant changes in the chemical composition of subglacial waters over the course of the melt season and they provide a basis for further examination of solute concentrations and other indices.

Concentrations of HCO_3^-, SO_4^{2-}, Ca^{2+} and Sr^{2+} show similar fluctuations throughout the course of the melt season (Figure 2:11). All are highly concentrated in outburst waters (Ca^{2+} = 4122.4μeq l^{-1}; SO_4^{2-} = 2796.1μeq l^{-1}; HCO_3^- = 2440.9μeq l^{-1}; Sr^{2+} = 50.8μeq l^{-1}), but decline to more steady values (Ca^{2+} ~ 1575μeq l^{-1}; SO_4^{2-} ~ 1200μeq l^{-1}; HCO_3^- ~ 660μeq l^{-1}; Sr^{2+} ~ 19μeq l^{-1}) by Day 180. Concentrations then peak again towards the end of the melt season, after Day 205. However, some low concentration samples are seen during this period (Days 207 and 208). These samples were collected prior to peak discharge, suggesting the possibility of diurnal fluctuations in solute concentration during this period.

Likewise, concentrations of Cl^-, Na^+, K^+ and Mg^{2+} fluctuate simultaneously for most of the melt season, but not synchronously with HCO_3^-, SO_4^{2-}, Ca^{2+} and Sr^{2+}, except during the outburst, when all concentrations were high (Figure 2:12). After the outburst, the main peak in these records is from Days 193-196, where concentrations increase by 110-225% (Cl^- = 213%; Na^+ = 223%; K^+ = 154%; Mg^{2+} = 111%). A further peak in Cl^-, Na^+ and K^+ is seen in conjunction with the low concentrations of HCO_3^-, SO_4^{2-}, Ca^{2+} and Sr^{2+} on Days 207 and 208. Mg^{2+} does not fluctuate at this time (Figure 2:12b). Li^+ is seen in trace amounts in outburst waters only (0.1-0.3μeql^{-1}; Days 174-175). NO_3^- also appears in significant quantities only in outburst waters (~3.5μeql^{-1}; Day 174). It is seen in most samples after this date, but only at concentrations close to detection limits (~1.5μeql^{-1}).

The seasonal mean value for Ca^{2+}: SO_4^{2-} in subglacial waters is 1.395, and most values are close to this mean (Figure 2:13a). However, from Day 205, a sharp increase to values close to 1.7 occurred. Seasonal Ca^{2+}: Mg^{2+} is much more variable (Figure 2:13b). The lowest values are seen in the outburst waters (~5.5), but they increase rapidly to ~9. A further increase is seen after Day 203 to a high value of 16.46 on Day 210.

PCO_2 has 4 phases (Figure 2:14a). Outburst waters have pCO_2 values greater than $10^{-3.5}$, but by Day 180, values are closer to 10^{-4}. A further period of high pCO_2 is seen from Days 187-195, with the final phase (Day 201 onwards) characterized by very low ($10^{-5.47}$) values. The series is cut short as pH values after JD210 are thought to have been affected by re-equilibration with the atmosphere prior to analysis, as a result of long-term storage in containers that were not full. Saturation indices for calcite (SI_{cal}) and dolomite (SI_{dol}) show that the outburst water was supersaturated with respect to both minerals (Figure 2:14b). Waters remained supersaturated with respect to calcite for the majority of the melt season, except on Days 175, 187, 190-195 and 199. Runoff was most supersaturated with respect to calcite on Day 209 (SI_{cal} = 1.42). However, once the saturation state of runoff with respect to dolomite had dropped below equilibrium (SI_{dol} < 0) following the outburst, the water remained undersaturated until Day 202. From Day 205 onwards, runoff was more supersaturated with respect to dolomite than with respect to calcite, with a peak on Day 208 (SI_{dol} = 1.81). In contrast, runoff was never saturated with respect to gypsum (Figure 2:14b). It was closest to saturation on Day 174, when the outburst occurred (SI_{gyp} = -0.96).

Changes in composition of runoff as an indicator of chemical weathering regime

It is clear that both solute concentration and composition of subglacial runoff are highly variable. Results allow for the identification of three distinct phases based upon changing chemical composition (Table 2:8).

Phase 1: Days 174-179 -

Phase 1 is characterized by the highly concentrated initial outburst waters, and their apparent dilution by low concentration snowmelt. Other key aspects of the chemistry are the low Ca^{2+}: Mg^{2+}, pCO_2 values of greater than $10^{-3.5}$, and the rapid switch from supersaturation to undersaturation with respect to calcite and dolomite on Day 175, with return to saturated conditions on Day 176. The high concentrations of solutes in the outburst waters are a result of dissolution of minerals in the subglacial environment, although there may be a contribution from

early season snowmelt that helps to produce the high concentrations of NO_3^- and Cl^-. The high concentrations of Na^+ and K^+ are too high to be derived from sea-salt, and are instead likely to be derived from the dissolution of feldspars:

$$KAlSi_3O_8 + H_2CO_3 + 9/2H_2O \Leftrightarrow K^+ + HCO_3^- + 2Si(OH)_4 + 1/2Al_2Si_2O_5(OH)_4$$

This is an incongruent reaction, and is therefore slower than the dissolution of gypsum, calcite or dolomite (Stumm and Morgan, 1981). The presence of high concentrations of Na^+ and K^+ are therefore indicative of a high degree of rock-water contact, allowing feldspar dissolution reactions to take place. Low Ca^{2+}: Mg^{2+} is also indicative of this, as dolomite dissolution is slower than calcite dissolution. Dissolution of calcite slows as water approaches saturation with respect to calcite (Stumm and Morgan, 1981). However, it takes longer for water to become saturated with respect to dolomite, so dolomite dissolution continues at a more rapid pace. Therefore, as residence time increases, Ca^{2+}: Mg^{2+} will decrease. Precipitation of calcite will also drive Ca^{2+}: Mg^{2+} down.

The mixing of high concentration subglacial waters with acidic early season snowmelt may have produced the high pCO_2 values as subglacial drainage is established. It is more likely though that precipitation of calcite in the subglacial system prior to the outburst could also have driven pCO_2 up, as $CO_2(aq)$ released by this reaction would not have been able to degas. Dilution by snowmelt is apparent based upon saturation indices. SI_{cal}, SI_{dol} and SI_{gyp} all decrease sharply on Day 175, as dilute snowmelt mixes with the high concentration subglacial waters. By Day 176, discharge may have been high enough to mobilize sediment and induce further dissolution in the subglacial environment that returned saturation indices to higher values, and allowed waters to once again become supersaturated with respect to calcite.

Phase 2: Days 180-204 -

Phase 2 starts once dilution of outburst waters by snowmelt is complete. The major weathering regime is the dissolution of gypsum, as indicated by a Ca^{2+}: SO_4^{2-} only slightly greater than 1 throughout the phase. However, the phase divides into three sub-phases. Phases 2a (JD180-189) and 2c (JD197-204) are characterized mostly by gypsum dissolution. Phase 2b (JD190-196) though is associated with a period of cold weather and precipitation, and exhibits peaks of Na^+, K^+ and Cl^- and high pCO_2. Waters are also undersaturated with respect to calcite, as well as dolomite and gypsum from Day 190-196.

The subglacial - supraglacial ratio indicates that the solute peaks are not derived from the supraglacial environment, so Cl^-, as well as Na^+ and K^+ must be produced in the subglacial

environment. Dye tracing tests revealed an increase in residence times during this period of cold weather, so feldspar dissolution may explain the increase in concentration of Na^+ and K^+. However, an alternative explanation must be found for the enhanced Cl^- concentration. It is possible that trace amounts of halite (NaCl) and sylvite (KCl) are found in the bedrock in association with other evaporites, for example in the Baumann Fjord Formation located in an overdeepening just downglacier of the bedrock bump (Figure 2:2). However, this is thought to be unlikely, based on studies of this and similar formations in other parts of the Arctic (B.Jones, pers.comm.). The freezing of water in the subglacial environment may cause solutes already present in the water to be precipitated as halite and sylvite, which are subsequently re-dissolved once in contact with water again. However, the glacier bed is isolated from surface temperature changes, so there is unlikely to be a location where sufficient freezing can occur. The most likely explanation is that precipitation of halite and sylvite is caused by glaciohydraulic super-cooling, linked to a drop in water pressure, either at the end of the melt season as discharge drops, or as water flows out of overdeepened areas of the bed and into subglacial channels.

High pCO_2 values during Phase 2b may be as a result of the rejection of CO_2 from the ice lattice as some of the subglacial water freezes as the pressure drops with decreasing discharge during the cold period. Another possible explanation is the of precipitation of calcite that releases CO_2(aq) that is unable to degas. However, the system is not likely to be closed at this time, as channels that have started to develop under parts of the glacier would not be full, and water would have access to the atmosphere. It is therefore possible that precipitation of calcite occurred in the distributed system whilst it was at high pressure, and that the waters in the subglacial outflow during Phase 2b have retained the characteristics imparted onto them by the high pressure distributed system.

Phase 3: Days 205-215 -

Phase 3 is characterized by a high degree of variability in the chemical composition of runoff. It is dominated by high concentrations of HCO_3^-, SO_4^{2-}, Ca^{2+} and Sr^{2+}, although peaks of Na^+, K^+ and Cl^- are seen when lower discharge is inferred, based on sampling time (JD207-208). Examination of the EC and SSC records (Figure 2:15) shows that peaks in EC and SSC are closely correlated with peaks in HCO_3^-, SO_4^{2-}, Ca^{2+} and Sr^{2+}, suggesting that the high rates of gypsum and calcite dissolution are associated with high concentrations of freshly mobilized suspended sediment in the water column. At lower discharges, both earlier in the melt season and

during Phase 3, there is less suspended sediment in the water column, so in-channel weathering rates are reduced.

High rates of calcite dissolution require consumption of large quantities of CO_2. The very low pCO_2 values observed suggest that the CO_2 supply is not replenished as rapidly as it is consumed, and supports the rapid weathering hypothesis. Further support for the increase in the weathering rate of calcite is provided by the increases in Ca^{2+}: SO_4^{2-}, and Ca^{2+}: Mg^{2+}. These both indicate that relatively more Ca^{2+} is being produced during this phase than at other times during the melt season. The dominance of calcite and gypsum dissolution indicate that water is being evacuated rapidly, with little rock-water contact, except for the in-channel weathering of suspended sediment.

Runoff is supersaturated with respect to both calcite and dolomite throughout Phase 3. However, concentrations of Ca^{2+}, Mg^{2+} and HCO_3^- continue to increase, suggesting that little or no precipitation of these minerals is taking place, despite the supersaturated state. If gypsum was dissolved faster than calcite was precipitated, the common ion effect could be used to explain this. However, Ca^{2+}: SO_4^{2-} increases throughout Phase 3, and this should drive calcite precipitation rather than prevent it. It is thus possible that water in the system is at high enough pressure for this to affect saturation indices. Increased water pressure means that more $CO_2(g)$ may be dissolved into the water column, hence driving the sequence of carbonic acid and calcite dissolution. This could have the effect that waters that appear supersaturated at atmospheric pressure may in fact be undersaturated at higher than atmospheric pressure. Alternatively, precipitation of minerals (calcite and dolomite) may be prevented by the lack of nucleation sites within or close to the solution.

The samples rich in Na^+, K^+ and Cl^- collected at lower discharge during Phase 3 appear to have a similar composition to Phase 2b, suggesting significantly longer residence times than other Phase 3 waters collected at high discharge. Like Phase 2b waters, these waters could be derived from an alternative carbonate-free source that is more important at low-flow.

Inferences about drainage system structure and development:

Based on the evaluation of runoff chemistry in terms of dominant ions and weathering regimes, it is possible to make inferences about the structure and development of the drainage system over the course of the melt season. Outburst waters have been subject to a high degree of rock-water contact whilst in storage in the subglacial environment. Although some small channels may exist at this time, the majority of the system is likely to be distributed in nature,

possibly as a saturated till layer (Copland, 2001). The opening up of surface moulins at the beginning of phase 1 is likely to have induced major drainage system restructuring, as moulins provide few discrete inputs to the subglacial drainage system, from which an efficient channelised drainage system may develop rapidly (Hock and Hooke, 1993). A decrease in dye residence times indicates that this is indeed the case, as do observations of tunnel development at the terminus, where the upwelling observed as the outburst occurred evolved rapidly into a tunnel carved upwards into the ice by Day 181 (Table 2:1). Discharge also increased at this time, allowing for further channel enlargement.

Hence, when the cold weather started (Day 190), subglacial channels are likely to have been established between surface moulins and the proglacial area. At high discharge these channels would have been full of water and the system would have been closed with no access to the atmosphere. As air temperatures fell and melt decreased, channels would have become only partially full, allowing ingress of atmospheric gases and renewed dissolution of CO_2 into the water. A distributed system would still be present in the areas surrounding the channels, which may now contribute a larger proportion of meltwater to total runoff, as recession flow (Collins, 1982). This water has experienced a high degree of rock-water contact, but based on the enhanced concentrations of Cl^-, it seems feasible that it comes from a location in the subglacial environment that has not previously been accessed by the drainage network.

At the end of Phase 2 and into Phase 3, there is much hydrological evidence for the expansion of the drainage system upglacier. During Phase 3, two moulins opened up high on the glacier (Table 2:1) and were proved to be connected to the subglacial drainage system by dye-tracing. The large crevasse lake also drained, although there is no solid evidence that it drained into the subglacial system. The switch of weathering regime in Phase 3 was initiated by increased discharge and increased suspended sediment load in the "bulk" meltwaters, allowing rapid in-channel calcite and gypsum dissolution. However, the peaks of Na^+, K^+ and Cl^- at times of lower flow indicate that the two-component system is still in operation, with the channelised system dominating high-flow chemistry, and the remaining distributed system playing a part in the chemical composition of runoff at low flow.

This 3-phase development of the subglacial drainage system allows a modeling strategy to be devised, in order to investigate the processes of mineral dissolution and precipitation in a more quantitative manner. This modeling procedure, and the results from it are presented in the next chapter, and further inferences are made regarding the nature of the drainage system.

Table 2:1 Major hydrometeorological events observed during the 2000 field season

DAY (DATE)	METEOROLOGICAL EVENT	HYDROLOGICAL EVENT
172 (20 Jun)		Nunatak Stream moulin opens
174 (22 Jun)		Subglacial Outburst – upwelling through frozen sediment and artesian fountains through cracks in ice surface
175 (23 Jun)		Ridge Lake drains
176 (24 Jun)		Nunatak Lake drains
181 (29 Jun)		Subglacial outflow now through ice tunnel
185 (3 Jul)		Lake by Nunatak moulin drains
186 (4 Jul)	Rainfall	
188 (6 Jul)	Rainfall	Ridge Lake refilling
189 (7 Jul)	Rain and mist	Subglacial discharge increases
192 (10 Jul)	Snow	Ridge Lake empty
193-195 (11-13 Jul)	Rain and snow	Low supra- and subglacial discharge; supraglacial channels freeze up
200 (18 Jul)	Overcast and rainy	
201 (19 Jul)	Overcast	Upper moulin observed
203 (21 Jul)		Major subglacial discharge event
207 (25 Jul)	Warm and sunny	High supraglacial discharge Major subglacial discharge event; large quantities of sediment moved
210-211 (28-29 Jul)	Chinook	Ice surface melted down to smooth ice; Nunatak Lake fills and drains (5m); major subglacial discharge events
212 (30 Jul)		2nd upper moulin observed
213 (31 Jul)		Crevasse Lake drains
215 (2 Aug)	Overcast	Subglacial discharge much reduced

Table 2:2 Seasonal mean and standard deviation Charge Balance Error (CBE) for each sampling site.

MONITORING SITE	MEAN CBE	STANDARD DEVIATION	N
Subglacial	12.80	6.42	36
Nunatak Stream	19.9	10.62	19
Ridge Stream	23.65	4.17	19
Stream 1	14.19	26.31	5
Stream 2	19.77	1.87	2
Stream 4	26.56	26.01	11
Nunatak Lake	18.96	3.62	4
Ridge Lake	25.05	3.975	3
Crevasse Lake	-25.28	47.83	5
Nunatak Str. Snow	8.03	23.81	15

Table 2:3 Equilibrium constants for common dissolution reactions in a carbonate – evaporite system, where T = 0°C

(Ford and Williams, 1989; Morse and MacKenzie, 1988)

EQUILIBRIUM CONSTANT	DISSOLUTION REACTION	LOG K VALUE
K_{CO2}	$CO_2(g) \Leftrightarrow CO_2(aq)$	-1.12
K_1	$CO_2(aq) + H_2O(l) \Leftrightarrow HCO_3^-(aq) + H^+(aq)$	-6.58
K_2	$HCO_3^-(aq) \Leftrightarrow CO_3^{2-}(aq) + H^+(aq)$	-10.63
$K_{calcite}$	$CaCO_3(s) \Leftrightarrow Ca^{2+} + CO_3^{2-}$	-8.38
$K_{dolomite}$	$CaMg(CO_3)_2 \Leftrightarrow Ca^{2+} + Mg^{2+} + 2CO_3^{2-}$	-16.56
K_{gypsum}	$CaSO_4.2H_2O \Leftrightarrow Ca^{2+} + SO_4^{2-} + 2H_2O$	-4.65
K_{halite}	$NaCl \Leftrightarrow Na^+ + Cl^-$	1.51

Table 2:4 Supraglacial discharge measurements (m^3/s), and calculation of proportional discharge from each channel.

	Time	Stream 1 discharge	Stream 1 proportion	Stream 2 discharge	Stream 2 proportion	Ridge Stream discharge	Ridge Stream proportion	Stream 4 discharge	Stream 4 proportion	Nunatak Stream discharge	Nunatak Stream proportion	Total Discharge
196	14:30-16:00	0.195	0.141	0.294	0.213	0.292	0.212	0.442	0.320	0.159	0.115	1.382
207	11:00-12:30	1.394	0.241	1.217	0.210	0.942	0.163	1.863	0.322	0.377	0.065	5.792
207	13:30-15:00	1.748	0.230	1.536	0.202	1.484	0.195	2.289	0.301	0.546	0.072	7.603
	Mean	1.112	**0.204**	1.016	**0.208**	0.906	**0.190**	1.531	**0.314**	0.360	**0.084**	4.926

Table 2:5 Principal Components Analysis; factor loadings and groupings from snowpack and supraglacial channels.

	FACTOR 1:	FACTOR 2:	FACTOR 3:
SNOWPACK	49% (Cl, SO_4^{2-}, Na^+, K^+)	31% (HCO_3^-, Mg^{2+}, Ca^{2+})	13.5% (NO_3^-)
STREAM 4	36% (Cl^-, Na^+, K^+)	37% (HCO_3^-, Mg^{2+}, Ca^{2+})	20% (NO_3^-)
NUNATAK	38% (HCO_3^-, Mg^{2+}, Ca^{2+})	37% (Cl^-, Na^+, K^+)	15.5% (SO_4^{2-})
RIDGE	37.5% (HCO_3^-, Mg^{2+}, Ca^{2+})	34% (Cl^-, Na^+, K^+)	19% (NO_3^-, SO_4^{2-})

Table 2:7 Seasonal mean subglacial: supraglacial ratios. Outburst ratio has been excluded from one calculation, due to difference in concentration on Day 174. For details of calculation procedure, see Appendix 1.

SUBGLACIAL/SUPRAGLACIAL RATIO		
Ion	Seasonal mean	Outburst ratio excl.
Cl	1.77	1.56
Na	6.47	5.57
K	12.05	11.66
HCO3	4.14	2.31
SO4	249.57	214.19
Ca	11.11	7.42
Mg	5.78	4.05

Table 2:6 Seasonal mean solute concentrations (μeq/l) in snowpack, supraglacial and subglacial streams.

		EC (μs)	pH	HCO_3^-	Cl^-	NO_3^-	SO_4^{2-}	Li^+	Na^+	K+	Mg^{2+}	Ca^{2+}	Sr^{2+}
SNOWPACK	mean	3.7	7.0	63.1	8.6	0.6	2.0	0	13.6	2.0	15.2	43.5	0
N=15	s.d.	1.6	0.8	40.8	7.0	0.4	0.5	0	11.1	2.3	9.1	33.0	0
RIDGE LAKE	mean	47.8	7.8	723.0	9.5	0.7	16.1	0	14.1	1.6	80.8	652.9	0
N=3	s.d.	10.4	0.4	112.1	1.5	0.6	3.1	0	2.3	0.9	6.6	109.2	0
NUNATAK LAKE	mean	41.8	8.3	595.4	9.3	1.0	13.8	0	12.9	1.7	89.8	515.1	0
N=4	s.d.	3.4	0.7	19.0	2.4	0.7	14.6	0	3.1	1.4	13.5	22.9	0
STREAM 1	mean	6.6	7.5	128.9	10.5	0.9	4.2	0	13.1	1.6	24.1	105.6	0
N=5	s.d.	2.7	0.4	116.6	2.7	0.6	0.6	0	5.3	1.9	18.3	97.6	0
STREAM 2	mean	8.7	7.4	135.5	10.9	1.0	4.4	0	15.9	1.6	21.1	113.2	0
N=2	s.d.	2.3	0.2	30.2	1.9	0.2	0.0	0	5.0	1.7	3.3	28.8	0
RIDGE STREAM (pre-outburst)	mean	6.4	6.4	80.6	11.1	0.5	3.9	0	15.4	2.3	21.6	56.8	0
N=2	s.d.	0.4	0.9	0.1	0.5	0.7	0.9	0	0.3	0.2	0.5	1.3	0
RIDGE STREAM (post-outburst)	mean	32.5	7.7	504.7	9.7	0.7	6.5	0	14.6	1.5	62.3	443.2	0
N=19	s.d.	4.2	0.5	76.6	1.7	0.6	1.2	0	3.8	1.4	12.4	67.9	0
STREAM 4	mean	4.5	7.2	92.9	9.0	0.4	3.8	0	12.5	0.8	19.2	73.7	0
N=12	s.d.	1.3	0.8	66.1	1.4	0.5	0.6	0	3.0	0.5	9.7	56.4	0
NUNATAK STREAM	mean	18.6	7.5	279.5	13.0	0.7	7.4	0	17.2	2.1	47.9	233.4	0
N=19	s.d.	4.8	0.4	70.5	4.6	0.7	3.7	0	7.1	3.3	11.4	59.9	0
SUBGLACIAL	mean	160.1	8.4	864.2	19.0	1.3	1334.4	0.3	101.6	12.7	211.4	1859.4	26.2
N=39	s.d.	51.5	0.6	443.5	11.0	0.8	515.1	0.1	72.3	8.4	139.6	760.7	13.7

Table 2:8 Mean concentrations of solutes (μeq/l) in each subglacial phase and sub-phase. (Phase 1 – Day 174-179; Phase 2 – Day 180-204; Phase 3 – Day 205-215; Phase 2a – Day 180-189; Phase 2b – Day 190-196; Phase 2c – Day 197-204)

		EC	pH	HCO3	Cl	NO3	SO4	Li	Na	K	Mg	Ca	Sr
PHASE 1	mean	219	8.1	1374.1	30.0	2.3	2010.1	0.1	179.8	24.5	418.0	2760.6	33.5
	s.d.	89.0	0.3	745.3	20.8	0.9	855.6	0.2	123.6	16.5	282.3	1154.5	15.7
	n=	5	5	6	6	6	6	6	6	6	6	6	6
PHASE 2	mean	141.6	8.3	636.9	17.3	1.0	1175.8	0.0	89.1	10.2	174.8	1524.5	19.6
	s.d.	21.7	0.6	148.5	7.9	0.7	174.2	0.0	51.3	3.4	35.9	254.7	3.7
	n=	23	22	23	23	23	23	23	23	23	23	23	23
PHASE 3	mean	174.7	9.4	1080.8	16.2	1.4	1293.8	0.0	83.6	11.3	171.5	2088.9	36.8
	s.d.	57.3	0.3	332.3	5.1	0.6	518.7	0.0	48.1	3.2	35.5	810.9	18.9
	n=	9	4	10	10	10	10	10	10	10	10	10	10
SEASONAL	mean	160.1	8.4	864.2	19.0	1.3	1334.4	0.0	101.6	12.7	211.4	1859.4	26.2
	s.d.	51.5	0.6	443.5	11.0	0.8	515.1	0.1	72.3	8.4	139.6	760.7	13.7
	n=	37	31	39	39	39	39	39	39	39	39	39	39
PHASE 2A	mean	145.0	8.1	662.7	14.6	0.8	1199.7	0.0	78.4	9.3	169.7	1574.5	18.7
	s.d.	15.1	0.5	150.3	2.7	0.8	111.7	0.0	19.4	2.2	27.9	226.8	2.8
	n=	11	11	11	11	11	11	11	11	11	11	11	11
PHASE 2B	mean	144.5	7.8	677.9	31.0	1.1	1177.1	0.0	175.2	14.4	187.8	1490.4	19.4
	s.d.	18.3	0.3	81.3	9.6	0.7	149.1	0.0	55.5	3.7	28.0	154.2	2.0
	n=	4	3	4	4	4	4	4	4	4	4	4	4
PHASE 2C	mean	135.4	8.7	581.1	14.2	1.2	1142.2	0.0	60.7	9.1	175.2	1472.7	21.0
	s.d.	30.8	0.5	169.1	3.9	0.3	256.6	0.0	32.7	3.2	49.7	335.5	5.2
	n=	8	8	8	8	8	8	8	8	8	8	8	8

Figure 2:1 Location map of John Evans Glacier (from Copland, 2001)

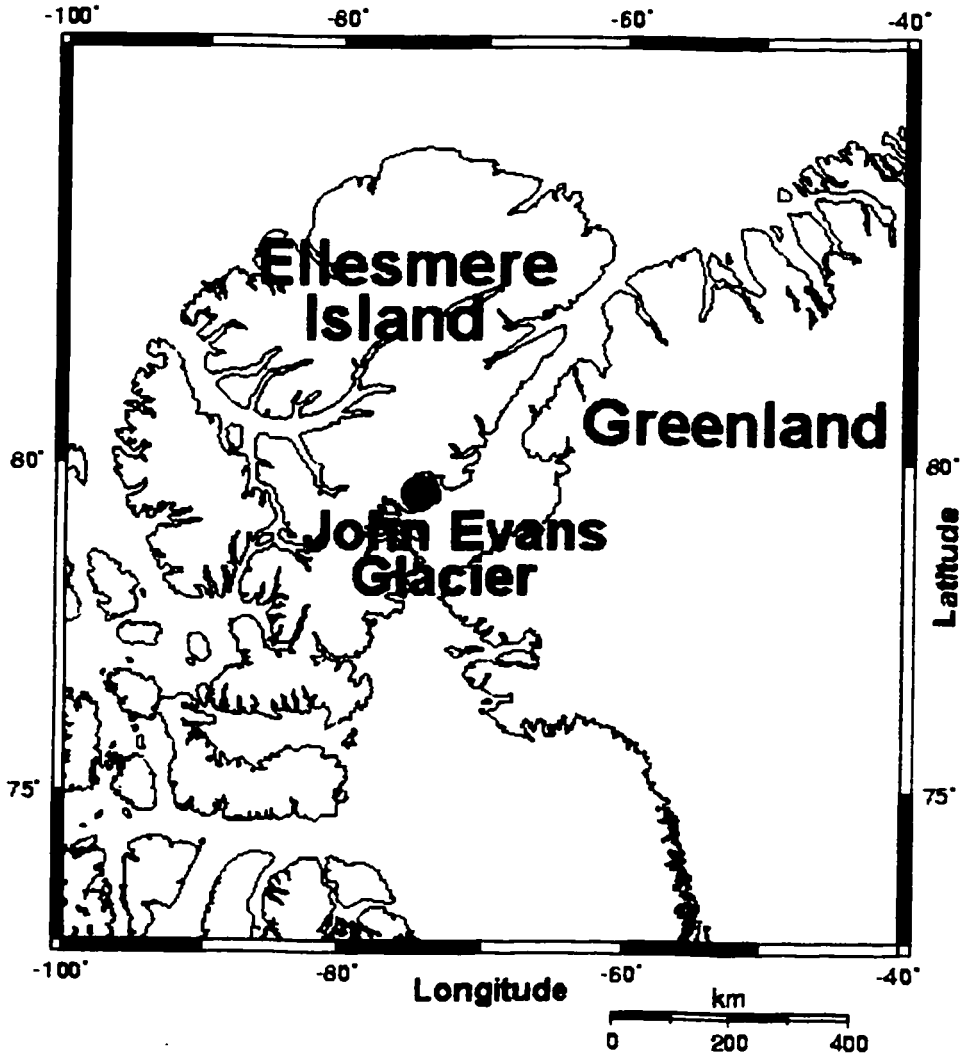

Figure 2:2 (next page) Bedrock geology in the John Evans Glacier area (from Kerr, 1972).

Key to geological abbreviations, with formations and major minerals listed:

O-Dar	Upper Ordovican, Silurian and Lower Devonian
	Douro and Allen Bay Formations
	Limestone, dolomite and siltstone
Oe-c	Lower and middle Ordovician
	Irene Bay, Thumb Mountain, Bay Fjord and Eleanor River Formations
	Limestone, dolomite, siltstone, anhydrite and gypsum
Ob	Lower Ordovician
	Baumann Fjord Formation
	Anhydrite and gypsum
Oco	Lower Ordovician
	Copes Bay Formation
	Limestone
Cpg	Middle Cambrian
	Parrish Glacier Formation
	Limestone, with shale interbeds, overlain by stream and glacial sediments
Csb	Lower Cambrian
	Scoresby Bay Formation
	Dolomite
P-Cu	Proterozoic and Cambrian
	Kane Basin, Rawlings Bay and Ella Bay Formations
	Sandstone, siltstone and conglomerate
O-Du	Lower Ordovician to Lower Devonian
	Douro, Allen Bay, Cornwallis Group and Eleanor River Formations

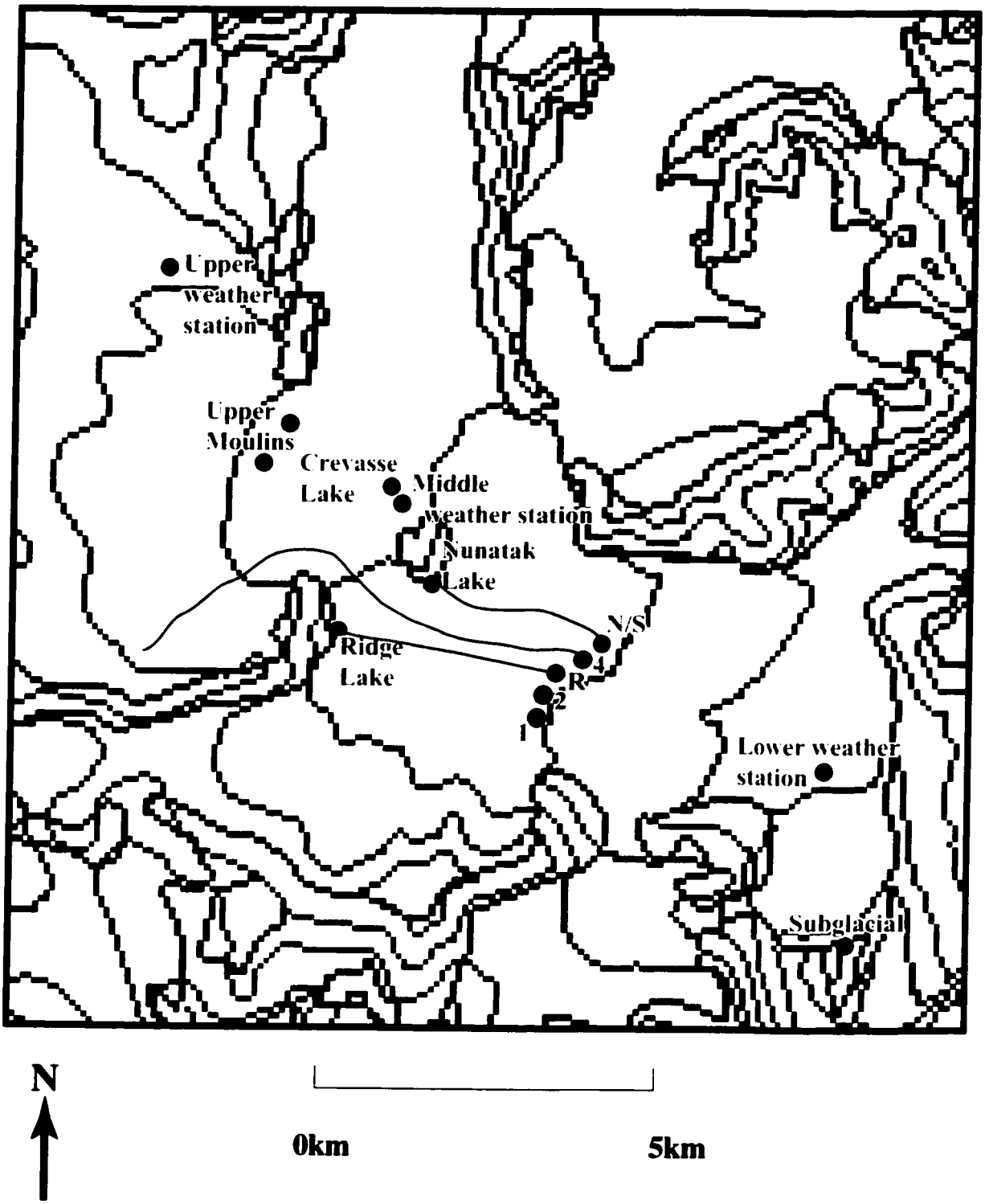

Figure 2:3 John Evans Glacier, showing supraglacial streams, water and snow sampling sites, and automated weather stations. 1 - Stream 1 moulin; 2 - Stream 2 moulin; R - Ridge Stream datalogger; 4 - Stream 4 moulin; N/S - Nunatak Stream datalogger and snow sampling site.

Figure 2:4 Daily mean temperature and Net radiation during the 2000 melt season

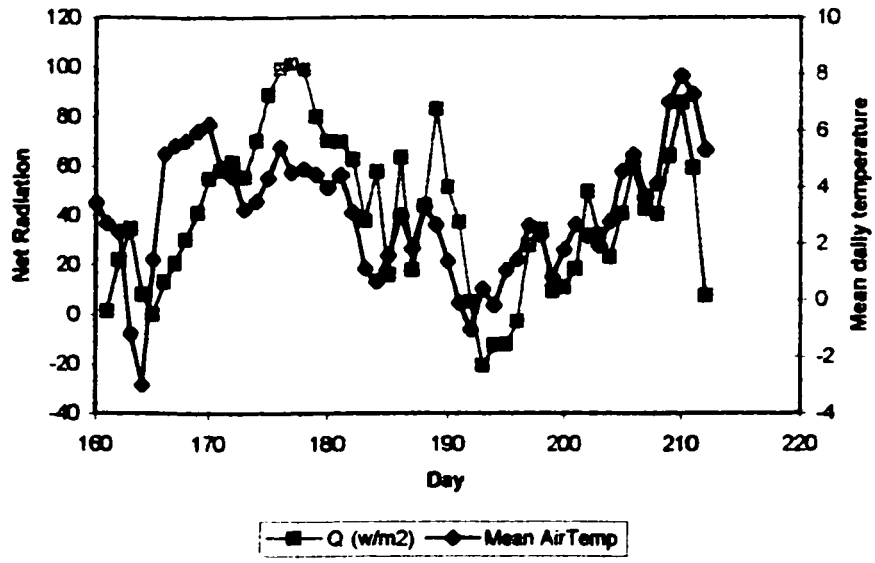

Figure 2:5 Suspended sediment concentration measured by filtration regressed on OBS values showing regression line and equation

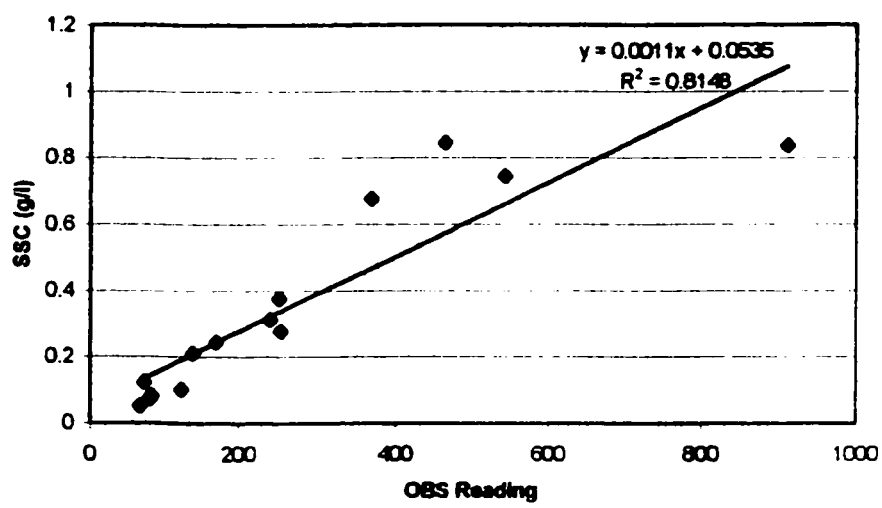

Figure 2:6 Mean air temperature and subglacial discharge collected manually whenever possible

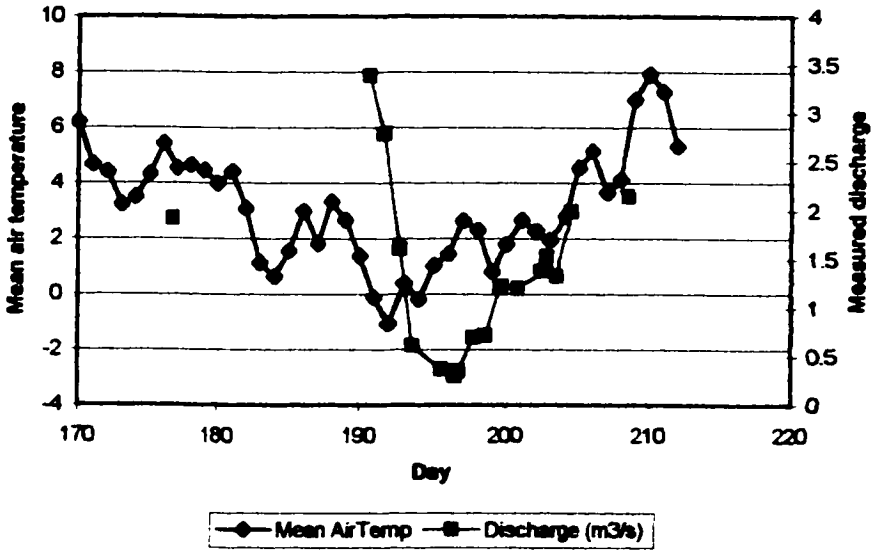

Figure 2:7 Seasonal variations (a) HCO3, (b) Ca and (c) Mg in supraglacial streams,snowpack and lakes (Key on figure 2:8)

(a)

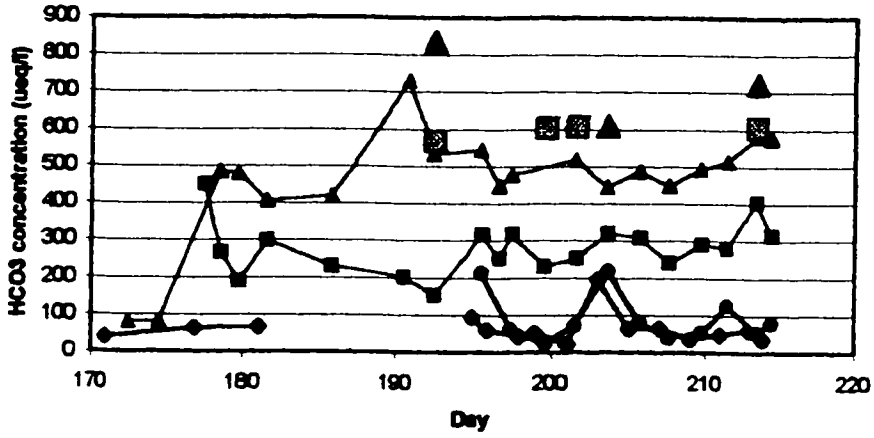

(b)

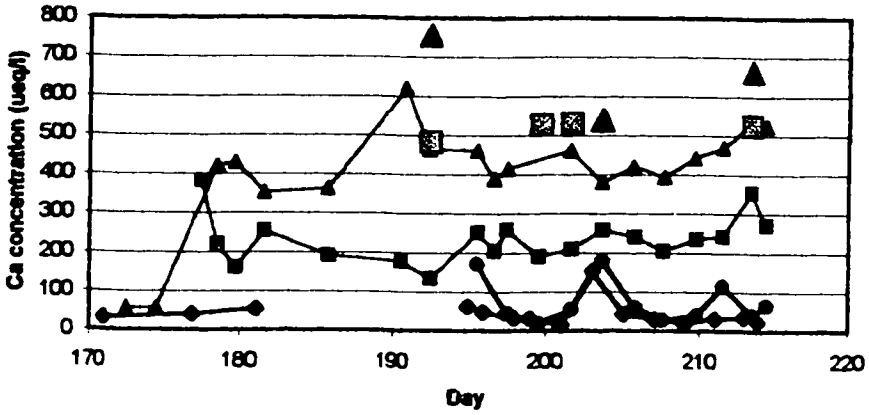

(c)

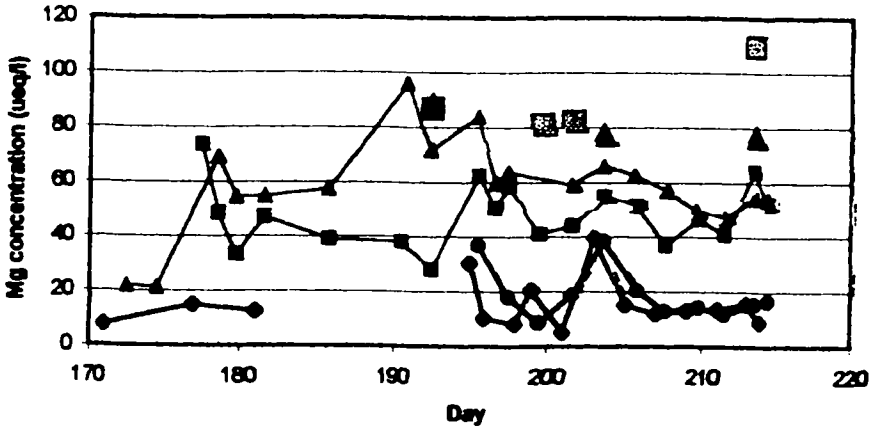

Figure 2:8 Seasonal variation of (a) Cl and (b) Na in supraglacial streams,snowpack and lakes

(a)

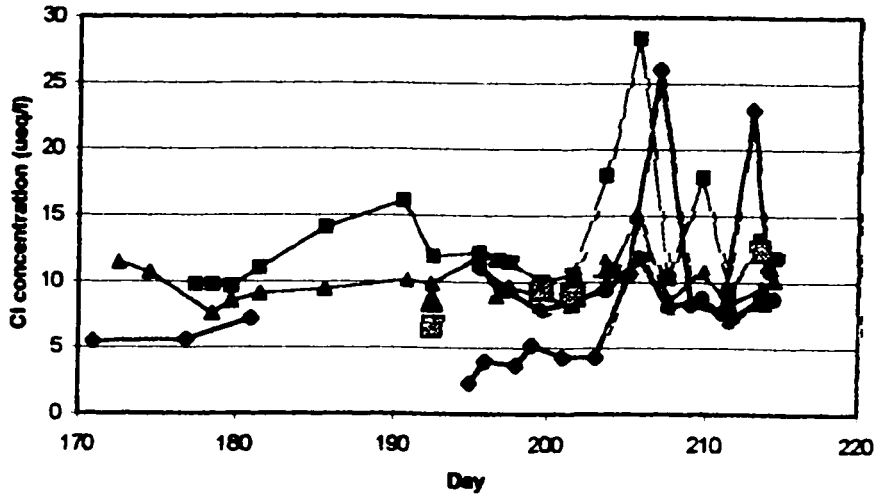

(b)

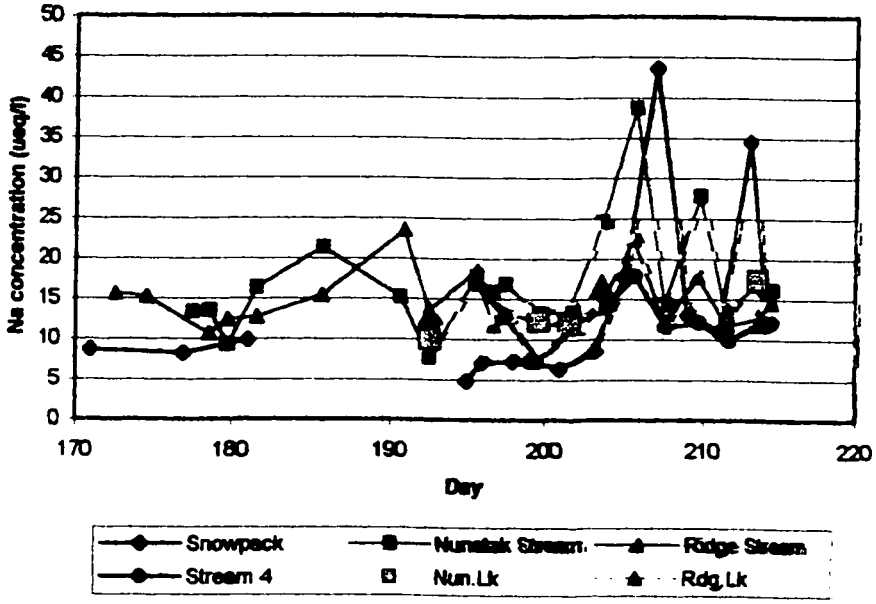

Figure 2:9 Seasonal subglacial - supraglacial ratios, (a) carbonate-derived ions, (b) sea-salt ions, and (c) SO4 ratio

(a)

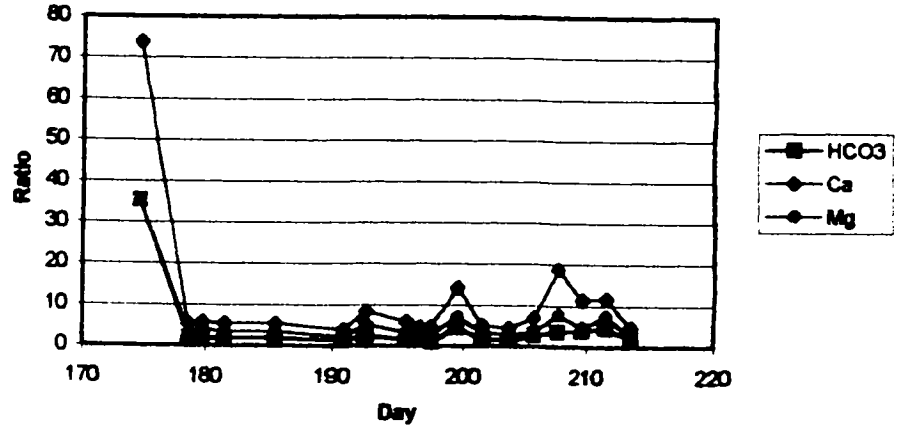

(b)

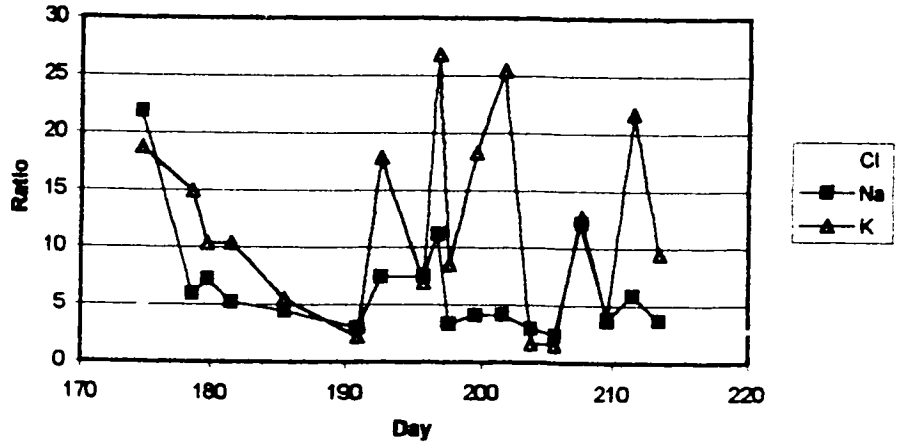

(c)

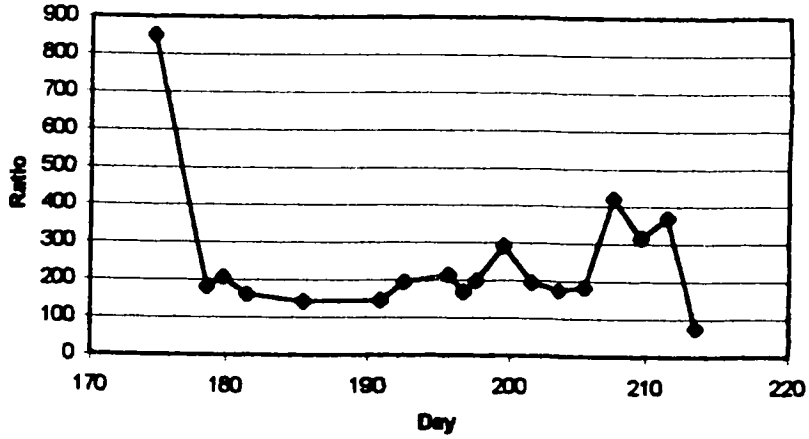

Figure 2:10 PCA Factor scores against time for subglacial samples (F1 - Na, K, Mg, Cl, Li, NO3; F2 - HCO3, Ca, SO4, Sr)

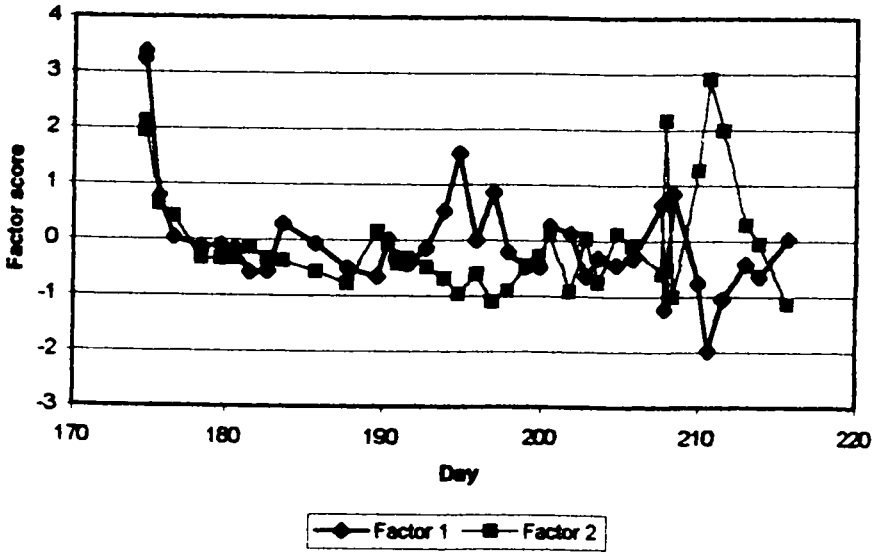

Figure 2:11 Seasonal variations in subglacial (a) HCO3, SO4 and Ca, and (b) Sr

(a)

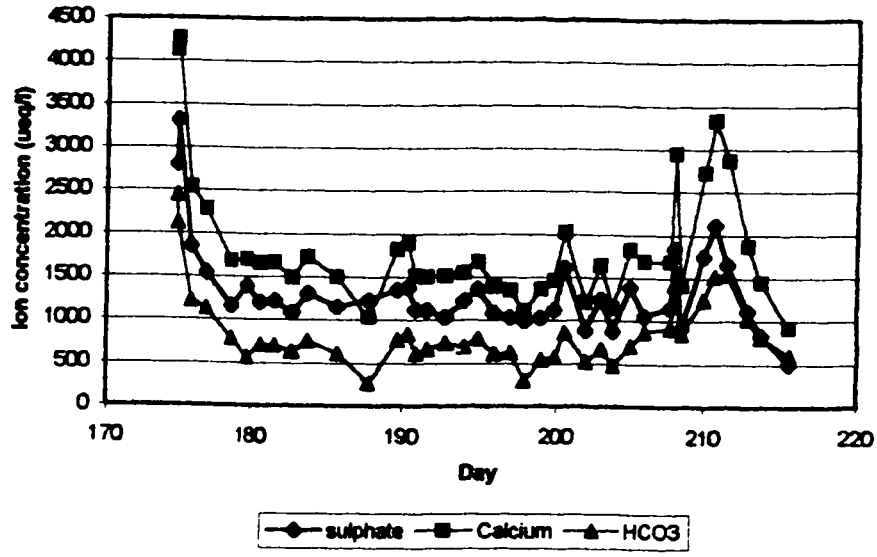

(b)

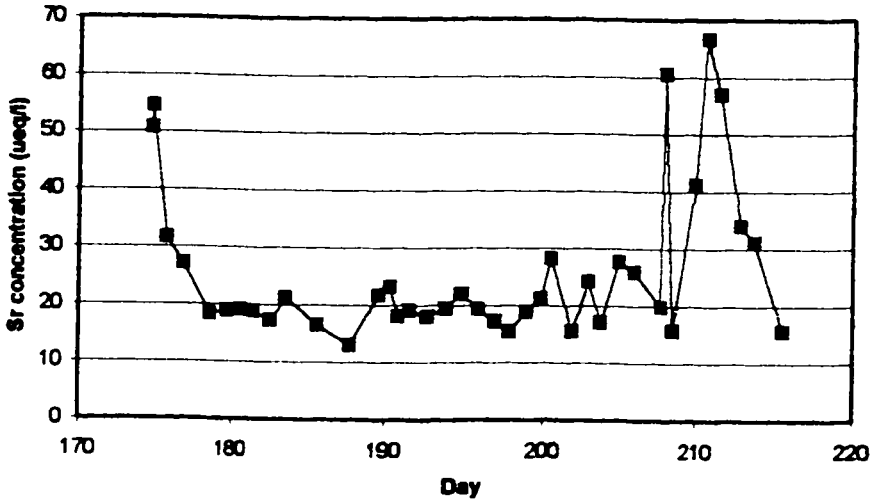

Figure 2:12 Seasonal variations in subglacial (a) K and Cl, and (b) Na and Mg

(a)

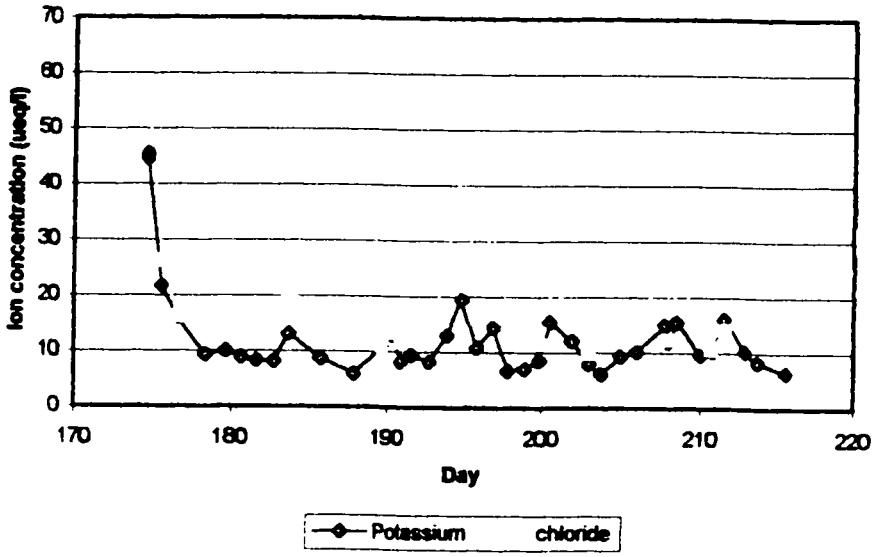

(b)

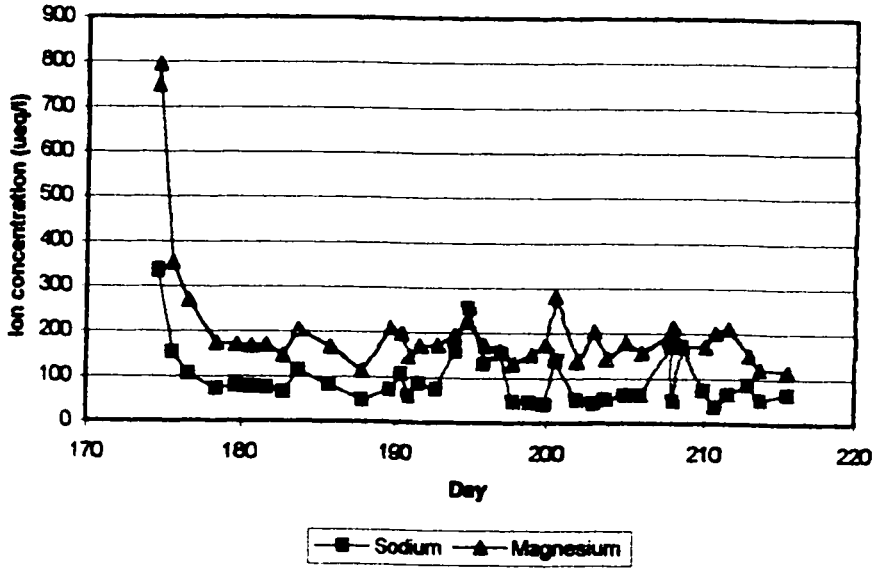

Figure 2:13a Seasonal Ca:SO4 in subglacial waters

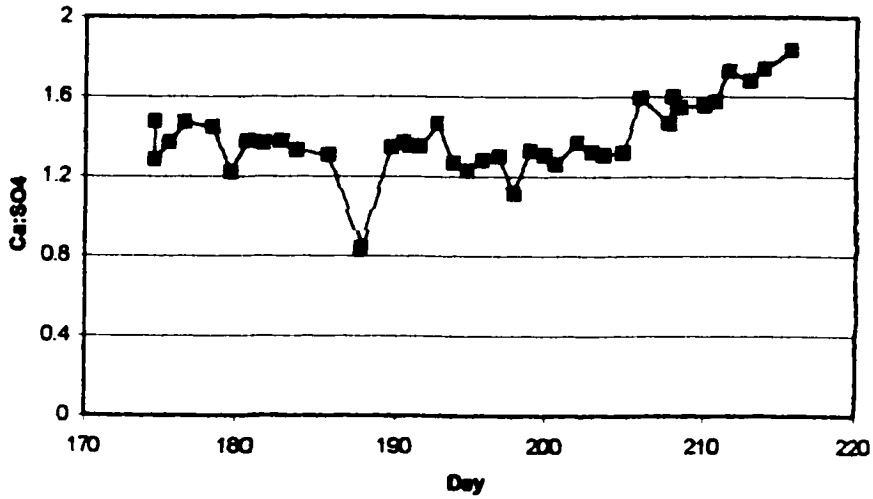

Figure 2:13b Seasonal Ca:Mg in subglacial waters

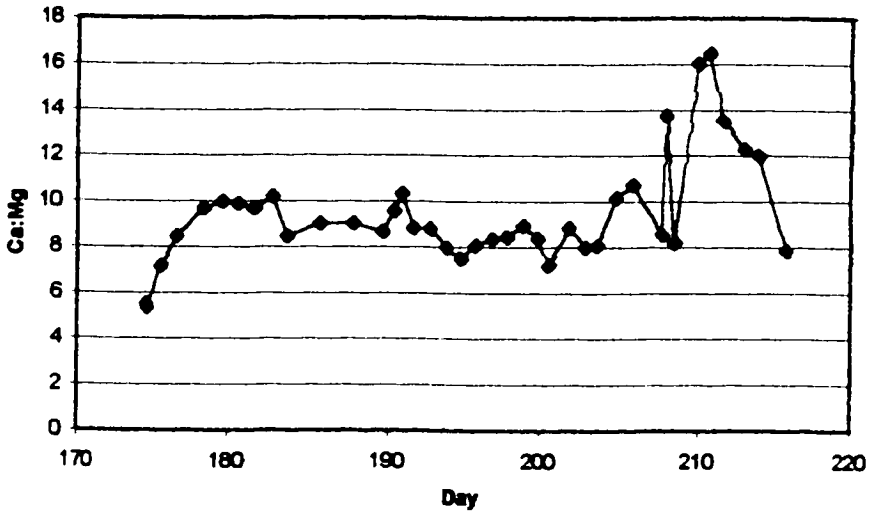

Figure 2:14a Seasonal log(pCO2) of subglacial waters, calculated by WEB-PHREEQC

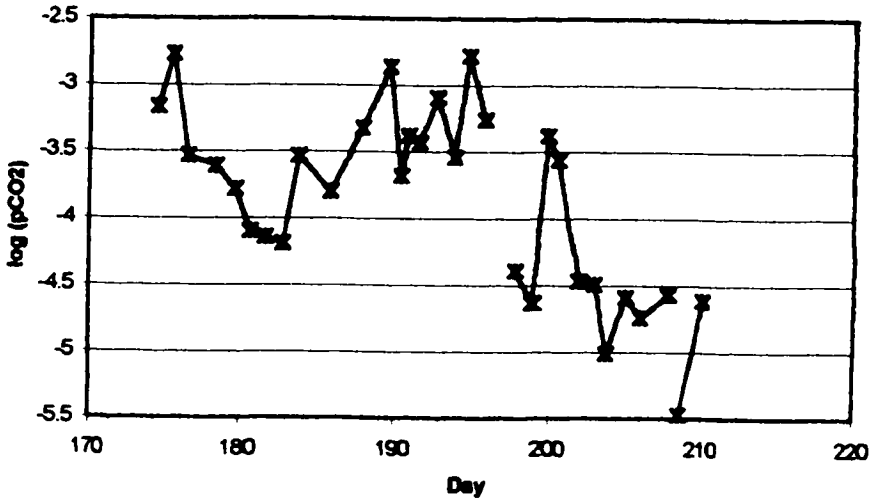

Figure 2:14b Seasonal saturation indices for calcite, dolomite and gypsum, calculated by WEB-PHREEQC

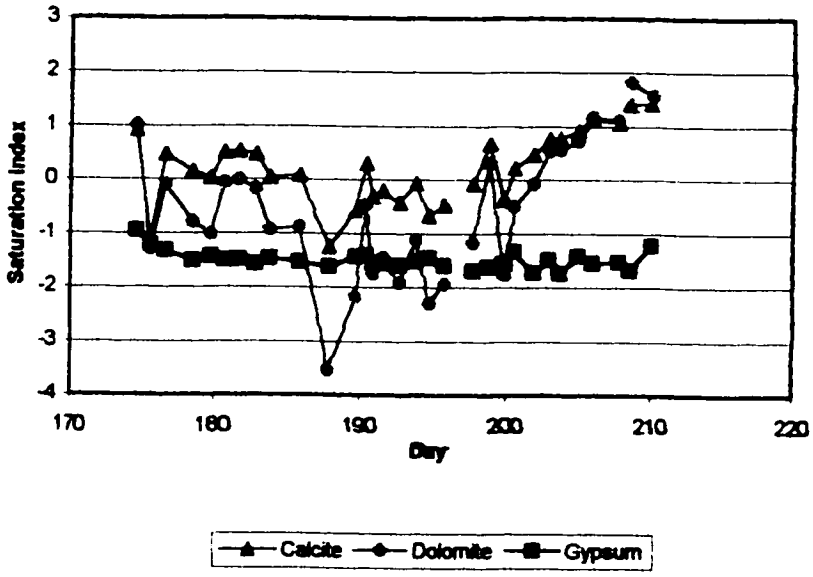

Figure 2:15 Seasonal variations in subglacial SSC and EC, and phases of subglacial drainage development

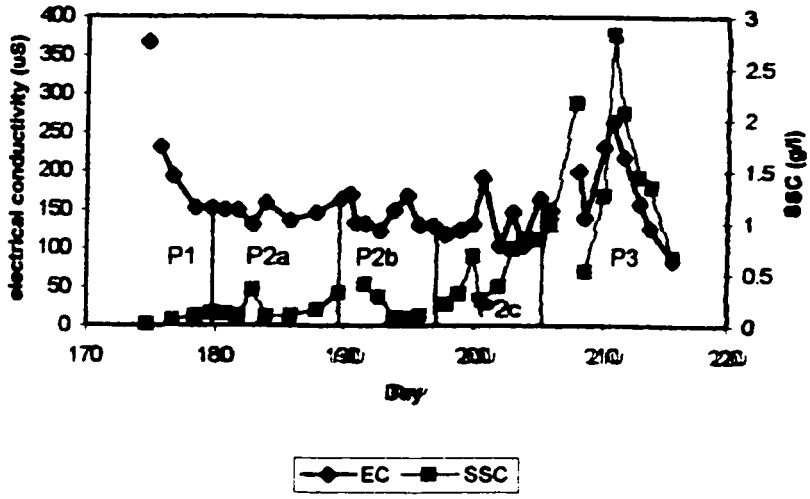

Chapter 3 – Quantification of chemical weathering reactions using PHREEQC

The concepts of chemical weathering in the subglacial environment and the seasonal evolution of solutes in subglacial water were introduced qualitatively in the previous chapter, and discussed in relation to field data collected during the 2000 melt season at John Evans Glacier, Ellesmere Island (Figure 2:1). A 3-phase development of the subglacial drainage system was proposed based upon the chemical data. It is suggested that a 2-component drainage system underlies the glacier, and that the channelised component expanded throughout the course of the 2000 melt season at the expense of the distributed component. These conclusions are similar to those made in other studies (e.g. Nienow et al, 1998, Haut Glacier d'Arolla; Wadham et al, 1998, Finsterwalderbreen), and are based upon a qualitative analysis of potential chemical weathering reactions occurring in different parts of the drainage system. The goal of this chapter is to provide a more quantitative interpretation of the observed temporal changes in water chemistry. A variety of geochemical modeling programs now exist, which may be used to quantify chemical weathering reactions in a variety of different environments. This chapter reviews a number of different models written in PHREEQC designed to examine chemical weathering reactions at different stages throughout the 2000 melt season at John Evans Glacier, and to identify phases that must be dissolved or precipitated to explain the observed changes in water chemistry. These results are then used to develop inferences made in the preceding chapter regarding subglacial hydrological system evolution at John Evans Glacier.

An introduction to PHREEQC:

PHREEQC (version 2) is described as "a program for simulating chemical reactions and transport processes in natural or polluted water" (Parkhurst and Appelo, 1999; pg.1). The program uses a series of equations based upon the laws of thermodynamics to perform a number of different modeling tasks specified by the user. The program is supported by a large database that includes listings of master species for most elements and dissolution reactions for common phases (minerals), along with thermodynamic data, including values for $log\ K$ (thermodynamic equilibrium constant) and ΔH (enthalpy change), for the master species and phases listed. For any specified task, there are a number of assumptions, unknowns and master unknowns that dictate those equations to be used in subsequent calculations.

The initial task performed prior to any other calculations is the speciation of an aqueous solution, and the calculation of saturation indices for a number of relevant phases. The key

assumption is that all dissolved species (denoted i) are in thermodynamic equilibrium, and therefore follow the Law of Mass Action, $K_i = a_{(product)} / a_{(reactant)}$. Unknowns for i are: activity (a_i), activity coefficient (γ_i), molality (m_i) and number of moles in solution (n_i). Master unknowns for the aqueous solution are: natural log (ln) a_m (where $_m$ denotes master species), $ln\ a_{H2O}$, ionic strength (μ) and mass of solvent (water) in aqueous solution (W_{aq}). Equations required to perform the speciation calculations include f_m, f_{H2O}, f_μ, and f_{Alk}, where f indicates function and Alk represents alkalinity (Parkhurst and Appelo, 1999). In order to solve all the functions within given tolerance limits, a Newton-Raphson iteration method is used until all equations are satisfied. The speciation process therefore calculates activities of all species, and takes account of ion pairs that form between some ions in solution (Appendix 2). Saturation indices for all relevant solid phases (according to input for solution) are then calculated using:

$$SI_p = log\ K_p$$

assuming that phases are pure (For full derivation and listing of all equations refer to Parkhurst and Appelo, 1999). Calculation of saturation indices and pCO_2 for all subglacial samples followed this procedure (Chapter 2).

Following speciation, numerous other tasks may be performed by PHREEQC. This chapter examines only mixing and inverse modeling. The mixing application requires input of two or more aqueous solutions and one or more suggested mixing ratios. Once each input solution has been speciated, solutions are mixed at given ratios, producing a new solution that is also speciated. Possible applications for this task are the dilution of one highly concentrated body of water (e.g. outburst water) by a less concentrated body of water (e.g. snowmelt / supraglacial input) to obtain a set of possible solutions that might occur following a period of dilution (e.g. Phase 2 waters).

The inverse modeling application is used predominantly to identify a range of possible reactions that can account for changes in water composition in either time or space. The reactions are defined by a series of mole transfers calculated to explain the difference in composition of two (or more) input waters, within given uncertainty limits. The approach used in the application is to solve a set of linear equalities to calculate a set of unknowns: mixing fraction for each solution (α_q), mole transfer of minerals and gases into / out of solution (α_p), aqueous mole transfer of redox elements (α_r), and a set of uncertainty terms to account for analytical error of the solution ($\delta_{m,q}$). The equations used are (1) mole balance equation for each element; (2) mole balance equation for alkalinity; (3) mole balance equation for electrons; (4) mole balance equation for water, that accounts for water gained and lost from minerals; (5) mole balance

equation for isotopes; (6) charge balance for each aqueous solution; (7) equation relating uncertainty terms for pH, alkalinity and total dissolved inorganic carbon (DIC); (8) inequalities used to constrain the size of the uncertainty terms, and (9) inequalities used to constrain the sign of mole transfer of reactants (see Parkhurst and Appelo, 1999 for details of equations). For modeling of John Evans Glacier solutions, redox elements and isotopes are not included, so α_r and equations (3) and (5) are not considered. The remaining equations are solved using an algorithm that uses L1 optimization (minimizes the sum of absolute values) and 3 matrix equations that describe all the equalities and inequalities listed above. This technique determines whether any models exist based upon constraints, and finds one (unique) set of mixing fractions and phase mole transfers that satisfies the input values and uncertainty constraints. A second algorithm is used to test every possible combination of phases and solutions. At this stage, "minimal models" are defined as being models that have the minimum number of phases possible where an inverse model may still be derived.

Required input for an inverse model consists of the description of two or more aqueous solutions (in ppm or mol/l), uncertainty limits for all aqueous species, pH and alkalinity, and a list of possible phases or reactants that the aqueous solution may encounter on its path. For modeling of John Evans Glacier solutions, NO_3^-, Li^+ and Sr^{2+} were excluded from the solution description. Li^+ and Sr^{2+} are thought to be derived from impurities in the bedrock (M.Sharp, pers.comm.), and cannot therefore be explained by weathering of pure phases. NO_3^- is derived mostly from atmospheric deposition to the supraglacial environment (Tranter et al, 1993), and concentrations may not be accurate as they are close to detection limits (cf. chapter 2). It was not possible to keep uncertainty limits for aqueous species constant throughout the modeling, as the program could not always produce models at low uncertainty limits. Limits were, however, always kept as low as the program would allow. pH balance was set at 0.1unit throughout. Phases included in the model were: CO_2(g), calcite, dolomite, gypsum, halite, sylvite, albite, k-feldspar, quartz (set to precipitate only), illite (set to precipitate only) and kaolinite (set to precipitate only). This choice of phases was based upon known geology (Kerr, 1972; figure 2:2 – calcite, dolomite and gypsum and feldspars from siltstone), mineralogical analysis of sediments (feldspars, illite, kaolinite), and inferences from water chemistry. It was apparent that a subglacial source for Cl^- was required, so halite and sylvite were included to provide this, although it should be noted that they may not be derived directly from the bedrock, but could have been precipitated from freezing subglacial waters.

The phases included allow all aspects of water chemistry to be explained by common reactions, and limit the number of possible models to facilitate analysis. In addition, the program was set to show minimal models only, in order that only the simplest models are available for discussion and analysis. Output of the model is in mol/l.

Following the qualitative analysis in chapter 2, a number of water types were identified. These water types and the investigation of the linkages between them form the basis for the modeling procedure adopted (Figure 3:1). Every simulation produced several different models, each of which was considered individually in terms of the reactions required to account for the changes in chemistry between the water types included in the model. Phase mole transfer ratios were calculated for CO_2: calcite, calcite: dolomite, calcite: gypsum, calcite: (halite + sylvite), calcite: feldspar, dolomite: gypsum, dolomite: feldspar and gypsum: feldspar. As there were only two different values for phase mole transfer of calcite in most simulations, ratios were calculated for two models only in each simulation. The modles used for this are highlighted in the results tables. For simplicity, they were chosen so that no negative mole transfers were included in the ratio calculations. Tabulated mean ratios were then obtained by averaging the ratios of the two selected models.

Supraglacial water evolution

Introduction

As discussed in chapter 2, the supraglacial channel network that feeds the subglacial drainage system of John Evans Glacier is comprised of 5 major supraglacial channels, 2 of which drain from ice marginal lakes (Figure 2:3). In terms of chemical composition, 3 out of 5 streams (Streams 1, 2 and 4) had solute concentrations very similar to the snowpack (Appendix 3; figure 2:7a-c), but the Nunatak and Ridge Streams had higher solute concentrations, with a greater abundance of crustally derived ions (Ca^{2+}, Mg^{2+}, HCO_3^-). However, concentrations in the Nunatak and Ridge Lakes were higher than in both the snowmelt-fed streams and the Nunatak and Ridge Streams. Thus, although the Nunatak and Ridge Streams are fed by their respective lakes, water entering the streams from the lakes must be later diluted by less concentrated snow- and ice-melt.

Lake water evolution

It is likely that the high solute concentrations in the Nunatak and Ridge Lakes are derived from chemical weathering of rock and sediment in the catchments of the small ice marginal

channels that flow into the lake basins (Hodgkins et al, 1998). The evolution of the lake waters (Appendix 3) from seasonal Stream 4 concentrations (as a proxy for snowmelt) was therefore investigated by inverse modeling (Simulation A1, Figure 3:1).

Results (Table 3:1) suggest that the change in lake water composition results predominantly from dissolution of calcite, dolomite and gypsum, although small amounts of trace minerals (sylvite and K-feldspar) were also dissolved in some models. Chemical equations accounting for all weathering reactions may be written as follows (Stumm and Morgan, 1981; Ford and Williams, 1989; Andrews et al, 1996):

Calcite dissolution:

[3-1] $$CaCO_3 + CO_2 + H_2O \Leftrightarrow Ca^{2+} + 2HCO_3^-$$

Dolomite dissolution:

[3-2] $$CaMg(CO_3)_2 + CO_2 + 2H_2O \Leftrightarrow Ca^{2+} + Mg^{2+} + 4HCO_3^-$$

Gypsum dissolution:

[3-3] $$CaSO_4.2H_2O \Leftrightarrow Ca^{2+} + SO_4^{2-} + 2H_2O$$

Sylvite dissolution:

[3-4] $$KCl \Leftrightarrow K^+ + Cl^-$$

Ion exchange (feldspars):

[3-5] $$KAlSi_3O_8 + Na^+ \Leftrightarrow NaAlSi_3O_8 + K^+$$

K-Feldspar dissolution:

[3-6a] $$KAlSi_3O_8 + H_2CO_3 + 9/2H_2O \Leftrightarrow K^+ + HCO_3^- + 2Si(OH)_4 \text{ (silicic acid)} + 1/2Al_2Si_2O_5(OH)_4 \text{ (kaolinite)}$$

[3-6b] $$3KAlSi_3O_8 + 2H_2CO_3 + 12H_2O \Leftrightarrow 2K^+ + 2HCO_3^- + 6Si(OH)_4 + KAl_2(Si_3Al)O_{10}(OH)_2 \text{ (illite)}$$

where silicic acid releases water to become quartz:

[3-7] $$2Si(OH)_4 \rightarrow 2SiO_2 + 4H_2O$$

very rapidly, in order to gain a more stable form (Andrews et al, 1996). Comparison of the mole transfers required by the measured input values with the model output values (Table 3:1) shows that there is a good correspondence between measured and modeled mole transfer, which is consistent with the equations listed above. Mole transfers are generally larger in the Ridge Lake basin, as runoff in this basin appears to have had more contact with sediment than runoff in the Nunatak Lake basin. However, dolomite dissolution is more prevalent in the Nunatak Lake basin. Based upon mineralogical analysis of sediments collected in the lake basins it is only a trace mineral in the Ridge Lake basin, but is a dominant mineral in the Nunatak Lake basin.

Lake water dilution

In order to calculate the proportions of lake water and snowmelt in each of the Nunatak and Ridge Streams (Simulation A2), the mixing application was used. A range of mixing ratios was explored in order to find the one that provided the best fit with observations. Seasonal mean values from Stream 4 (snowmelt) and the lakes were used as input data, and output was compared with mean values from the Nunatak and Ridge Streams collected at the same time as lake samples at locations where water flowed into moulins (Table 3:2).

In chapter 2, it was seen that some species did not behave conservatively in the supraglacial channels (Figure 2:6, Na^+ and Cl^-), so these could not be used as a "best fit" measure. As Ca^{2+} and Mg^{2+} are derived mostly from chemical weathering of crustal material (Souchez and Lemmens, 1987), they should behave conservatively within an ice-walled channel with little access to rock or dust. These species were therefore used to determine the mixing ratio for the dilution of lake water, although it is likely that the calculations provide a maximum estimate of the lake water input to each stream. Based on this assumption, results (Table 3:2) show that Nunatak Stream water is diluted at an approximate ratio of 0.66 snowmelt: 0.34 lake water. The Ridge Stream ratio is 0.32 snowmelt: 0.68 lake water. Therefore, the Ridge Stream receives less snowmelt input prior to entering the subglacial system than the Nunatak Stream. As the Nunatak Stream has more tributaries draining the ice surface than the Ridge Stream, this result seems realistic.

Most species are matched well using these mixing ratios. However, HCO_3^- is significantly overestimated in both simulations. This is likely due to an error in the HCO_3^- data, as discussed in chapter 2. However, an approximation of the stream water composition may still be derived through a mixing model where concentrated lake waters are mixed with dilute snowmelt.

Developing mean supraglacial input using proportional mixing of 5 streams

Based on calculations of discharges in the 5 supraglacial streams (Table 2:4), a composite supraglacial water composition was derived using the mixing program (Simulation A3). Input concentrations for the model were mean seasonal values from each of the five streams (Appendix 3), and mixing proportions were as follows: Stream 1 (0.204); Stream 2 (0.208); Ridge Stream (0.190); Stream 4 (0.314); Nunatak Stream (0.084). The resulting solution (Table 3:3) was then used as an input solution for several of the inverse modeling simulations performed on subglacial

waters, to investigate various aspects of subglacial chemical weathering. Comparison of this solution with other supraglacial solutions illustrates that the waters entering the subglacial system from the surface have a mean composition that is slightly modified from that of snowmelt, mainly by dissolution of small amounts of calcite and dolomite derived in basins draining to the ice marginal lakes, as suggested by the snowmelt: lake water ratios discussed above.

Subglacial water evolution

Introduction

Most of the water draining across the glacier bed appears to be derived from the supraglacial environment. Based on dye tracing results, minimum estimates of residence times of these waters in the subglacial environment during the melt season vary from 11.5 hours to less than 2 hours (R.Bingham, pers.comm.). Even longer residence times may occur if waters are stored at the glacier bed over winter, or if water gets trapped in the distributed system. These residence times, in association with the consideration that much of the material available for dissolution is freshly ground rock flour, are long enough to allow a wide range of chemical weathering reactions to take place (Tranter et al, 1993). Many of these reactions were discussed at a qualitative level in chapter 2.

Based on temporal variations in the concentration and composition of solutes in subglacial runoff, the melt season can be divided into 3 phases (Table 2:8; Figure 3:2). Changes in composition between each of these phases were modeled using inverse modeling or dilution by mixing, following figure 3:1. All subglacial waters are thought to evolve from a combination of chemical weathering reactions adding solute to the composite supraglacial input. However, some insight into changes in the balance of reactions involved in the initial and final stages of evolution of the water chemistry can be gained by comparing the chemistry of more concentrated solutions with that of a water with a composition intermediate between that of the composite supraglacial input and that of the more concentrated water. Intermediate waters chosen as the starting points for simulations were usually examples of more dilute subglacial water types that drained from the glacier in a period immediately preceding that in which the more concentrated water was sampled (Figure 3:2). Where it was necessary to evolve a dilute solution from a more concentrated solution (e.g. Phase 2a waters from outburst waters), a mixing (dilution) step was added. In some cases, a second inverse modeling step was required to simulate the addition of some solute to the mixed solution by post-mixing reactions.

Outburst water evolution

Subglacial drainage commenced on Day 174, when slightly turbid water was observed upwelling through ice-marginal sediment in the proglacial area and through newly formed cracks on the ice surface close to the glacier snout. These waters were very solute-rich (Figure 2:11 – 2:12; Appendix 4). In order to investigate the source of these solutes, two simulations were performed using the inverse modeling application. Simulation B1 (Figure 3:1) modeled composition changes between pure early season snowmelt runoff and outburst waters (Appendix 4). Because the outburst took place prior to the connection of the supraglacial lakes to the rest of the drainage system, it is more realistic to use the very dilute solutions from early snowmelt as the initial solution rather than the composite supraglacial solution (Appendix 2). This simulation examines the net changes that took place in the solution prior to the outburst. Simulation B2 modeled changes in composition between mean values for subglacial low-flow conditions (Phase 2c) and outburst waters (Appendix 4). Phase 2c waters are dominated by the products of gypsum dissolution and are characteristic of periods of relatively stable water flux from the subglacial drainage system, as described by Skidmore and Sharp (1999; Table 1). Late season observations in 2000 suggest that following the discharge peak on Days 210 – 211, water composition returned to this steady state (Days 213-215) prior to freeze-up (Figures 2:11; 2:12). These waters thus provide a good initial solution from which to examine the later stages of evolution of the outburst waters, thus providing insight into the suite of reactions that add solute to waters with long rock-water contact times.

These simulations saw the greatest mole transfers of any of the inverse modeling simulations performed (Table 3:4a). In terms of the absolute contributions from different minerals, the only difference between the two simulations is that mole transfers were greater in the snowmelt simulation than the Phase 2c simulation. However, $CO_2(g)$ transfers were approximately equal in both simulations. Most phases were dissolved, and the only removal of solutes from solution resulted from ion exchange between sylvite and halite.

[3-8] $$NaCl + K^+ \Leftrightarrow KCl + Na^+$$

The largest phase mole transfers were from the dissolution of gypsum [3-3] and calcite [3-1], but other reactions needed to explain the inferred phase mole transfers are dolomite dissolution [3-2], halite [3-9] and sylvite [3-4] dissolution, and incongruent dissolution of feldspar (K-feldspar [3-6] and albite [3-10]) that left illite and kaolinite as solid phases (Ford and Williams, 1989; Andrews et al, 1996).

[3-9] $NaCl \Leftrightarrow Na^+ + Cl^-$

[3-10a] $NaAlSi_3O_8 + H_2CO_3 + 9/2H_2O \Leftrightarrow Na^+ + HCO_3^- + 2Si(OH)_4 + 1/2Al_2Si_2O_5(OH)_4$ (kaolinite)

[3-10b] $3NaAlSi_3O_8 + H_2CO_3 + 12H_2O + K^+ \Leftrightarrow 3Na^+ + 2HCO_3^- + 2Si(OH)_4 + KAl_2(Si_3Al)O_{10}(OH)_2$ (illite)

These reactions account for all the changes in chemical composition required by the measured input values.

Examination of the relative contributions of different reactions did, however, reveal subtle differences between the simulations (Table 3:4b). Comparison of phase mole transfer ratios showed that calculated net weathering (from snowmelt) saw a greater proportion of gypsum and calcite dissolution, whereas later stages of weathering showed a greater contribution from dissolution of dolomite, halite, sylvite and feldspars. Relative to calcite, more $CO_2(g)$ is consumed in the simulation from Phase 2c waters than in the simulation from snowmelt, indicating that more CO_2 is consumed for the dissolution of dolomite and feldspars during the later stages of evolution of outburst waters.

Outburst water dilution

Following the outburst, subglacial waters were rapidly diluted by snowmelt. To investigate the evolution of Phase 2 waters from outburst water, it is most appropriate to perform a mixing simulation, due to both the extremely high solute concentrations in the outburst waters, and the fact that dilute snowmelt was constantly being fed into the subglacial system from the supraglacial environment during this period. The mixing simulation provides an estimate of the fraction of "outburst" type water in subglacial flow at the end of Phase 1, as well as providing an indication of whether any post-mixing reactions are required to produce Phase 2 waters. Input solutions for simulation B3 (figure 3:1) were the modeled composite supraglacial water (Table 3:3) and the measured outburst water (Day 174; Appendix 4). These were mixed in different proportions until the result matched up as closely as possible with a measured sample from Day 180. As Cl^- is considered to be a conservative species in most subglacial systems (Sharp et al., 1995), and the subglacial: supraglacial Cl^- ratio on Day 180 is close to 1 (Figure 2:9b), this species was used to match measured and calculated solutions.

Results (Table 3:5) show that, when measured and calculated Cl^- concentrations match, the ratio of snowmelt: outburst water is 0.935:0.065. This suggests that by Phase 2, the chemical signature of bulk subglacial water is barely influenced by the characteristics of the old outburst

water. However, the concentration of all other species, especially Ca^{2+} and SO_4^{2-}, is underestimated by this mixing ratio. This suggests that mixing is not conservative, and that some chemical weathering is required to produce Phase 2 waters. The nature of this chemical weathering was thus examined using inverse modeling.

Post-mixing reactions

Simulation B4 (Figure 3:1) was used to investigate the nature and magnitude of the post-mixing reactions required to explain the changes in water composition between the water produced by the outburst dilution simulation (using 0.935:0.065 mixing ratio) and the water sampled on Day 180 (Appendix 4). As a comparison, simulation B5 was also performed to simulate the evolution from the modeled composite supraglacial solution (Table 3:3) to the Day 180 sample. It is expected that most post-mixing reactions will have involved the weathering of suspended sediment in subglacial channels.

Model results (Table 3:6a) indicate that the magnitudes of phase mole transfers were larger when starting with the more dilute snowmelt solution. The balance of phase mole transfers was also different with different starting solutions (Table 3:6b). Ratios of phase mole transfers for different mineral pairs suggest that calcite and gypsum dissolution become more important than dolomite and feldspar dissolution during the later stages of evolution (i.e. in the simulation from the diluted outburst waters). This indicates that rather than slow reactions dominating the later stages of evolution as in the outburst evolution simulations, ions released by such reactions are introduced to the solution with old subglacial water during the mixing stage, and rapid reactions dominate solute acquisition during the post-mixing stage whilst water is being evacuated efficiently from the glacier. Most of the specified phases must be dissolved to produce the required changes in composition. Chemical reactions needed to explain the observed changes in water composition are the dissolution of calcite [3-1], dolomite [3-2] and gypsum [3-3], ion exchange [3-8] and dissolution of sylvite [3-4] and halite [3-9], and incongruent dissolution of feldspars (k-feldspar [3-6] and albite [3-10]) that left illite and kaolinite as solid phases.

The magnitude of post-mixing reactions was calculated for each individual solute (Table 3:6c). A large percentage (75 – 85%) of total SO_4^{2-}, Sr^{2+} and Ca^{2+} in Day 180 waters was derived through post-mixing reactions, with a smaller percentage of HCO_3^-, K^+, Na^+ and Mg^{2+} (~50%) resulting from post-mixing reactions. This shows that gypsum dissolution was the most important reaction in the evolution of Day 180 waters, although it also suggests that residence times were still long enough for some dolomite and feldspar dissolution to occur.

Phase 2b

During Phase 2 there was a short period (Days 193-196) when the chemical composition of subglacial waters was distinct from any other period of the season. This period coincided with a period of cold weather (Figure 2:4; Figure 2:12), and was characterized by particularly high concentrations of Na^+, K^+ and Cl^- that were not matched in the supraglacial record. In order to investigate the possible origins for these solutes, two inverse model simulations (B6 and B7, figure 3:1) were performed. Simulation B6 examined the change in composition between Phase 2a and Phase 2b waters (Appendix 4). Simulation B7 used the modeled composite supraglacial solution (Table 3:3) as the initial solution.

The simulation starting with the composite supraglacial solution illustrated the net changes required to account for the observed changes in chemistry. As with other simulations from an initial dilute solution, it required dissolution of most specified phases in order to produce the correct chemical composition (Table 3:7). However, comparison of the phase mole transfer ratios for this simulation with other simulations where the composite supraglacial solution was the initial solution (Table 3:8) show that cal:dol, cal:(hal+syl), cal:feld and gyp:feld are lowest for this simulation. This means that, relative to calcite and gypsum dissolution, this simulation requires more dissolution of dolomite, halite, sylvite and feldspars to match the observed solute concentrations than other simulations from snowmelt or the composite supraglacial input (e.g. snowmelt – outburst; composite supraglacial – Day 180).

Results of the simulation starting from Phase 2a waters produced similar results, although extra $CO_2(g)$ was not consumed in all models. The most important reactions were the incongruent dissolution of feldspars (k-feldspar [3-6] and albite [3-10]) that left illite and kaolinite as solid phases, and dolomite dissolution [3-2]. Precipitation of calcite also released H^+ that was subsequently used in feldspar dissolution reactions. Ion exchange reactions also took place involving both sylvite and halite [3-8] and occasionally feldspars [3-5]. As $CO_2(g)$ was not transferred in all simulations starting from Phase 2a waters, the later stages of evolution of Phase 2b waters may have taken place within a closed system without access to the atmosphere. The importance of dolomite and feldspar weathering in the later stages of evolution indicate that these waters were subject to a high duration of rock-water contact.

The models created by this simulation do not account for all aspects of the changing water composition. Transfers calculated for input solutions indicate that there should be removal of Ca^{2+} and SO_4^{2-} by precipitation. Removal of Ca^{2+} is mostly accounted for in model results, but that of SO_4^{2-} is not. By examining input concentrations and model output, it is apparent that the

observed change in SO_4^{2-} is less than specified uncertainty constraints in the model. Therefore, the program has calculated $\delta_{m,q}$ (where $|\delta_{m,q}| \leq u_{m,q}$) for SO_4^{2-} so that $m_{SO4(p2a)} = m_{SO4(p2b)}$ for all models. [$\delta_{m,q}$ is the change in molar concentration calculated by PHREEQC, $u_{m,q}$ is the uncertainty limit specified by user, and $m_{SO4(x)}$ is the molar concentration of SO_4^{2-} in solution x]

Phase 3 evolution

Phase 3 saw the greatest variability in water chemistry. This is in part due to the occurrence of high discharge events and of diurnal variability in discharge and suspended sediment concentration (SSC). The inverse models developed for Phase 3 are intended to investigate the causes of this variability in chemistry, and to establish possible sources for solutes. 6 different simulations were performed (B8 – B13, Figure 3:1).

Simulation B8 examines the transition from Phase 2 to early Phase 3 waters, and compares solutions from Phase 2c and Day 205 (Appendix 4). This simulation should establish the fundamental differences in chemistry between Phases 2 and 3. Only one model was produced, and requires calcite dissolution [3-1] in association with the consumption of $CO_2(g)$ and an increase in pH (Table 3:9a). As SSC was increasing at this time (Figure 2:15), this is attributable to in-channel dissolution of suspended sediment. All other mole transfers lie within the 10% uncertainty limit, and are therefore accounted for using $|\delta_{m,q}| \leq 10\%$.

Simulations B9 and B10 examine the evolution of the measured high discharge solution (Day 209; Appendix 4) from measured values for Day 205 (Appendix 4) and from the modeled composite supraglacial water (Table 3:3). As with all other simulations from dilute solutions, the simulation from supraglacial water produced models requiring dissolution of most phases (Table 3:9b). Comparison of phase mole transfer ratios (Table 3:8) indicates that relatively more calcite and gypsum are dissolved in this simulation than in any other simulations from snowmelt. The simulation involving measured solute concentrations from JD205 and JD209 produced only one model (Table 3:9b). The reactions in this model are calcite dissolution [3-1] and gypsum dissolution [3-3], and $CO_2(g)$ is consumed. Once again, all other transfers required may be accounted for by $|\delta_{m,q}| \leq 10\%$. The evolution of both Day 205 and Day 209 waters from intermediate precursor waters thus resulted from rapid reactions, with little or no contribution from reactions that require extended rock-water contact.

Simulations B11 and B12 examine the evolution of low discharge water sampled during phase 3. On some days during phase 3, samples were collected well in advance of diurnal peak discharge. These samples are significantly different in chemical composition from those

collected at or after peak discharge (e.g. Day 208; Figure 2:12; Appendix 4). Therefore, to investigate the causes of these differences in chemistry, the composition of the measured Day 208 solution was compared with (a) measured solute concentrations from Day 205 (B11); and (b) the modeled composite supraglacial solution (B12). The simulation from the supraglacial solution produces similar results to all other simulations using this initial solution (Table 3:9c), although comparison of phase mole transfers with other simulations from snowmelt (Table 3:8) indicates a relatively high solute input from dissolution of dolomite and feldspars relative to dissolution of calcite and gypsum, although the ratios are not as extreme as in the Phase 2b and outburst water simulations. Hence, there is an "old water" signature in the bulk runoff. Results from the Day 205 - Day 208 simulation (B12; Table 3:9c) show that the most important reactions are precipitation of gypsum [3-3] or calcite [3-1]. In models where gypsum is precipitated there is no $CO_2(g)$ transfer, whereas in models with calcite precipitation, $CO_2(g)$ is released from solution. When $CO_2(g)$ is released, phase mole transfers for dolomite are an order of magnitude greater than in solutions where this is not the case. Other important reactions are the dissolution of halite [3-9] and sylvite [3-4] and the incongruent dissolution of feldspar (k-feldspar [3-6] and albite [3-10]) that left illite and kaolinite as solid phases. Ion exchange reactions involving halite and sylvite [3-8] also occur in some models.

Simulation B13 is intended to investigate the changes in composition between low (Day 208) and high (Day 209) discharge, as discharge variability seems to be an important factor in determining the chemical composition of runoff. Initially, the program was unable to produce any models using the same constraints as other simulations, due to the requirement for the precipitation of feldspars as a result of weathering of clay minerals (illite and kaolinite). Instead, a simulation was performed that included a mixing stage prior to inverse modeling. With increasing discharge, surface meltwater input must increase. This leads to the dilution of the high concentration subglacial waters characteristic of low flow conditions, and decreases the concentration of solutes characteristic of slow reactions (Na^+, K^+, Mg^{2+} and Cl^-). However, concentrations of some species (Ca^{2+}, SO_4^{2-}, HCO_3^-) increase between low and high flow conditions, suggesting a significant input from post-mixing reactions. This simulation highlights the nature of these reactions. Only one model was produced (Table 3:9d). This required a mixing ratio of 0.5358 supraglacial: 0.4642 Day 208. Reactions required to produce Day 209 waters from the diluted Day 208 waters were calcite dissolution [3-1], dolomite dissolution [3-2] and gypsum dissolution [3-3]. All of these are relatively rapid reactions, and likely indicate post-mixing in-channel weathering of suspended sediment mobilized at high flow.

Interpretation of modeling results:

Two sets of simulations were performed – those with dilute initial waters, where the final solution was evolved from snowmelt or from composite supraglacial waters, and those where initial waters were more concentrated than snowmelt, but more dilute than the final water. In the latter case, the initial waters were sampled in a time period preceding that in which the final waters were collected. In two cases, the initial solution was more concentrated in some or all solutes than the final solution, and an initial mixing step representing dilution by supraglacial waters was required, as well as a dissolution phase.

Subglacial water evolution from supraglacial meltwater input –

At first glance, all simulations starting from a dilute initial solution appear to produce similar results, with dissolution of all specified phases. The simulation with the highest magnitude of phase mole transfers was that of the evolution of outburst waters from pre-outburst Ridge Stream waters. The simulations that produced the lowest magnitude of phase mole transfers vary depending upon the initial and final solute concentrations for each individual ion. As the initial solution is identical for all three simulations involved (evolution of Day 180 waters, evolution of Phase 2b waters, and evolution of Day 208 waters from composite supraglacial input), this is therefore indicative of differential weathering of phases in each simulation, and is highlighted by a selection of calculated phase mole transfer ratios (Table 3:8).

All models starting from dilute solutions require consumption of CO_2(g) that is subsequently used in dissolution of calcite, dolomite and feldspar. When CO_2: cal ~ 1, this indicates the importance of carbonation of calcite, (e.g. supraglacial to Day 209 simulation; Table 3:8). If CO_2: cal > 1, CO_2(g) is consumed in other dissolution reactions. In the supraglacial to Phase 2b simulation, CO_2: cal = 7.866, so a large amount of CO_2(g) is used to drive feldspar and dolomite dissolution. Ratios are also fairly high in the snowmelt to outburst simulation, and the supraglacial to Day 180 simulation.

Gypsum is always dissolved more than any other phase (cal: gyp and dol: gyp are always < 1; gyp: feld is always > 1), although relative to other phases, it appears to be dissolved more during phase 2, especially in the evolution of Day 180 waters (cal: gyp = 0.25), and during peak discharge in Phase 3 (Day 209; gyp: feld = 11.59). Calcite also appears to be dissolved proportionally more than most other phases, particularly halite and sylvite. The exception is during the evolution of Phase 2b waters, where dissolution of both dolomite and feldspars is higher than calcite dissolution. Proportionally more halite and sylvite are also dissolved in this

simulation relative to calcite (cal: hal+syl - P2b = 2.433; Outburst = 11.644; Day 180 = 48.252). Generally, more feldspar dissolution occurs than dolomite dissolution, except in the evolution of outburst waters, where slightly more dolomite dissolution is seen (dol: feld = 1.06). Dissolution of feldspars seems to be particularly important in the evolution of Phase 2b waters, even in the early stages of evolution.

Apart from the precipitation of quartz, illite and kaolinite as products of feldspar dissolution, the only phases that are lost from solution during the evolution of subglacial waters from dilute supraglacial solutions are halite and sylvite. In most instances, this can be accounted for by ion exchange between halite and sylvite [3-8], and in the instances where mole transfers are not comparable (indicating ion exchange only), there is always extra dissolution of halite or sylvite, and never extra precipitation. It should be noted however that there is no evidence of the presence of halite and sylvite in the bedrock. Instead, halite and sylvite may have been precipitated as a result of pressure-induced freezing in the subglacial environment, and re-dissolved upon subsequent contact with water.

Thus it is clear that, in most instances, evolution of subglacial waters from dilute supraglacial solutions is dominated by calcite, gypsum and sometimes dolomite dissolution. This dominance is due to the rapid dissolution kinetics of calcite and gypsum that allow them to be weathered rapidly in the presence of water until waters are saturated, or, in the case of calcite, until the proton supply is exhausted in a system that has no access to the atmosphere (also leading to the saturation of waters with respect to calcite). Two exceptions to this rule are seen - the evolution of Day 180 waters and of Phase 2b waters from the composite supraglacial solution. For Day 180 waters, the early stages of evolution, represented by this simulation, are dominated by dolomite and feldspar dissolution, whilst water is still in the distributed system. Calcite and gypsum dissolution only become more important in the later stages, once water reaches the channelised system (Table 3:6b). For Phase 2b waters, the situation is different, with calcite and gypsum dissolution never playing a dominant role in their evolution. This is indicative of two distinct weathering environments that are likely to be in distinct hydrological or geological settings, as discussed in chapter 2. An evaporite-rich area of the bed (Baumann Fjord Formation) is found in an overdeepening just downglacier of the bedrock bump and crevasse field, where Phase 2b waters are likely to have been stored at high pressure. However, as evaporites seem to be less important in outburst waters than in other waters, this may suggest that outburst waters were not stored in this area of the bed, and were instead stored even closer to the glacier terminus in an area of limestone outcrop (Copes Bay Formation).

Late stages of subglacial water evolution from previously evolved subglacial waters -

These simulations all represent the later stages of evolution of waters, but produce distinctive results that highlight the existence of two different weathering environments – those of long-term storage of water, and of in-channel post-mixing reactions. Release of water that has undergone prolonged subglacial storage is seen during periods of low subglacial discharge (Outburst water evolution from Phase 2c water; Phase 2b water evolution from Phase 2a water; Day 208 water evolution from Day 205 water). Simulations of these waters show that dolomite, halite, sylvite and feldspar dissolution are important during the later stages of evolution. In-channel, post-mixing reactions are important when suspended sediment concentrations are high and / or discharge is high relative to that when the initial solution was collected (Day 180 water evolution from diluted outburst; Day 205 water evolution from Phase 2c water; Day 209 water evolution from Day 205 water; Day 209 water evolution from diluted Day 208 water). In these cases, calcite and / or gypsum dissolution dominate either throughout or in the later stages of evolution.

CO_2(g) transfers during the later stages of water evolution are potentially very informative when considering the state of the system relative to chemical equilibrium and access to the atmosphere. In general, those simulations indicating long-term storage of water exhibit reduced uptake of CO_2(g) in the later stages of solute acquisition (e.g. Phase 2b water evolution from Phase 2a waters; Table 3:7). However, in outburst water evolution, CO_2(g) transfers are similar in the simulation from dilute snowmelt and in that from Phase 2c waters (Table 3:4), with a significantly higher transfer of CO_2(g) used in the weathering of dolomite and feldspars in the later stages of solute acquisition. In the later stages of Phase 2b and Day 208 water evolution, the precipitation of calcite or gypsum is seen, in association with either no uptake of CO_2(g), or even the release of CO_2(g) from solution (in the evolution of Day 208 water from Day 205).

Precipitation of calcite in model results-

Precipitation of calcite requires that waters must be supersaturated with respect to calcite at some point during their evolution, and that nucleation sites are available for the formation of calcite crystals. However, during Phase 2b, waters are not supersaturated with respect to calcite (mean SI_{cal} = -0.37). It is thus apparent that the precipitation of calcite must have occurred sometime in advance of sampling of these waters, most likely in the distributed system where nucleation sites are available. As feldspar dissolution is the most important reaction in the

evolution of Phase 2b waters (Table 3:8), it is likely that the HCO_3^- released from these reactions is used in the precipitation of calcite given supersaturation of waters with respect to calcite. This situation is likely in the earlier stages of evolution of the waters, based on the solubility product for calcite (K_{cal} = -8.38) and the bedrock geology. Given precipitation, the waters will become less supersaturated with respect to calcite over time. Observations at John Evans Glacier (Skidmore, 2001) based on the occurrence of artesian fountains on the glacier surface, as well as results from a study of the $\delta^{13}C$ – DIC composition of subglacial outflow suggest that for the majority of the melt season much of the subglacial drainage system is at high pressure and thus cannot take in atmospheric CO_2. PCO_2 values during Phase 2a ($10^{-3.5}$ – $10^{-4.2}$, figure 2:14a) indicate that this is indeed the case. Hence, it is not usually possible for waters to become undersaturated with respect to calcite once they are supersaturated. However, during Phase 2b, discharge was significantly reduced (Figure 2:6), and subglacial channels would no longer have been full. As suggested by Skidmore (2001), this would allow uptake of CO_2, raise pCO_2 values (figure 2:14a) and allow waters to become undersaturated with respect to calcite. SSC was very low during Phase 2b (Figure 2:15), so no post-mixing reactions were likely (Brown et al, 1996b).

Evolution of Day 208 waters required not only calcite precipitation, but also gypsum precipitation and degassing of CO_2. Saturation indices for Day 208 suggest that water is supersaturated with respect to both calcite and to dolomite, but not to gypsum. pCO_2 is also very low ($10^{-5.47}$), indicating that CO_2 was being consumed more rapidly than it is being replaced. This suggests that degassing of CO_2 within the outflow channel itself is unlikely. As with the evolution of Phase 2b waters, the precipitation of calcite in association with CO_2 degassing may have occurred in the distributed system, in advance of the emergence of Day 208 waters in the proglacial area. Thus, as pressure dropped in the channelised system at low discharge in the diurnal cycle (particularly on Day 208), water in the distributed system could flow towards the channels (Hubbard et al, 1995). Calcite precipitation and degassing of CO_2 probably took place in the channel marginal areas of the distributed system where pressure was lower than in the main part of the distributed system. Once this "old water" entered the channelised system, it mixed with surface runoff and became diluted; however, discharge on Day 208 was still high enough that suspended sediment was mobilized, although the concentration was much lower than at peak discharge (e.g. Days 205 and 209). In-channel weathering of suspended sediment, possibly through carbonate hydrolysis [3-12] led to the low pCO_2 and high values for SI_{cal} and SI_{dol} seen in the subglacial outflow (Skidmore, 2001).

[3-12] $$CaCO_3 + H_2O \Leftrightarrow Ca^{2+} + OH^- + HCO_3^-$$

Data from speciation calculations indicate that carbonate hydrolysis is likely, due to the higher concentration of OH^- in Day 208 waters (Table 3:10).

Precipitation of gypsum in model results -

The precipitation of gypsum predicted in the simulation of Day 208 water evolution from Day 205 seems unlikely, given that SI_{gyp} = -1.68 for Day 208, and waters are not saturated with respect to gypsum at any point during the melt season. There are, however, two possible explanations for its predicted occurrence.

(1) Sampling of subglacial waters could only take place at the outflow during its period of operation. It is likely that if waters become supersaturated with respect to gypsum, it will occur very early in the evolution of the waters, based upon the high solubility product of gypsum (K_{gyp} = -4.65; Ford and Williams, 1989). Gypsum precipitation will then occur to restore equilibrium. As waters become supersaturated with respect to calcite, precipitation of gypsum will be halted, and calcite will precipitate instead, as it less soluble than gypsum (K_{cal} = -8.38; Ford and Williams, 1989). Evidence for the precipitation of gypsum can be found at various points on the glacier surface, where deposits of $CaSO_4$ are seen, in association with artesian fountain locations.

(2) Day 208 waters were less concentrated in Ca^{2+} and SO_4^{2-} than Day 205 waters not because gypsum had precipitated out of them, but because Day 205 waters had been subject to rapid in-channel dissolution of suspended sediment, whereas Day 208 waters had not. This is possible, as the appearance of old waters in bulk runoff during peak discharge suggests that there had been a reduction in water pressure in the subglacial system that allowed drainage of the distributed system into the outflow channel. However, the observed pCO_2 value ($10^{-5.47}$) does require some rapid weathering of carbonates that is best explained by in-channel dissolution of suspended sediment.

Post-mixing reactions -

In contrast to these situations, $CO_2(g)$ is consumed in all simulations that indicate in-channel post-mixing reactions that weather calcite and, in one simulation, dolomite. pCO_2 values from Day 205 – 209 are low, which is either a result of limited access to the atmosphere, or of rapid consumption of CO_2 in the weathering of carbonates (Tranter et al, 1993). Closer examination of the relative amounts of $CO_2(g)$ consumption to its use in dissolution reactions indicate that in all cases, with the exception of the evolution of Day 180 waters ($pCO_2 = 10^{-4.1}$)

from diluted outburst waters, more CO_2 was used in dissolution reactions than was taken in from the atmosphere. This clearly supports depletion of CO_2 in waters where rapid post-mixing reactions are occurring. The situation is likely to be different for Day 180 because there is significantly less suspended sediment in the water (Figure 2:15), and in-channel dissolution reactions are therefore not happening as rapidly. It is also clear that the later stages of Day 180 water evolution were dominated by gypsum dissolution (Table 3:9c) that does not require CO_2.

Synthesis -

In summary, three distinct subglacial weathering environments are defined, based upon important reactions in their evolution, both in the early stages, as indicated by simulations from snowmelt, and in the later stages, as indicated by simulations from suitable intermediate waters (Table 3:11). Some waters (e.g. outburst waters) exhibit characteristics of long-term storage only, suggesting they were evolved in the distributed system, although they may have experienced some dilution by snowmelt. However, most waters experienced at least some of their evolution within the channelised system. If the channel system is at low pressure, waters from the distributed system may drain into the channel. These waters re-equilibrate with the atmosphere by taking up $CO_2(g)$, producing low SI_{cal} and high pCO_2 (e.g. Phase 2b). They are diluted and may experience some post-mixing reactions, depending upon SSC (e.g. Day 208). Conversely, when channels are highly pressurized at peak discharge, waters are characterized by high SI_{cal} (and SI_{dol}, Day 209) and low pCO_2 as a result of rapid in-channel dissolution of suspended sediment.

Implications of chemical weathering environments for subglacial hydrology:

Evolution of outburst waters suggests that water is stored in the subglacial environment for a fairly long period of time prior to the outburst. Over-winter and early season storage is likely to have been widespread within a saturated till layer, not only allowing for the extended duration of rock-water contact, but also for exposure of a large reactive surface area to subglacial waters. Chemical composition of the water suggests that the majority of this storage was over an outcrop rich in limestone close to the glacier terminus. Radar data indicate that this is indeed the case (Copland and Sharp, in press). Ice motion data from 1999 (Copland, 2001) indicated that enhanced horizontal motion was observed in association with the outburst, but that there was very little surface uplift as would be expected if water inputs resulted in storage in subglacial cavities at the ice-bed interface (Iken and Bindschadler, 1986). In 2000, surface melt commenced on 7

June (Day 159), 16 days before the subglacial outburst on Day 174. Thus, if most of the outburst water originated as Summer 2000 melt, this is likely to be sufficient time for waters to become supersaturated with respect to calcite and dolomite (Figure 2:14b), as well as for a feldspar signal to be evolved. Recent work however, suggests that there is a significant delay (c.12 days) between first surface melt and runoff to the bed due to storage and refreezing in the snowpack (D.Lewis, pers.comm.), indicating that outburst waters may be comprised predominantly of water stored over-winter. At the time of the outburst, given the composition of runoff, as well as the extended residence times of surface meltwater detected by dye-tracing results (R.Bingham, pers.comm.), the entire drainage system was likely to have been distributed in structure.

The opening of surface moulins just prior to the outburst, along with increased surface input, is likely to have destabilized the distributed system, and allowed rapid development of channels at the bed between the moulins and the outflow (Kamb, 1987; Nienow et al, 1998). These channels would have been surrounded by the pre-existing distributed system, still covering the majority of the glacier bed. As these channels developed, they may have allowed more rapid evacuation of the remaining stored water, which would also have been diluted as it mixed with the new surface input. By the end of phase 1 (Day 180), this old water made only a small contribution to the bulk meltwaters at times of high discharge, and solute chemistry was dominated instead by the products of rapid in-channel weathering of suspended sediment (predominantly gypsum dissolution). However, at times of maximum discharge, water pressure in the channels may have been high, preventing inflow of old waters from the surrounding distributed system. Thus, the low contribution from the distributed system may reflect the inability of old water to exit the distributed system as channel discharge and water pressure rose progressively over time rather than exhaustion of the supply of old water.

Shortly after this, air temperatures and surface melt decreased dramatically (Figure 2:4), leading to a situation where subglacial channels were no longer full. The direction of the pressure gradient switched, so that water could flow from the distributed system into the channelised system as recession flow (Hubbard et al, 1995). This water is likely to have been stored in the distributed system since the outburst due to the negative pressure gradient between the distributed system and the channels, although its composition in comparison to outburst waters suggests that storage was in a different location over an outcrop rich in evaporites (Baumann Fjord Formation, Figure 2:2) further up-glacier than the waters stored before the outburst. This location is an overdeepening on the glacier bed, where water would be stored at high pressure. As water flowed out of this overdeepening, water pressure would have dropped, causing freezing that could have

induced the precipitation of halite and sylvite, that would have then been available for re-dissolution. The water may have experienced some dilution by snow and ice-melt but still carried the imprint of weathering of feldspars. Calcite precipitation occurred in association with feldspar dissolution in order to push the water towards equilibrium with respect to calcite, although waters may not have achieved chemical equilibrium with respect to calcite until access to the atmosphere allowed the uptake of CO_2.

As air temperatures recovered, and surface melt increased (Day 200 onwards) a significant increase in subglacial discharge was observed in the proglacial area, and a number of major subglacial drainage events were seen. At high discharge, old recession flow waters were no longer seen, indicating that the increase in discharge had re-established the pressure gradient away from the channelised system (i.e. channels were once again at high pressure). Chemistry was highly variable, depending upon sampling time in relation to discharge peaks. The observed discharge peaks were associated with high SSC, and the evolution of meltwater chemistry at this time reflected post-mixing in-channel weathering of this suspended sediment. Further supraglacial melt and drainage events (e.g. opening of two upper glacier moulins and drainage of Crevasse Lake (Day 213); Table 2:1) suggest that the channelised system may have been expanding up-glacier throughout Phase 3. At times of low discharge in the diurnal cycle (e.g. Day 208), old recession flow waters from the distributed system were observed in runoff. At these times, therefore, a smaller proportion of total discharge was derived from surface melt, and as a consequence there was less dilution of waters from the distributed system in association with the reversal in pressure gradient that allowed outflow from the distributed system.

In summary, the subglacial drainage system of John Evans Glacier in 2000 had a distributed configuration throughout the winter, and when the outburst occurred. Observational and ice motion evidence suggests that the system consisted of an unfrozen permeable till layer, rather than of linked subglacial cavities. Channel development is triggered by high levels of supraglacial input from moulins, particularly early in the melt season, and bulk meltwaters have a chemical signature from the channelised component of the drainage system at high discharge. As the season progresses, the channelised system expands up-glacier at the expense of the distributed system, driven by supraglacial drainage events (P.Nienow, pers.comm.), although in surrounding areas, an extensive distributed system is maintained throughout the melt season. When discharge is reduced as a result of cold or cloudy weather (e.g. Phase 2b), or as part of the diurnal cycle (e.g. JD208), the main contribution to bulk meltwater is provided by the distributed system, as

recession flow. At peak discharge, sediment is entrained and weathered in-channel, and water therefore has a distinct rapid-flow chemical signature.

Table 3:1 Results from lake water evolution inverse modeling simulations, showing required mole transfers from input solutions and calculated mole transfers from simulations. Italic grey numbers represent negative mole transfers (= phase removed from solution).

Nunatak Lake		Uncertainty=0.1						
	Input	Output	Transfer:	Model:	1	2	3	4
Moles	Stream 4	Nun Lake		moles				
PH	7.2	8.3		CO2(g)	2.59E-04	2.59E-04	2.59E-04	2.59E-04
HCO3	1.13E-04	7.26E-04	6.13E-04	calcite	2.00E-04	2.00E-04	2.00E-04	2.00E-04
Cl	9.05E-06	9.34E-06	2.83E-07	dolomite	3.79E-05	3.79E-05	3.76E-05	3.75E-05
SO4	1.92E-06	6.91E-06	5.00E-06	gypsum	5.00E-06	5.00E-06	5.00E-06	5.00E-06
Na	1.25E-05	1.29E-05	4.40E-07	halite				
K	7.42E-07	1.66E-06	9.20E-07	sylvite	9.21E-07			
Mg	9.63E-06	4.49E-05	3.53E-05	albite		*9.21E-07*		
Ca	3.69E-05	2.58E-04	2.21E-04	k-feldspar		9.21E-07	1.25E-06	9.21E-07
				quartz			*1.84E-06*	*1.84E-06*
				illite			*5.42E-07*	
				kaolinite				*4.60E-07*
Ridge Lake		Uncertainty=0.1						
	Input	Output	Transfer:	Model:	1	2	3	4
Moles	Stream 4	Ridge Lake		moles				
PH	7.2	7.8		CO2(g)	3.65E-04	3.65E-04	3.66E-04	3.66E-04
HCO3	1.13E-04	8.81E-04	7.68E-04	calcite	2.79E-04	2.79E-04	2.80E-04	2.80E-04
Cl	9.05E-06	9.56E-06	5.09E-07	dolomite	3.31E-05	3.33E-05	3.30E-05	3.29E-05
SO4	1.92E-06	8.03E-06	6.11E-06	gypsum	6.11E-06	6.11E-06	6.11E-06	6.11E-06
Na	1.25E-05	1.05E-05	*2.03E-06*	halite				
K	7.42E-07	1.56E-06	8.18E-07	sylvite	8.19E-07			
Mg	9.63E-06	4.04E-05	3.08E-05	albite		*8.19E-07*		
Ca	3.69E-05	3.26E-04	2.90E-04	k-feldspar		8.19E-07	1.11E-06	8.19E-07
				quartz			*1.64E-06*	*1.64E-06*
				illite			*4.81E-07*	
				kaolinite				*4.09E-07*

Table 3:2 Results from lake water dilution experiments, including measured input and comparison concentrations (in μeq/l). Bold numbers indicate the best mixing ratios, and closely matching concentrations in target sample.

Nunatak Lake

ueq/l	Snowmelt	Nun Lake	0.4snow:0.6nun	0.5:0.5	0.6snow:0.4nun	**0.66snow:0.34nun**	0.7snow:0.3nun	Nun Stream
pH	7.2	8.3	8.0	7.3	7.8	**7.8**	7.7	7.5
HCO3	92.9	595.4	496.1	436.7	377.3	**341.7**	318	259.4
Ca	73.7	515.1	338.6	294.4	250.2	**223.8**	206.2	**221.8**
Cl	9.0	9.3	9.2	9.2	9.2	**9.2**	9.1	11.418
K	0.8	1.7	1.3	1.2	1.1	**1.1**	1.0	0.723
Mg	19.2	89.8	61.6	54.5	47.5	**43.2**	40.4	**44.244**
Na	12.5	12.9	12.8	12.7	12.7	**12.6**	12.6	12.891
SO4	3.8	13.8	9.8	8.8	7.8	**7.2**	6.8	8.496

Ridge Lake

ueq/l	Snowmelt	Ridge Lake	0.2snow:0.8ridge	0.3snow:0.7ridge	**0.32snow:0.68ridge**	0.4snow:0.6ridge	0.5:0.5	Ridge Stream
pH	7.2	7.8	7.8	7.7	**7.7**	7.7	7.7	7.7
HCO3	92.9	723.0	772	692.9	**677.1**	613.9	534.9	519.9
Ca	73.7	652.9	537	479.2	**467.6**	421.2	363.2	**458.8**
Cl	9.0	9.5	9.5	9.4	**9.4**	9.4	9.3	9.7
K	0.8	1.6	1.4	1.3	**1.3**	1.2	1.2	0.9
Mg	19.2	80.8	68.5	62.3	**61.1**	56.2	50.0	**63.9**
Na	12.5	14.1	13.7	13.6	**13.6**	13.4	13.3	**13.6**
SO4	3.8	16.1	13.6	12.4	**12.1**	11.2	9.9	7.0

Table 3:3 Results from supraglacial mixing simulation, used as input for subglacial simulations.

COMPOSITE SUPRAGLACIAL WATER (MOL/L)	
pH	7.5
HCO3	2.27E-04
Ca	8.60E-05
Cl	1.02E-05
K	1.37E-06
Mg	1.53E-05
Na	1.41E-05
SO4	2.41E-06

Table 3:4 (a – pg.75) Results from inverse modeling of outburst water evolution, showing input and output solutions, required and modeled phase mole transfers; (b – pg.76) Phase mole transfer ratios of snowmelt and Phase 2a simulations. Italic grey numbers are negative mole transfers.

Table 3:4a

From early season snowmelt

moles	Input pre-outburst ridge	Output Day 174	Transfer:
pH	6.4	8.2	
HCO3	9.82E-05	2.98E-03	2.88E-03
Cl	1.11E-05	5.75E-05	4.64E-05
SO4	1.94E-06	1.40E-03	1.40E-03
Na	1.54E-05	3.32E-04	3.17E-04
K	2.28E-06	4.46E-05	4.23E-05
Mg	1.08E-05	3.74E-04	3.63E-04
Ca	2.84E-05	2.06E-03	2.03E-03
Sr	0.00E+00	2.54E-05	2.54E-05

Uncertainty=0.1

Model: moles	1	2	3	4	5	6	7
CO2(g)	1.15E-03	1.46E-03	1.42E-03	**1.42E-03**	1.42E-03	1.46E-03	**1.46E-03**
calcite	5.18E-04	5.64E-04	5.18E-04	**5.18E-04**	5.18E-04	5.61E-04	**5.64E-04**
dolomite	4.08E-04	3.62E-04	4.08E-04	**4.08E-04**	4.08E-04	3.62E-04	**3.62E-04**
gypsum	1.31E-03	1.31E-03	1.31E-03	**1.31E-03**	1.31E-03	1.31E-03	**1.31E-03**
halite	3.17E-04	3.17E-04	*-1.06E-04*	**4.64E-05**			**4.64E-05**
sylvite	*-2.71E-04*	*-2.71E-04*	1.53E-04		4.64E-05	4.23E-05	
albite			4.23E-04	**2.71E-04**	3.17E-04	3.17E-04	**2.71E-04**
k-feldspar	4.23E-04	3.13E-04		**1.53E-04**	1.06E-04		**4.23E-05**
quartz	*-6.26E-04*	*-6.26E-04*	*-6.26E-04*	***-6.26E-04***	*-6.26E-04*	*-6.34E-04*	***-6.26E-04***
illite	*-1.84E-04*		*-1.84E-04*	***-1.84E-04***	*-1.84E-04*		
kaolinite		*-1.56E-04*				*-1.59E-04*	***-1.56E-04***

From subglacial low-flow waters

moles	Input mean P2c	Output Day 174	Transfer:
pH	8.7	8.2	
HCO3	7.09E-04	2.98E-03	2.27E-03
Cl	1.42E-05	5.75E-05	4.33E-05
SO4	5.71E-04	1.40E-03	8.27E-04
Na	6.06E-05	3.32E-04	2.72E-04
K	9.13E-06	4.46E-05	3.54E-05
Mg	8.76E-05	3.74E-04	2.86E-04
Ca	7.37E-04	2.06E-03	1.33E-03
Sr	1.05E-05	2.54E-05	1.49E-05

Uncertainty=0.1

Model: moles	1	2	3	4	5	6	7
CO2(g)	1.26E-03	1.31E-03	1.26E-03	**1.26E-03**	1.30E-03	1.26E-03	**1.30E-03**
calcite	3.91E-04	4.26E-04	3.91E-04	**3.91E-04**	4.30E-04	3.91E-04	**4.30E-04**
dolomite	3.25E-04	2.86E-04	3.25E-04	**3.25E-04**	2.86E-04	3.25E-04	**2.86E-04**
gypsum	7.42E-04	7.46E-04	7.42E-04	**7.42E-04**	7.42E-04	7.42E-04	**7.42E-04**
halite			2.72E-04	**4.33E-05**	2.72E-04	*-8.53E-05*	**4.33E-05**
sylvite	4.33E-05	3.75E-05	*-2.28E-04*		*-2.28E-04*	1.29E-04	
albite	2.72E-04	2.72E-04		**2.28E-04**		3.57E-04	**2.28E-04**
k-feldspar	8.53E-05		3.57E-04	**1.29E-04**	2.64E-04		**3.54E-05**
quartz	*-5.28E-04*	*-5.43E-04*	*-5.28E-04*	***-5.28E-04***	*-5.28E-04*	*-5.28E-04*	***-5.28E-04***
illite	*-1.55E-04*		*-1.55E-04*	***-1.55E-04***		*-1.55E-04*	
kaolinite		*-1.36E-04*			*-1.32E-04*		*-1.32E-04*

Table 3:4b

Mole transfer ratios:

	cal:dol	cal:gyp	cal:(hal+syl)	cal:feld	dol:gyp	dol:feld	gyp:feld
Snowmelt	1.41	0.41	11.64	1.51	0.29	1.06	3.64
Phase 2c	1.35	0.55	9.48	1.36	0.41	1.00	2.45

Table 3:5 Results from outburst water dilution experiments, including measured input and comparison concentrations (μeq/l). Bold numbers indicate the best mixing ratio, and closely matching concentrations in target sample.

Solute Ueq/l	Composite supraglacial	outburst Day 174	0.5:0.5	0.7snow:0.3out	0.8snow:0.2out	0.9snow:0.1out	0.92snow:0.08out	**0.935snow:0.065out**	Day 180
pH	7.5	8.2	8.2	8.1	8.0	7.8	7.8	**7.7**	8.7
HCO3	227.4	2440.8	1627	1078	803.5	529.1	474.2	**433.1**	711.2
Ca	172.1	4122.4	2148	1357.6	962.4	567.2	488.2	**429**	1658.9
Cl	10.2	57.4	33.9	24.4	19.7	14.9	14.0	**13.3**	**13.1**
K	1.4	44.5	23.0	14.3	10.0	5.7	4.8	**4.2**	8.9
Mg	30.6	747.3	389	245.8	174.0	102.3	88.0	**77.2**	167.7
Na	14.1	332.3	173.2	109.6	77.8	45.9	39.6	**34.8**	76.9
SO4	4.8	2796.1	1400.2	842.2	563	284	228.2	**186.2**	1205.6
Sr	0	50.8	25.4	15.2	10.2	5.1	4.1	**3.3**	19.1

Table 3:6 (a) Results from post-mixing inverse modeling simulations, showing input and output solutions, required and modeled phase mole transfers; (b) Phase mole transfer ratios for diluted outburst and composite supraglacial simulations. Italic grey numbers indicate negative mole transfers; (c) Proportions of solutes derived from post-mixing reactions in Day 180 waters.

From diluted outburst — **Uncertainty=0.1**

moles	Input diluted outburst	Output Day 180	Transfer:
pH	7.7	8.7	
HCO3	4.33E-04	8.67E-04	4.34E-04
Cl	1.33E-05	1.32E-05	*-1.30E-07*
SO4	9.31E-05	6.03E-04	5.09E-04
Na	3.48E-05	7.70E-05	4.22E-05
K	4.18E-06	8.88E-06	4.70E-06
Mg	3.86E-05	8.39E-05	4.53E-05
Ca	2.15E-04	8.30E-04	6.15E-04
Sr	1.65E-06	9.54E-06	7.89E-06

Model: moles	1	2	3	4	5	6
CO2(g)	2.19E-04	**2.25E-04**	2.19E-04	2.25E-04	2.25E-04	**2.18E-04**
calcite	1.18E-04	**1.25E-04**	1.18E-04	1.25E-04	1.25E-04	**1.18E-04**
dolomite	5.22E-05	**4.53E-05**	5.22E-05	4.53E-05	4.53E-05	**5.22E-05**
gypsum	5.06E-04	**5.06E-04**	5.06E-04	5.06E-04	5.06E-04	**5.06E-04**
halite	4.22E-05		*-2.14E-05*	4.22E-05	*-4.84E-06*	
sylvite	*-4.23E-05*		2.13E-05	*-4.23E-05*	4.70E-06	
albite		**4.22E-05**	6.36E-05		4.70E-05	**4.22E-05**
k-feldspar	6.36E-05	**4.70E-06**		4.70E-05		**2.12E-05**
quartz	*-9.40E-05*	***-9.37E-05***	*-9.40E-05*	*-9.40E-05*	*-9.40E-05*	***-9.37E-05***
illite	*-2.76E-05*		*-2.76E-05*			***-2.76E-05***
kaolinite		*-2.34E-05*		*-2.35E-05*	*-2.35E-05*	

From composite supraglacial — **Uncertainty=0.05**

moles	Input Supragl.	Output Day 180	Transfer:
pH	7.5	8.7	
HCO3	2.27E-04	8.67E-04	6.40E-04
Cl	1.02E-05	1.32E-05	2.95E-06
SO4	2.41E-06	6.03E-04	6.00E-04
Na	1.41E-05	7.70E-05	6.29E-05
K	1.37E-06	8.88E-06	7.51E-06
Mg	1.56E-05	8.39E-05	6.83E-05
Ca	8.60E-05	8.30E-04	7.44E-04
Sr	0.00E+00	9.54E-06	9.54E-06

Model: moles	1	2	3	4	5	6	7	8
CO2(g)	3.06E-04	3.15E-04	3.06E-04	3.06E-04	**3.06E-04**	3.15E-04	3.15E-04	**3.15E-04**
calcite	1.37E-04	1.47E-04	1.37E-04	1.37E-04	**1.37E-04**	1.47E-04	1.47E-04	**1.47E-04**
dolomite	7.82E-05	6.83E-05	7.82E-05	7.82E-05	**7.82E-05**	6.83E-05	6.83E-05	**6.83E-05**
gypsum	5.70E-04	5.70E-04	5.70E-04	5.70E-04	**5.70E-04**	5.70E-04	5.70E-04	**5.70E-04**
halite	6.29E-05	6.29E-05	*-2.84E-05*	2.95E-06		*-4.56E-06*	2.95E-06	
sylvite	*-5.99E-05*	*-5.99E-05*	3.13E-05		**2.95E-06**	7.51E-06		**2.95E-06**
albite			9.12E-05	5.99E-05	**6.29E-05**	6.74E-05	5.99E-05	**6.29E-05**
k-feldspar	9.12E-05	6.74E-05		3.13E-05	**2.84E-05**		7.51E-06	**4.56E-06**
quartz	*-1.35E-04*	*-1.35E-04*	*-1.35E-04*	*-1.35E-04*	***-1.35E-04***	*-1.35E-04*	*-1.35E-04*	***-1.35E-04***
illite	*-3.97E-05*		*-3.97E-05*	*-3.97E-05*	***-3.97E-05***			
kaolinite		*-3.37E-05*				*-3.37E-05*	*-3.37E-05*	***-3.37E-05***

Table 3:6b

Mole transfer ratios:							
	cal:dol	cal:gyp	cal:(hal+syl)	cal:feld	dol:gyp	dol:feld	gyp:feld
Snowmelt to Day 180	1.95	0.25	48.25	1.84	0.13	0.93	7.35
dilute outburst to Day 180	2.52	0.24		2.27	0.10	0.89	9.39

Table 3:6c

	TOTAL DAY 180	DILUTED OUTBURST		POST-MIXING REACTIONS	
	concentration	concentration	% of Total	concentration	% of Total
HCO3	867	433.1	50	434	50
Ca	1659	429	26	1230	74
Cl	13	13	100	0	0
K	8.9	4.2	47	4.7	53
Mg	167.7	77.2	46	90.6	54
Na	769	34.8	45	42.2	55
SO4	1206	186	15	1018	85
Sr	19.1	3.3	17	15.8	83

Table 3:7 Results from inverse modeling simulation of Phase 2b water evolution, showing input and output solutions, and observed and modeled phase mole transfers. Italic grey numbers are negative mole transfers.

From composite supraglacial				Uncertainty=0.05									
	Input	Output	Transfer	Model:	1	2	3	4	5	6	7	8	9
moles	Supragl.	Phase 2b		moles									
pH	7.5	7.8		CO2(g)	3.71E-04	3.94E-04	3.71E-04	**3.71E-04**	3.71E-04	**3.94E-04**	3.94E-04	3.94E-04	3.91E-04
HCO3	2.27E-04	8.27E-04	5.99E-04	calcite	3.96E-05	6.21E-05	3.96E-05	**3.96E-05**	3.96E-05	**6.21E-05**	6.21E-05	6.21E-05	5.88E-05
Cl	1.02E-05	3.11E-05	2.09E-05	dolomite	1.01E-04	7.83E-05	1.01E-04	**1.01E-04**	1.01E-04	**7.83E-05**	7.83E-05	7.83E-05	8.16E-05
SO4	2.41E-06	5.88E-04	5.86E-04	gypsum	5.57E-04	5.57E-04	5.57E-04	**5.57E-04**	5.57E-04	**5.57E-04**	5.57E-04	5.57E-04	5.57E-04
Na	1.41E-05	1.75E-04	1.61E-04	halite	2.09E-05	1.61E-04	*-4.62E-05*		1.61E-04	**7.83E-06**	2.09E-05		
K	1.37E-06	1.44E-05	1.31E-05	sylvite		*-1.40E-04*	6.71E-05	**2.09E-05**	*-1.40E-04*	**1.31E-05**		2.09E-05	2.09E-05
Mg	1.56E-05	9.39E-05	7.83E-05	albite	1.40E-04		2.07E-04	**1.61E-04**		**1.53E-04**	1.40E-04	1.61E-04	1.61E-04
Ca	8.60E-05	7.45E-04	6.59E-04	k-feldspar	6.71E-05	1.53E-04		**4.62E-05**	2.07E-04		1.31E-05	-7.83E-06	
Sr	0.00E+00	9.71E-06	9.71E-06	quartz	*-3.06E-04*	*-3.06E-04*	*-3.06E-04*	***-3.06E-04***	*-3.06E-04*	***-3.06E-04***	*-3.06E-04*	*-3.06E-04*	*-3.06E-04*
				illite	*-9.01E-05*		*-9.01E-05*	***-9.01E-05***	*-9.01E-05*				*-1.31E-05*
				kaolinite		*-7.66E-05*				***-7.66E-05***	*-7.66E-05*	*-7.66E-05*	

Table 3:7 (cont.)

From P2a **Uncertainty=0.1**

	Input Phase 2a	Output Phase 2b	Transfer:
moles			
pH	8.1	7.8	
HCO3	8.08E-04	8.27E-04	1.86E-05
Cl	1.46E-05	3.11E-05	1.65E-05
SO4	6.00E-04	5.88E-04	*-1.13E-05*
Na	7.10E-05	1.75E-04	1.04E-04
K	9.36E-06	1.44E-05	5.07E-06
Mg	8.49E-05	9.39E-05	9.05E-06
Ca	7.87E-04	7.45E-04	*-4.21E-05*
Sr	9.36E-06	9.71E-06	3.54E-07

Model:	1	2	3	4	5	6	7
moles							
CO2(g)						1.26E-04	
calcite	*-1.37E-04*	*-1.18E-04*	*-1.37E-04*	*-1.37E-04*	*-1.37E-04*		*-1.18E-04*
dolomite	2.27E-05		2.27E-05	2.27E-05	2.27E-05		
gypsum							
halite	1.65E-05	1.65E-05	1.04E-04	*-2.13E-05*		1.65E-05	1.04E-04
sylvite			*-8.77E-05*	3.78E-05	1.65E-05		*-8.77E-05*
albite	8.77E-05	8.77E-05		1.26E-04	1.04E-04	8.77E-05	
k-feldspar	3.78E-05	5.06E-06	1.26E-04		2.13E-05	5.06E-06	9.28E-05
quartz	*-1.86E-04*	*-1.86E-04*	*-1.86E-04*	*-1.86E-04*	*-1.86E-04*	*-1.86E-04*	*-1.86E-04*
illite	*-5.46E-05*		*-5.46E-05*	*-5.46E-05*	*-5.46E-05*		
kaolinite		*-4.64E-05*				*-4.64E-05*	*-4.64E-05*

	8	9	10	11	12	13	14	15	16	17	18
CO2(g)				1.16E-04	1.26E-04	1.26E-04	1.26E-04	1.16E-04	1.16E-04	1.16E-04	1.16E-04
calcite	*-1.18E-04*	*-1.18E-04*	*-1.09E-04*								
dolomite				8.48E-06				8.48E-06	8.48E-06	8.48E-06	
gypsum											
halite	1.14E-05			1.65E-05	1.04E-04	1.14E-05		1.04E-04	*-2.13E-05*		
sylvite	5.06E-06	1.65E-05	1.65E-05		*-8.77E-05*	5.06E-06	1.65E-05	*-8.77E-05*	3.78E-05	1.65E-05	1.65E-05
albite	9.28E-05	1.04E-04	1.04E-04	8.77E-05		9.28E-05	1.04E-04		1.26E-04	1.04E-04	1.04E-04
k-feldspar		*-1.14E-05*		3.78E-05	9.28E-05		*-1.14E-05*	1.26E-04		2.13E-05	
quartz	*-1.86E-04*	*-1.86E-04*	*-1.86E-04*	*-1.86E-04*	*-1.86E-05*	*-1.86E-04*	*-1.86E-04*	*-1.86E-04*	*-1.86E-04*	*-1.86E-04*	*-1.86E-04*
illite			*-1.90E-05*	*-5.46E-05*				*-5.46E-05*	*-5.46E-05*	*-5.46E-05*	*-1.90E-05*
kaolinite	*-4.64E-05*	*-4.64E-05*			*-4.64E-05*	*-4.37E-05*	*-4.64E-05*				

Table 3:8 Phase mole transfer ratios for all simulations from snowmelt or composite supraglacial solution

	CO2:cal	cal:dol	cal:gyp	cal:(hal+syl)	cal:feld	dol:gyp	dol:feld	gyp:feld
Snowmelt - outburst	2.40	1.41	0.41	11.64	1.51	0.29	1.06	3.64
Snowmelt – Day 180	2.19	1.95	0.25	48.25	1.84	0.13	0.93	7.35
Snowmelt – P2b	7.87	0.59	0.09	2.43	0.30	0.16	0.50	3.16
Snowmelt – Day 208	1.43	2.19	0.41	12.28	1.75	0.19	0.89	4.38
Snowmelt – Day 209	1.08	6.44	0.56	123.66	6.47	0.09	1.00	11.59

Table 3:9 (next 4 pages) (a) Results from inverse modeling simulation of Phase 2c waters to Day 205. (b) Results from inverse modeling simulations of evolution of Day 209 waters from composite supraglacial and Day 205 waters. (c) Results from inverse modeling simulations of evolution of Day 208 waters from composite supraglacial and Day 205 waters. (d) Results from inverse modeling simulation of Day 208 waters evolving into Day 209 waters, including dilution by supraglacial solution. All tables include input and output solutions, and observed and modeled phase mole transfers. Italic grey numbers indicate negative mole transfer.

Table 3:9(a)

Mean P2c to Day 205				Uncertainty=0.1	
	Input	Output	Transfer:	Model:	1
moles	mean P2c	Day 205		moles	
pH	8.7	9.3		CO2(g)	1.04E-04
HCO3	7.09E-04	1.06E-03	3.47E-04	calcite	1.73E-04
Cl	1.42E-05	1.52E-05	9.60E-07	dolomite	
SO4	5.71E-04	5.28E-04	*-4.26E-05*	gypsum	
Na	6.06E-05	6.30E-05	2.35E-06	halite	
K	9.13E-06	1.02E-05	1.02E-06	sylvite	
Mg	8.76E-05	7.85E-05	*-9.13E-06*	albite	
Ca	7.37E-04	8.42E-04	1.06E-04	k-feldspar	
Sr	1.05E-05	1.29E-05	2.44E-06	quartz	
				illite	
				kaolinite	

Table 3:9(b)

Day 205 to Day 209				Uncertainty=0.1	
	Input	Output	Transfer:	Model:	1
moles	Day 205	Day 209		moles	
pH	9.3	9.3		CO2(g)	1.80E-04
HCO3	1.06E-03	1.53E-03	4.69E-04	calcite	2.34E-04
Cl	1.52E-05	1.41E-05	*-1.13E-06*	dolomite	
SO4	5.28E-04	8.77E-04	3.48E-04	gypsum	3.38E-04
Na	6.30E-05	7.38E-05	1.08E-05	halite	
K	1.02E-05	9.59E-06	*-5.58E-07*	sylvite	
Mg	7.85E-05	8.51E-05	6.63E-06	albite	
Ca	8.42E-04	1.36E-03	5.21E-04	k-feldspar	
Sr	1.29E-05	2.06E-05	7.71E-06	quartz	
				illite	
				kaolinite	

Table 3:9(b)

Snowmelt to Day 209 — **Uncertainty=0.1**

moles	Input snowmelt	Output JD209	Transfer:
pH	7.5	9.3	
HCO3	2.27E-04	1.53E-03	1.30E-03
Cl	1.02E-05	1.41E-05	3.85E-06
SO4	2.41E-06	8.77E-04	8.74E-04
Na	1.41E-05	7.38E-05	5.97E-05
K	1.37E-06	9.59E-06	8.23E-06
Mg	1.56E-05	8.51E-05	6.95E-05
Ca	8.60E-05	1.36E-03	1.28E-03
Sr	0.00E+00	2.06E-05	2.06E-05

Model: moles	1	2	3	4	5	6	7	8
CO2(g)	5.11E-04	5.20E-04	5.11E-04	5.11E-04	5.11E-04	5.20E-04	5.20E-04	5.20E-04
calcite	4.71E-04	4.81E-04	4.71E-04	4.71E-04	4.71E-04	4.81E-04	4.81E-04	4.81E-04
dolomite	7.89E-05	6.95E-05	7.89E-05	7.89E-05	7.89E-05	6.95E-05	6.95E-05	6.95E-05
gypsum	8.54E-04	8.54E-04	8.54E-04	8.54E-04	8.54E-04	8.54E-04	8.54E-04	8.54E-04
halite			5.97E-05	-2.70E-05	3.85E-06	5.97E-05	-4.38E-06	3.85E-06
sylvite	3.85E-06	3.85E-06	-5.58E-05	3.08E-05		-5.58E-05	8.23E-06	
albite	5.97E-05	5.97E-05		8.67E-05	5.58E-05		6.41E-05	5.58E-05
k-feldspar	2.70E-05	4.38E-06	8.67E-05		3.08E-05	6.41E-05		8.23E-06
quartz	-1.28E-04	-1.28E-04	-1.28E-04	-1.28E-04	-1.28E-04	-1.28E-04	-1.28E-04	-1.28E-04
illite	-3.77E-05		-3.77E-05	-3.77E-05	-3.77E-05			
kaolinite		-3.20E-05				-3.20E-05	-3.20E-05	-3.20E-05

Table 3:9(c)

Snowmelt to Day 208 — **Uncertainty=0.1**

moles	Input snowmelt	Output Day 208	Transfer:
pH	7.5	9.8	
HCO3	2.27E-04	1.03E-03	8.02E-04
Cl	1.02E-05	2.44E-05	1.42E-05
SO4	2.41E-06	4.57E-04	4.54E-04
Na	1.41E-05	1.70E-04	1.56E-04
K	1.37E-06	1.55E-05	1.41E-05
Mg	1.56E-05	8.60E-05	7.04E-05
Ca	8.60E-05	7.06E-04	6.20E-04
Sr	0.00E+00	7.88E-06	7.88E-06

Model: moles	1	2	3	4	5	6	7
CO2(g)	2.37E-04	2.60E-04	2.37E-04	2.37E-04	2.37E-04	2.60E-04	2.60E-04
calcite	1.63E-04	1.85E-04	1.63E-04	1.63E-04	1.63E-04	1.85E-04	1.85E-04
dolomite	9.33E-05	7.04E-05	9.33E-05	9.33E-05	9.33E-05	7.04E-05	7.04E-05
gypsum	4.26E-04	4.26E-04	4.26E-04	4.26E-04	4.26E-04	4.26E-04	4.26E-04
halite		1.56E-04	-5.50E-05	1.42E-05	1.56E-04		1.42E-05
sylvite	1.42E-05	-1.42E-04	6.91E-05		-1.42E-04	1.41E-05	
albite	1.56E-05		2.11E-04	1.42E-04		1.56E-04	1.42E-04
k-feldspar	5.50E-05	1.56E-04		6.91E-05	2.11E-04		1.41E-05
quartz	-3.12E-04	-3.12E-04	-3.12E-04	-3.12E-04	-3.12E-04	-3.12E-04	-3.12E-04
illite	-9.17E-05		-9.17E-05	-9.17E-05	-9.17E-05		
kaolinite		-7.80E-05				-7.80E-05	-7.80E-05

Table 3:9c (cont.)

Day 205 to Day 208 **Uncertainty=0.1**

moles	Input Day 205	Output Day 208	Transfer:
pH	9.3	9.8	
HCO3	1.06E-03	1.03E-03	-2.70E-05
Cl	1.52E-05	2.44E-05	9.19E-06
SO4	5.28E-04	4.57E-04	-7.16E-05
Na	6.30E-05	1.70E-04	1.07E-04
K	1.02E-05	1.55E-05	5.32E-06
Mg	7.85E-05	8.60E-05	7.53E-06
Ca	8.42E-04	7.06E-04	-1.36E-04
Sr	1.29E-05	7.88E-06	-5.05E-06

Model: moles	1	2	3	4	5	6	7
CO2(g)						-1.21E-04	
calcite						-1.43E-04	
dolomite	8.37E-06		8.37E-06	8.37E-06	8.37E-06	2.27E-05	
gypsum	-1.17E-04	-1.13E-04	-1.17E-04	-1.17E-04	-1.17E-04		-1.13E-04
halite	1.18E-04	1.07E-04	-4.13E-05	6.87E-06		1.07E-04	
sylvite	-1.11E-04	-9.79E-05	4.81E-05		6.87E-06	-9.79E-05	6.76E-06
albite			1.59E-04	1.11E-04	1.18E-04		1.07E-04
k-feldspar	1.59E-04	1.03E-04		4.81E-05	4.13E-05	1.40E-04	
quartz	-2.35E-04	-2.07E-04	-2.35E-04	-2.35E-04	-2.35E-04	-2.07E-04	-2.14E-04
illite	-6.92E-05		-6.92E-05	-6.92E-05	-6.92E-05	-6.07E-05	
kaolinite		-5.16E-05					-5.36E-05

	8	9	10	11	12	13	14	15	16	17
CO2(g)			-1.21E-04	-1.21E-04	-1.21E-04	-1.02E-04		-1.05E-04	-1.05E-04	
calcite		-9.56E-05	-1.43E-04	-1.43E-04	-1.43E-04	-1.12E-04	-9.56E-05	-1.12E-04	-1.12E-04	-9.28E-05
dolomite		1.61E-05	2.27E-05	2.27E-05	2.27E-05		1.61E-05			1.61E-05
gypsum	-1.13E-04									
halite	9.20E-06	1.30E-04	-3.26E-05	9.20E-06			8.73E-06	1.07E-04	9.20E-06	
sylvite		-1.22E-04	4.18E-05		9.20E-06	6.76E-06		-9.79E-05		6.76E-06
albite	9.79E-05		1.40E-04	9.79E-05	1.07E-04	1.07E-04	1.22E-04		9.79E-05	1.25E-04
k-feldspar	5.32E-06	1.27E-04		4.18E-05	3.26E-05		5.32E-06	1.03E-04	5.32E-06	
quartz	-2.07E-04	-2.54E-04	-2.07E-04	-2.07E-04	-2.07E-04	-2.14E-04	-2.54E-04	-2.07E-04	-2.07E-04	-2.50E-04
illite			-6.07E-05	-6.07E-05	-6.07E-05					
kaolinite	-5.16E-05	-6.35E-05				-5.36E-05	-6.35E-05	-5.16E-05	-5.16E-05	-6.24E-05

Table 3:9d

Day 208 to Day 209				Uncertainty=0.1
	Input	Output	Transfer:	
moles	Day 208	Day 209		
pH	9.8	9.3		
HCO3	1.03E-03	1.53E-03	4.96E-04	
Cl	2.44E-05	1.41E-05	*-1.03E-05*	
SO4	4.57E-04	8.77E-04	4.20E-04	
Na	1.70E-04	7.38E-05	*-9.63E-05*	
K	1.55E-05	9.59E-06	*-5.88E-06*	
Mg	8.60E-05	8.51E-05	*-9.00E-07*	
Ca	7.06E-04	1.36E-03	6.57E-04	
Sr	7.88E-06	2.06E-05	1.28E-05	
Dilution of Day 208 by snowmelt to Day 209				
			Model:	1
Mixed at fraction:			moles	
snowmelt:	0.5358		CO2(g)	4.10E-04
JD208:	0.4642		calcite	3.95E-04
			dolomite	3.68E-05
			gypsum	6.61E-04
			halite	
			sylvite	
			albite	
			k-feldspar	
			quartz	
			illite	
			kaolinite	

Table 3:10 Selected ion concentrations from speciation calculations for Days 205 and 208

ION	DAY 205	DAY 208
OH^-	2.327e-06	8.089e-06
HCO_3^-	8.856e-04	6.427e-04
CO_3^{2-}	4.845e-05	1.195e-04
CO_2	1.622e-06	3.444e-07

Table 3:11 Classification of water types, based upon initial water and important reactions leading to evolution of water type.

	IMPORTANT REACTIONS		
TIMES SEEN	SUPRAGLACIAL INPUT WATERS	PREVIOUS SUBGLACIAL WATERS	WEATHERING ENVIRONMENT
Outburst	Gypsum dissolution Calcite dissolution Dolomite dissolution	Dolomite dissolution Halite / sylvite dissolution Feldspar dissolution	Long-term water storage
Day 180	Gypsum dissolution Dolomite dissolution Feldspar dissolution	Gypsum dissolution Calcite dissolution	Post-mixing reactions (partially full channel)
Phase 2b	Dolomite dissolution Feldspar dissolution Halite / sylvite dissolution	Dolomite dissolution Feldspar dissolution Calcite precipitation	Long-term water storage
Day 205		Calcite dissolution	Post-mixing reactions (full channel)
Day 208	Calcite dissolution Gypsum dissolution Dolomite dissolution	Dolomite dissolution Feldspar dissolution Calcite precipitation Gypsum precipitation	Long-term water storage Post-mixing reactions (partially full channel)
Day 209	Calcite dissolution Gypsum dissolution	Calcite dissolution Gypsum dissolution Dolomite dissolution (from Day 208 only)	Post-mixing reactions (full channel)

Figure 3:1 Flow-chart of water types on John Evans Glacier, Summer 2000. Characteristics of output waters are determined by mixing of input waters, and by post-mixing reactions.

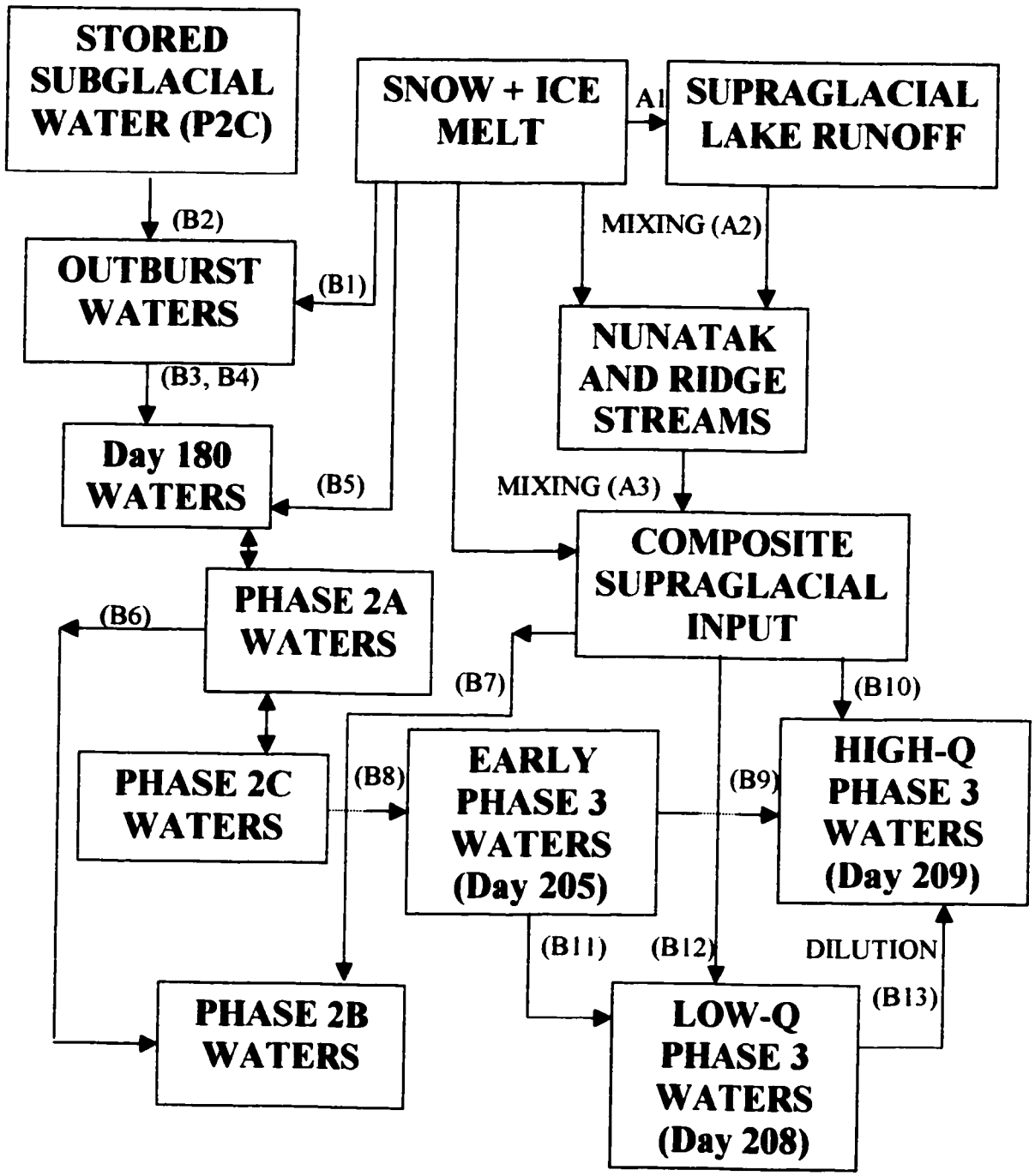

Figure 3:2 Subglacial Electrical Conductivity time series with subglacial drainage phases and selected days superimposed to illustrate modeling procedure

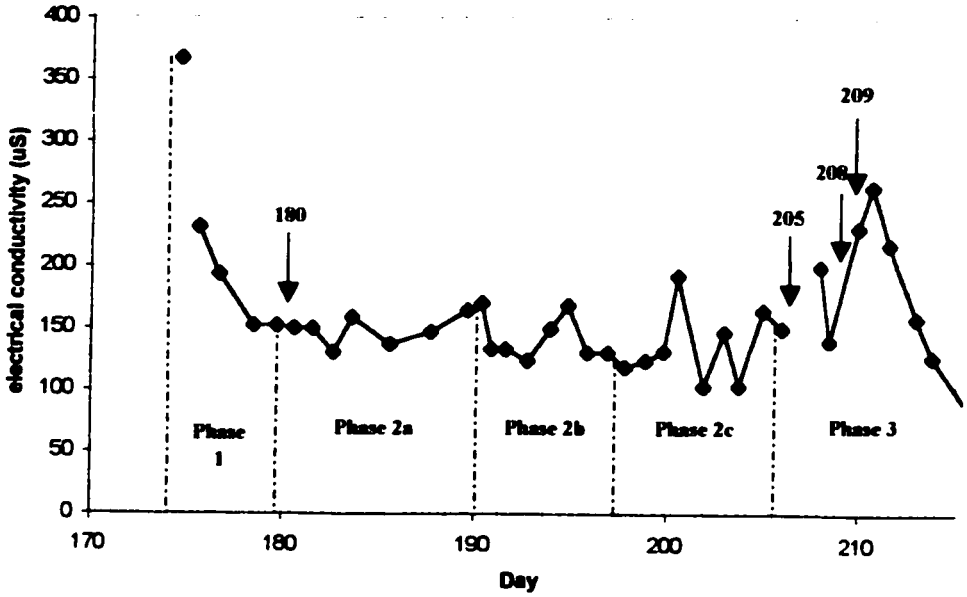

Chapter 4 – Summary and conclusions

Summary:

The material presented in this thesis represents the first documented evidence of the seasonal evolution of channelised subglacial drainage under a polythermal glacier based upon hydrochemical data. More importantly, the amount of solute in selected water samples derived from specified reactions in the subglacial environment has been quantified using geochemical modeling. As the relative importance of different reactions changes during the course of the season and with discharge, this has allowed inferences to be made about likely changes in the character of the weathering environments in which solute is acquired.

Chemical data were collected from supraglacial lakes and channels, from the snowpack and from the subglacial outflow at John Evans Glacier, Ellesmere Island, during the summer of 2000. Supraglacial channel and snowpack solute concentrations were similar, except in those channels draining two ice-marginal lakes, where subaerial weathering of carbonates elevated concentrations of Ca^{2+}, Mg^{2+} and HCO_3^-. However, supraglacial solute concentrations were seen to differ significantly from subglacial solute concentrations, indicating that a substantial amount of subglacial chemical weathering was taking place. Based on ratios of ion concentrations in subglacial and supraglacial waters and their variation over the course of the melt season, it was apparent that a greater proportion of some solutes was derived from weathering in the subglacial environment than that of others, and that the fractional contribution from subglacial weathering varied over the season.

Comparison of subglacial and supraglacial water chemistry allowed for the identification of 3 distinct chemical phases during the course of the melt season. Phase 1 was characterized by highly concentrated outburst waters, which were progressively diluted by low concentration snowmelt. These highly concentrated waters were the result of weathering of minerals, especially dolomite and feldspars, over an extended period of time. Phase 2 started on Day 180, after the phase of dilution of outburst waters by snowmelt. Modeling the dilution of outburst waters by snowmelt showed that dilution was not conservative, and that post-mixing reactions took place. The major weathering reaction in this post-mixing phase, and throughout Phase 2, was the dissolution of gypsum, as indicated by a Ca^{2+}: SO_4^{2-} ratio close to 1 throughout the period. However, the period divides into three sub-periods. Phases 2a (JD180-189) and 2c (JD197-204) were characterized by gypsum dissolution. Phase 2b (JD190-196) however coincided with a period of cold weather and snow, and waters exhibited peaks of Na^+, K^+ and Cl^-. The subglacial: supraglacial ratio indicates that these solute peaks were not derived from the supraglacial

environment, and thus must have been produced in the subglacial environment. Feldspar dissolution may explain the increase in concentration of Na^+ and K^+. However, the increased concentration of crustally derived Cl^- in association with increases in Na^+ and K^+ suggests that at least some runoff at this time was derived from a different part of the glacier bed where freezing induced precipitation of halite and sylvite could occur.

Phase 3 was characterized by a high degree of variability in the chemical composition of runoff. It was dominated by high concentrations of HCO_3^-, SO_4^{2-}, Ca^{2+} and Sr^{2+}, although peaks of Na^+, K^+ and Cl^- were observed in low discharge waters (Days 207-208). Examination of the EC and SSC records showed that peaks in EC and SSC were closely correlated with peaks in HCO_3^-, SO_4^{2-}, Ca^{2+} and Sr^{2+}, suggesting that the high rates of gypsum and calcite dissolution were caused by high concentrations of suspended sediment in the water column. Very low pCO_2 values suggest that the supply of CO_2 was not replenished as rapidly as it was consumed (Tranter et al., 1993), and supports the rapid weathering hypothesis. The Na^+, K^+ and Cl^- rich waters sampled at lower discharge appeared to have a composition similar to Phase 2b waters, and were therefore derived from the distributed system. As surface water input was reduced, these waters became less diluted, and comprised a larger proportion of bulk discharge during recession flow.

Modeling results allowed for the identification of three distinct weathering environments. Waters were evolved as a result of (1) long-term storage (LTS), (2) post-mixing reactions (PMR) in full channels where no uptake of CO_2 was possible, and (3) PMR in partially full channels where CO_2 uptake was possible. In most cases, outflowing waters were evolved in at least two of these weathering environments, and diluted to some extent by surface input. In the earlier stages of evolution of waters subject to long-term storage, calcite and gypsum dissolution reactions were found to be important, whereas in the later stages, dolomite, feldspar, halite and sylvite dissolution were more important, whilst precipitation of calcite and possibly gypsum occurred as a result of the water being supersaturated with respect to these minerals. For waters evolved through post-mixing reactions, calcite and gypsum dissolution were important in the later stages of evolution, although where there was significant mixing with long-term storage waters (Day 180), feldspar and dolomite dissolution were found to be important in the early stages of evolution while the water was still in the distributed system. The post-mixing reactions occurred in the channelised part of the system, in the last hours of evolution, just prior to the water emerging at the terminus.

The influence of these different weathering environments on bulk meltwater chemistry varied over time, and appeared to be closely related to rates of surface melt and subglacial

discharge. At peak discharge, PMR are dominant, and waters have high SI_{cal} and low pCO_2. As discharge decreases, the signal from LTS increases in magnitude as it experiences less dilution by surface inputs, and PMR become less important as SSC decreases in the subglacial outflow. These waters have low SI_{cal} and high pCO_2, due to the uptake of CO_2 by waters from the distributed system that have been isolated from the atmosphere for long periods of time.

Thus, during the summer of 2000, the subglacial drainage system of John Evans Glacier apparently consisted of two distinct components that contributed different amounts to bulk runoff depending upon surface meltwater input and pressure gradients within the drainage network. At the beginning of the melt season, prior to and during the outburst (Day 174), the drainage system consisted entirely of a distributed system, but once moulins opened up (Day 173 onwards), localized subglacial channel development was triggered by high levels of supraglacial input from them. At high discharge, solute composition in bulk meltwaters was evolved as a result of rapid in-channel dissolution of calcite and gypsum in a closed environment, but when discharge was reduced as a result of cold or cloudy weather (e.g. Phase 2b), or as part of the diurnal cycle (e.g. JD208), and pressure within the channelised component of the system returned to atmospheric, the main contribution to bulk meltwater was provided by the distributed system, as delayed or recession flow.

Comparison of results with previous work:

John Evans Glacier –

Hydrochemical chemical data have been collected at John Evans Glacier since 1994 (Skidmore, 2001). As well as the subglacial outflow, which has been the focus of most studies (Skidmore, 1995, 2001; Skidmore and Sharp, 1999), marginal and supraglacial streams have been monitored in various melt seasons. Distinct differences in hydrochemistry have been found between these different weathering environments (Skidmore, 1995).

Comparison of 2000 data from the subglacial outflow with data from previous years (Table 4:1) illustrates a high level of inter-annual variability in chemical composition of the subglacial outflow. Mean concentrations of all solutes apart from SO_4^{2-} are higher in 2000 than in any other year. The highest mean SO_4^{2-} was seen in 1994, and the 1996 value was also greater than the 2000 value. In 1994, concentrations of Ca^{2+} and SO_4^{2-} are approximately equal, indicating that most Ca^{2+} is a product of gypsum weathering. However, in 2000, there is significantly more (~500 μeq/l) Ca^{2+} than SO_4^{2-}, indicating that this Ca^{2+} is derived from dissolution of other minerals, for example calcite or dolomite. The increased HCO_3^-

concentration in 2000, as well as the greater proportion of total solutes made up of Ca^{2+} (47%) and HCO_3^- (11%) indicates that this is the case. To a lesser extent, this situation is seen in 1996, 1998 and 1999, although the number of samples collected in 1998 and 1999 is not enough to draw any significant conclusions. This is likely to reflect inter-annual variations in extent of PMR, and is thus linked to the degree of channel development and magnitude of water fluxes passing through channels, which affect the mobilization of suspended sediment. In 1994, although total solute concentration was highest, the contribution from SO_4^{2-} was much greater. This could be attributed to the high rates of gypsum weathering relative to the slower weathering of calcite, dolomite and feldspars, although as waters were supersaturated with respect to carbonates (Skidmore, 1995), it may be more indicative of a predominantly distributed drainage system where long residence times allowed high enough rates of dissolution of all minerals for supersaturation with respect to calcite to occur that may have led to precipitation of calcite, whilst gypsum could still continue to dissolve.

In 1994, subglacial weathering was dominated by gypsum dissolution throughout the season, although there was evidence of dissolution of feldspars (Skidmore and Sharp, 1999). Subglacial drainage was episodic, with three separate flood events, and it was suggested that later in the season the volume of the subglacial reservoir was large enough to filter out diurnal variations in the water input (Skidmore, 1995; pg.100). In 2000, although subglacial discharge was highly variable, it was maintained throughout the season following the outburst (as also in 1998 and 1999). However, chemical data in Phase 3 show high variability that seems to be linked to discharge. This is indicative of two sources for subglacial runoff that contribute different amounts to bulk meltwater chemistry depending upon surface meltwater input. At high discharge, surface meltwater input fills subglacial channels and mobilizes sediment. Water is evacuated rapidly, but high SSC means that rapid in-channel dissolution of calcite and gypsum imparts a distinct PMR signature on bulk meltwaters. Conversely, at low discharge, subglacial channels are not full, and water stored in the distributed system may enter the channel and is not diluted significantly. Storage of this water during periods of high discharge has allowed it to develop a chemistry rich in Na^+, K^+, Cl^- and Mg^{2+}.

In 1994 therefore, it is likely that the drainage system did not evolve to a point where two components of the drainage system co-existed, and subglacial flow never attained the critical flow rate at which there was sufficient suspended sediment within the water to allow rapid in-channel weathering of calcite, as was clearly seen in Phase 3 of the 2000 melt season. Comparison of

SSC data from 1994 and 2000 support this conclusion, as the highest SSC in 1994 was an order of magnitude less than the highest SSC in 2000 (0.2g/l in 1994; Skidmore, 1995; 2.8g/l in 2000).

Based on meteorological data (Table 4:2), seasonal averages cannot be used to explain the differences in the development of the drainage system seen in 1994 and 2000. The total number of positive degree-days (ΣPDD) was in fact greater in 1994 than in 2000. However, mean daily PDD prior to the outburst was high in 2000 compared to other years, which likely led to high early season melt rates, and contributed to the early occurrence of the subglacial outburst. Although the glacier surface near the supraglacial channels was still snow-covered at the time of the outburst in 2000, this was mostly clear by Day 190. By the end of the melt season, the snowline had retreated beyond the Nunatak to the Middle Meteorological Station and the Crevasse Lake (Figure 2:3), and discharge in supraglacial channels was high. If the glacier surface had become snow-free sooner in 2000 than in 1994, meltwater delivery to supraglacial channels would have been more rapid, and diurnal variations in melt rates would have been more distinct. It is also possible that as the years preceding 2000 were very warm, large englacial and subglacial channels may not have closed completely during the winter months, hence allowing more rapid development of the drainage system the next summer (M.Sharp, pers.comm.)

The most significant meteorological event in 2000, however, was a period of warm, dry winds (Days 210-211; Boon and Sharp, submitted) when mean daily temperatures substantially exceeded the monthly mean, and the warm winds enhanced surface melt rates and delivery of runoff to the subglacial system. High subglacial flow allowed for the mobilization of very large amounts of sediment (Figure 2:15), leading to extensive PMR and peak solute concentrations (Ca^{2+}, HCO_3^-, SO_4^{2-} and Sr^{2+}) in association with this event (Figure 2:11). This indicates that the inferred extensive channel development in Phase 3 could be attributed, at least partially, to this event. The opening of the upper moulins during this period allowed large amounts of runoff from the upper glacier to access the bed, and this is likely to have been the main cause for upglacier expansion of the channelised system. These events are uncommon in the Canadian Arctic (Boon and Sharp, submitted), and have not previously been recorded on John Evans Glacier.

Other Arctic glaciers –

Previous studies, mostly on Svalbard glaciers, have attempted to evaluate glacier hydrological systems of Arctic glaciers (Table 4:3). Based on results of this and other studies of John Evans Glacier, many similarities exist between it and other Arctic glaciers. Meltwater is ponded on the surface of the glacier to such an extent that deep supraglacial channels have

developed (e.g. Scott Turnerbreen; Hodgkins et al, 1997; Austre Brøggerbreen, Hagen et al, 1991). In areas of cold ice, water runs off in ice-marginal channels (west marginal and east marginal; Skidmore, 1995; Nunatak and Ridge Lake catchments; this thesis), and chemistry of these streams is dominated by subaerial carbonate dissolution (e.g. Scott Turnerbreen, Hodgkins et al, 1998). Ice-flow over bedrock bumps leads to the formation of crevasses and moulins, through which surface runoff is able to penetrate to the base of the glacier (e.g. Storglaciären, Hock and Hooke, 1993; Erikbreen, Vatne et al, 1995), and outflow from the subglacial system is often seen as a turbid upwelling at or close to the glacier snout (e.g. Finsterwalderbreen, Wadham et al, 1998; Midre Lovenbreen, Hodson et al, 2000).

Although the extent of subglacial channel development described in this thesis has not previously been documented on any polythermal glacier, it cannot be attributed to any specific characteristic of John Evans Glacier in comparison to other Arctic glaciers. As this level of development is not an annual occurrence on John Evans Glacier (Skidmore and Sharp, 1999), it must be attributed to carry-over effects from the previous summers and to the overall summer meltwater flux, as well as the extraordinary synoptic weather conditions, as discussed above (Boon and Sharp, submitted) that led to high levels of meltwater flux within the drainage system.

An Alpine Glacier (Haut Glacier d'Arolla)

The seasonal development of the subglacial drainage system at John Evans Glacier during the melt season of 2000 has many similarities to that of Haut Glacier d'Arolla, Switzerland (Nienow et al, 1998). At the beginning of the melt season, the drainage system has a predominantly distributed structure. Channels are established where meltwater input is so great that the distributed system is destabilized, and on Haut Glacier d'Arolla this is associated with the retreat of the snowline and exposure of the bare ice surface that has no storage capacity. Channels grow down-glacier from individual moulins. However, the net effect is an up-glacier expansion of the channelised drainage system as the snowline retreats. The distributed system remains in the area surrounding the channelised system, and although it covers an extensive area of the bed throughout the season, its contribution to subglacial discharge is negligible by the end of the melt season.

Nienow et al (1998) describe three factors that may control the seasonal evolution of subglacial drainage systems: (1) Weather conditions during a particular melt season; (2) the pattern of snowline retreat, and (3) the distribution of moulins and crevasses that allow supraglacial runoff to reach the bed. As already discussed, weather conditions during the 2000

melt season at John Evans Glacier are at least partly responsible for the substantial development of subglacial channels. A thin over-winter snowpack meant that the ice surface was exposed early across much of the glacier, enhancing waters fluxes as a result of the lower albedo of ice in comparison to snow. The pattern of snowline retreat has also been discussed briefly, although no quantitative data are available to substantiate any conclusions regarding this.

The distribution of moulins and crevasses on John Evans Glacier is potentially a very important control on subglacial channel development, as they are not as widespread as they are on some temperate glaciers, due to the low mass balance gradient seen on this and other Arctic glaciers. With fewer moulins, and major supraglacial channel development and ponding in the early melt season, meltwater flux draining into each moulin is likely to be greater than that seen on Haut Glacier d'Arolla. Hence, subglacial channels will develop given a large enough supraglacial drainage event. However, upglacier extension of the channel system may be prevented if no further moulins or crevasses are present to allow drainage to the bed. In 2000, the initial channelised system was established from the lower moulins at the outburst. Upglacier extension of the channelised system was then likely halted until the upper moulins opened and the Crevasse Lake drained late in the melt season.

Implications for Arctic glacier hydrology:

Observations on John Evans Glacier since 1994, and in particular during the summer of 2000 have increased knowledge and understanding of the hydrological processes driving the development of a subglacial drainage system on polythermal glaciers. This study has shown that significant development of a channelised drainage network may take place, even on an Arctic glacier, given a number of points of access from the supraglacial to the subglacial system, as well as a large enough meltwater flux to destabilize the existing distributed drainage system. This flux may be attributable to the early season storage of meltwater on the glacier surface , and its subsequent drainage into the subglacial drainage system (Nienow et al., submitted). Extra-ordinary weather conditions that produce extreme surface meltwater fluxes, such as the period of warm, dry winds seen late in the 2000 melt season, may be required for the development of a spatially extensive subglacial channel system on Arctic glaciers.

If global warming causes mean annual temperatures in Arctic regions to increase, it is likely that this level of development of subglacial drainage systems will be seen more regularly, both at John Evans Glacier, and at other polythermal glaciers in Arctic Canada, Svalbard and elsewhere. It has been shown on temperate glaciers that a widespread channelised drainage

system has the effect of slowing glacier velocity (Kamb, 1987). This will allow a greater proportion of the ice mass to remain at higher altitude, and may thus reduce the amount of melt occurring. This may mean that the rise in sea level is less than predicted, assuming no further feedbacks take place.

Conclusions:

1. Substantial chemical weathering is apparent in the subglacial drainage system of John Evans Glacier. This is due to extended residence times in the subglacial environment, and to the large quantities of eroded glacial sediment providing a large surface area of reactive material that is thought to make up the glacier bed. This chemical weathering is not constant throughout the melt season, requiring the melt season to be divided into 3 phases, each with distinct chemical composition.
2. A two-component subglacial drainage system is inferred. At the time of the subglacial outburst, the drainage system is distributed in nature, but channels develop downglacier of any point where surface meltwater may access the bed through moulins or crevasses.
3. At high discharge, the drainage system is full and highly pressurized. Little water from the distributed system is able to enter the channels, and the chemical signature is dominated by post-mixing in-channel dissolution of calcite and gypsum.
4. At low discharge, channels are only partially full, allowing ingress of atmospheric gases. A reversal of the pressure gradient allows water stored in the distributed system to enter the channels as recession flow, and dilution by surface waters is minimal. The chemical signature of this water is dominated by solutes that are derived from reactions that require long-term storage of waters. These waters may experience some post-mixing reactions, if suspended sediment concentration is high enough.
5. Substantial precipitation of calcite and gypsum is predicted in the distributed system, due to supersaturation of waters with respect to these minerals. Precipitation is unlikely to occur in channels where rapid in-channel weathering of suspended sediment seems to be more normal.
6. The high level of channel development observed in 2000 is attributed to (a) carry-over effects from the previous two warm summers; (b) a thin winter snowpack that melted very quickly, exposing the ice surface to melt earlier than usual and increasing meltwater flux; (c) Warm, dry winds at the end of the melt season that further enhanced surface

meltwater flux, and allowed the opening of two upper glacier moulins that diverted runoff to the bed.

7. If global warming occurs, this level of channel development will become more common on polythermal glaciers. Feedbacks from this may affect glacier motion, glacier geometry and melt rates.

Table 4:1 Seasonal mean solute concentrations from John Evans Glacier subglacial outflow, 1994 – 2000 (adapted from Skidmore, 2001). Solute concentrations ($\mu eq\ l^{-1}$) have been adjusted for atmospheric inputs, and represent solute derived from crustal sources only.

	Ca					Mg				
Year	94	96	98	99	2000	94	96	98	99	2000
Subglacial	1701	1610	852	1111	1859	175	176	74	120	208
% of Σsolute	42	43	46	43.5	47	4.3	4.7	4.0	4.7	5.3
	Na					K				
Year	94	96	98	99	2000	94	96	98	99	2000
Subglacial	54	45	26	38	85	10.7	9.5	2.2	6.4	12.3
% of Σsolute	1.3	1.2	1.4	1.5	2.2	0.3	0.3	0.1	0.25	0.3
	HCO3					SO4				
Year	94	96	98	99	2000	94	96	98	99	2000
Subglacial	269	342	246	272	426	1810	1521	662	1005	1328
% of Σsolute	7	9	13	11	11	45	41	36	39	34
	Sum solute					Log pCO2				
Year	94	96	98	99	2000	94	96	98	99	2000
Subglacial	4031	3736	1861	2552	3918	-4.6	-4.4	-4.4	-4.1	-3.9
										(n=31)
	n									
Year	94	96	98	99	2000					
Subglacial	38	8	11	7	39					

Table 4:2 Comparison of meteorological conditions between melt seasons on John Evans Glacier, from Boon and Sharp (submitted) and http://arctic.eas.ualberta.ca (LWS – Lower weather station; MWS – Middle weather station; figure 2:3)

YEAR	FIRST MELT (LWS)	DAY OF OUTBURST	ΣPDD BEFORE OUTBURST	MEAN PDD PRE-OUTBURST	SEASONAL ΣPDD
1994	164	190	92	3.53	207 (LWS)
1996	168	192	67	2.8	91 (LWS)
1998	150	180	96	3.2	216 (MWS)
1999	150	185	122	3.5	224 (MWS)
2000	159	174	101	7.2	174 (MWS)

Table 4:3 Comparison of hydrological studies on cold, polythermal and temperate glaciers.

Glacier:	Hydrology description:	Discharge range m^3/s
Scott Turnerbreen, Spitsbergen *Hodgkins et al., 1997* *Hodgkins et al., 1998*	two ice-marginal (subaerial) channels; ponding of runoff on surface of ice	0.8 - 1 (est.)
Austre Broggerbreen, Spitsbergen *Hagen et al., 1991*	some surface / ice-marginal drainage; some drainage into moulins, although these drain englacially; some surface storage of meltwater	mean: 2.1
Erikbreen, Spitsbergen (79N, 12E) *Vatne et al., 1995* *Hodson et al., 2000*	supraglacial water drains into crevasses; drains englacially and subglacially, directly into proglacial lake; in ablation area, low pressure channelised system exists; pressure increases upglacier; evolution of drainage system is apparent	1 - 2 (est.)
Finsterwalderbreen, Spitsbergen (77N, 15E) *Wadham et al., 1998* *Hodson and Ferguson, 1999*	runoff drains through subglacial(?) conduit, and through upwelling in proglacial area; small amount as ice-marginal runoff; upwelling and conduit have separate sources that are kept separate due to thermal regime in ablation area	4 - 25 (est.)
Storglaciaren, northern Sweden *Hock and Hooke, 1993*	two subglacial - englacial channels draining glacier; Nordjakk is clear and drains accumulation area; Sydjakk is turbid and drains moulins over bedrock bump; drainage network is believed to be braided	mean Nordjakk 1.1 Sydjakk 0.6
Haut Glacier d'Arolla, Switzerland *Nienow et al., 1998* *Brown et al., 1994*	major subglacial channel; channelised system expands up-glacier with retreat of snowline, at expense of distributed system	3.5 (est.)
John Evans Glacier, Ellesmere Island (80N, 78W) *This thesis* *Skidmore, 1995* *Skidmore, 2001* *Skidmore and Sharp, 1999*	major supraglacial channels draining into moulins above bedrock bump; two major ice marginal channels plus subglacial outflow in proglacial area; subglacial channel is initially turbid upwelling that subsequently develops into channel carved into ice; drainage system has 2 components, and channelised component grows at expense of distributed component	0.2 - >10

Hydrochemistry description:	Mean TDS:	Dye tracing results:
solute acquisition from icing; major snowmelt peak; subaerial chemical weathering; decrease in TDS as season progresses	1100	None
		where detected, throughflow velocities 0.4 - 0.8 m/s
SSC 0.05 - 0.7g/l		throughflow velocity 0.07 - 0.3 m/s; dispersivity 9 - 24m; increase in velocity and decrease in dispersivity at end of melt season
major early season snowmelt peak; upwelling had high solute concentrations throughout season; conduit had low solute concentrations	1500	None
		throughflow velocity 0.07 - 0.3 m/s; dispersivity 2.3 - 55m; velocity and dispersivity are dependent upon meltwater input
In June, dominant reaction is sulphide oxidation; In July, more carbonation reactions are evident; by August, waters were dominated by calcite dissolution (but SIcal < 1)		throughflow velocity stable at 0.37 - 0.72m/s; dispersivity rapidly decreasing to 2.8 - 7.5m, except for injections in upper glacier moulins
Outburst waters are highly concentrated; diluted by snowmelt then dominated by gypsum weathering for most of melt season; at peak discharge in-channel dissolution of calcite is apparent (low pCO2 and Sical >1)	3918	

Geometry:

catchment size (km^2)	% ice cover	length (km)	max depth (m)	altitude range (m)
12.8	26		76	230 - 680
9.8	71	6	153	40 - 600
12.4	73		270	0 - 650
44	76	11	220	100 - 900
12	54	4.2		2560 - 3500
220	75	21	<150	100 - 1350

References:

Andrews, J.E., Brimblecombe, P., Jickells, T.D. and Liss, P.S. (1996) *Introduction to Environmental Chemistry*. Blackwell Science.

Arendt, A. (1995) Mass balance simulations using a positive degree-day model for John Evans Glacier, N.W.T., Canada. *Unpublished term paper*, University of Alberta.

Baranowski, S. (1973) Geyser-like water spouts at Werenskioldbreen, Spitsbergen. *IAHS Publication* **95**, pgs.131-133

Barrie, L.A. (1985) Atmospheric particles: their physical and chemical characteristics, and deposition processes relevant to the chemical composition of glaciers. *Annals of Glaciology* **7**, pgs.100-108

Blatter, H. (1987) On the thermal regime of an Arctic valley glacier: a study of White Glacier, Axel Heiberg Island, N.W.T., Canada. *Journal of Glaciology* **33**, pgs.200-211

Blatter, H. and Hutter, K. (1991) Polythermal conditions in Arctic glaciers. *Journal of Glaciology* **37**, pgs.261-269

Boon, S. and Sharp, M.J. (submitted) Impact of a Chinook-type event on the runoff and hydrology of a high Arctic glacier. *Hydrological Processes*

Brown, G.H., Sharp, M., Tranter, M., Gurnell, A.M. and Nienow, P. (1994) Impact of post-mixing chemical reactions on the major ion chemistry of bulk meltwaters draining the Haut Glacier d'Arolla, Valais, Switzerland. *Hydrological Processes* **8**, pgs.465-480

Brown, G.H., Sharp, M.J. and Tranter, M. (1996a) Subglacial chemical erosion: seasonal variations in solute provenance, Haut Glacier d'Arolla, Valais, Switzerland. *Annals of Glaciology* **22**, pgs.25-31

Brown, G.H. Tranter, M. and Sharp, M.J. (1996b) Experimental investigations of the weathering of suspended sediment by Alpine glacial meltwater. *Hydrological Processes* **10**, pgs.579-597

Collins, D.N. (1979) Hydrochemistry of meltwaters draining from an Alpine glacier. *Arctic and Alpine Research* **11**, pgs.307-324

Collins, D.N. (1982) Water storage in an Alpine glacier. *IAHS Publication* **138**, pgs.113-122

Copland, L. (2001) Polythermal glacier hydrology and ice flow dynamics. *Unpublished PhD thesis,* Department of Earth and Atmospheric Sciences, University of Alberta. 138pp.

Copland, L. and Sharp, M.J. (2000) Radio-echo sounding determination of polythermal glacier hydrology. *Proceedings, GPR 2000: Eighth International Conference on Ground Penetrating Radar, Gold Coast, Australia.*

Copland, L. and Sharp, M.J. (in press) Mapping hydrological conditions beneath a polythermal glacier using radio-echo sounding. *Journal of Glaciology*

Dowdeswell, J.A. (1995) Glaciers in the High Arctic and recent environmental change. *Philosophical Transactions of the Royal Society, Series A* **352**, pgs.321-334

Etzelmüller, B. et al (1993) Dynamics of two subpolar valley glaciers – Erikbreen and Hannabreen, Liedefjorden, northern Spitsbergen. *Geografiska Annaler* **75A**, pgs.41-54

Fairchild, I.C., Bradby, L., Sharp, M.J. and Tison, J-L. (1994) Hydrochemistry of carbonate terrains in alpine glacial settings. *Earth Surface Processes and Landforms* **19**, pgs.33-54

Ford, D.C. and Williams, P. (1989) *Karst Geomorphology and Hydrology.* Unwin Hyman, London. 601pp

Fountain, A.G. (1989) The storage of water in, and hydraulic characteristics of, the firn of South Cascade Glacier, Washington State, U.S.A. *Annals of Glaciology* **13**, pgs.69-75

Fountain, A.G. (1996) Effect of snow and firn hydrology on the physical and chemical characteristics of glacial runoff. *Hydrological Processes* **10**, pgs.509-521

Fountain, A.G. and Walder, J.S. (1998) Water flow through temperate glaciers. *Reviews of Geophysics* **36**, pgs.299-328

Gardiner, V. and Dackcombe, R. (1983) *Geomorphological Field Manual.* Allen & Unwin, London. 254pp

Hagen, J.O., Korsen, O.M. and Vatne, G. (1991) Drainage pattern in a subpolar glacier, Brøggerbreen, Svalbard. In Gjessing, Y., Hagen, J.O., Hassel, K.A., Sand, K. and Wold, B. eds. *Arctic Hydrology. Present and Future Tasks*, pgs.121-131

Hock, R. and Hooke, R. LeB. (1993) Evolution of the internal drainage system in the lower part of the ablation area of Storglaciären, Sweden. *Geological Society of America Bulletin* **105**, pgs.537-546

Hodgkins, R. (1997) Glacier hydrology in Svalbard, Norwegian High Arctic. *Quaternary Science Reviews* **16**, pgs.957-973

Hodgkins, R., Tranter, M. and Dowdeswell, J.A. (1997) Solute provenance, transport and denudation in a High Arctic glacierized catchment. *Hydrological Processes* **11**, pgs.1813-1832

Hodgkins, R., Tranter, M. and Dowdeswell, J.A. (1998) The hydrochemistry of runoff from a 'cold-based' glacier in the High Arctic (Scott Turnerbreen, Svalbard). *Hydrological Processes* **12**, pgs.87-103

Hodson, A.J. and Ferguson, R.I. (1999) Fluvial suspended sediment transport from cold and warm-based glaciers in Svalbard. *Earth Surface Processes and Landforms* **24**, pgs.957-974

Hodson, A.J. Tranter, M. and Vatne, G. (2000) Contemporary rates of chemical denudation and atmospheric CO_2 sequestration in glacier basins: an Arctic perspective. *Earth Surface Processes and Landforms* **25**, pgs. 1447-1471

Holland, H.D. (1978) *The Chemistry of Atmosphere and Oceans.* Wiley-Interscience, New York.

Holmlund, P. and Eriksson, M. (1989) The cold surface layer on Storglaciären. *Geografiska Annaler* **71A**, pgs.241-244

Hooke, R.LeB., Gould, J.E. and Brozozowski, J. (1983) Near-surface temperatures near and below the equilibrium line on polar and subpolar glaciers. *Zeitschrift für Gletscherkunde und Glazialgeologie* **19**, pgs.1-25

Hubbard, B.P. et al (1995) Borehole water-pressure variations and the structure of the subglacial hydrological system of the Haut Glacier d'Arolla, Valais, Switzerland. *Journal of Glaciology* **41**, pgs.572-583

Iken, A. and Bindschadler, R.A. (1986) Combined measurements of subglacial water pressure and surface velocity of the Findelengletscher, Switzerland: conclusions about the drainage system and sliding mechanism. *Journal of Glaciology* **32**, pgs.101-109

Johannessen, M. and Henriksen, A. (1978) Chemistry of snow meltwater: changes in concentration during melting. *Water Resources Research* **14**, pgs.615-619

Johnston, R.J. (1978) *Multivariate Statistical Analysis in Geography.* Longman Group, London. 280pp.

Kamb, W.B. (1987) Glacier surge mechanism based on linked cavity configuration of the basal conduit system. *Journal of Geophysical Research* **92 (B9)**, pgs.9083-9100

Kerr, J.W. (1972) Map 1358A Geology: Dobbin Bay, District of Franklin 1:250000, *Geological Survey of Canada.*

Killawee, J.A., Fairchild, I.J., Tison, J-L., Janssens, L. and Lorrain, R. (1998) Segregation of solutes and gases in experimental freezing of dilute solutions: Implications for natural glacial systems. *Geochimica et Cosmochimica Acta* **62**, pgs.3637-3655

Koerner, R.M. (1979) Accumulation, ablation and oxygen isotope variations on the Queen Elizabeth Islands Ice Caps, Canada. *Journal of Glaciology* **22**, pgs.25-41

Kretz, R. (1985) Calculation and illustration of uncertainty in geochemical analyses. *Journal of Geological Education* **33**, pgs.40-44

Morse, J.W. and Mackenzie, F.T. (1990) *Geochemistry of sedimentary carbonates*. Elsevier Science. Amsterdam. 707pp.

Nienow, P. Sharp, M.J. and Willis, I. (1998) Seasonal changes in the morphology of the subglacial drainage system, Haut Glacier d'Arolla, Switzerland. *Earth Surface Processes and Landforms* **23**, pgs. 825-843

Nienow, P., Sharp, M.J., Boon, S., Bingham, R. and Heppenstall, K. (submitted) The hydrochemistry of runoff from a High Arctic polythermal glacier. *Journal of Geophysical Research*

Parkhurst, D.L. and Appelo, C.A.J. (1999) User's Guide to PHREEQC (Version 2) – a computer program for speciation, batch-reaction, one-dimensional transport, and inverse geochemical calculations. *U.S.Geological Survey*. 326pp.

Paterson, W.S.B. (1994) *The Physics of Glaciers (3ed.)* Pergamon, Oxford. 480pp.

Pelto, M.S., Higgins, S.M., Hughes, T.J. and Fastook, J.L. (1990) Modeling mass-balance changes during a glaciation cycle. *Annals of Glaciology* **14**, pgs.238-241

Rabus and Echelmeyer (1997) The flow of a polythermal glacier: McCall Glacier, Alaska, U.S.A. *Journal of Glaciology* **43**, pgs.522-536

Raymo, M.E. and Ruddiman, W.F. (1992) Tectonic forcing of late Cenozoic climate. *Nature* **359**, pgs.117-122

Röthlisberger, H. (1972) Water pressure in intra- and subglacial channels. *Journal of Glaciology* **11**, pgs.177-203

Rouse, W.R. (1993) Northern Climates. In French, H.M. and Slaymaker, O. (eds) *Canada's Cold Environments.* McGill-Queens University Press, pgs.65-92

Sharp, M.J., Gemmell, J.C. and Tison, J-L. (1989) Structure and stability of the former subglacial drainage system of the Glacier de Tsanfleuron, Switzerland. *Earth Surface Processes and Landforms* **14**, pgs.119-134

Sharp, M.J., Tranter, M., Brown, G.H. and Skidmore, M.L. (1995) Rates of chemical denudation and CO_2 drawdown in a glacier-covered alpine catchment. *Geology* **23**, pgs.61-64

Sharp, M.J., Skidmore, M.L. and Nienow, P.W. (in review) The chemistry of a high Arctic supraglacial snowcover. *Journal of Glaciology.*

Shoemaker, E.M. (1994) Sub-permafrost water storage beneath subpolar ice sheets. *Cold Regions Science and Technology* **23**, pgs. 83-91

Skidmore, M.L. (1995) The hydrology and hydrochemistry of a High Arctic glacier. *Unpublished MSc thesis,* Department of Geography, University of Alberta. 114pp.

Skidmore, M.L. (2001) Hydrology, microbiology and carbon cycling at a high Arctic polythermal glacier (John Evans Glacier, Ellesmere Island, Canada). *Unpublished PhD thesis,* Department of Earth and Atmospheric Sciences, University of Alberta. 139pp.

Skidmore, M.L. and Sharp, M.J. (1999) Drainage system behaviour of a High Arctic polythermal glacier. *Annals of Glaciology* **28**, pgs. 209-215

Souchez, R.A. and Lemmens, M.M. (1987) Solutes. In Gurnell, A.M. and Clark, M.J. (eds) *Glacio-fluvial sediment transfer: An Alpine perspective.* Wiley, Chichester, pgs.285-303

Stumm, W. and Morgan, J.J. (1981) *Aquatic Chemistry (2ed.)*. Wiley Interscience, New York. 780pp.

Sugden, D.E. and John, B.S. (1976) *Glaciers and Landscape. A geomorphological approach.* Edward Arnold, London. 376pp.

Tranter, M. Brown, G. Raiswell, R. Sharp, M.J. and Gurnell, A. (1993) A conceptual model of solute acquisition by Alpine glacial meltwaters. *Journal of Glaciology* **39**, pgs. 573-581

Tranter, M. Brown, G.H. Hodson, A. Gurnell, A.M. and Sharp, M.J. (1994) Variations in the nitrate concentration of glacial runoff in Alpine and sub-Polar environments. In Jones, H.G. Davies, T.D. Ohmura, A. and Morris, E.M. (eds) *Snow and Ice Covers: Interactions with the atmosphere and ecosystems* IAHS Publication **223**, pgs. 299-311

Tranter, M. Brown, G.H. Hodson, A.J. and Gurnell, A.M. (1998) Hydrochemistry as an indicator of subglacial drainage system structure: A comparison of Alpine and Sub-Polar environments. In Sharp, M. Richards, K. and Tranter, M (eds), *Glacier hydrology and hydrochemistry.* Wiley-Chichester.

Vatne, G., Etzelmüller, B., Sollid, J.L. and Ødegard, R-S. (1995) Hydrology of a polythermal glacier, Erikbreen, Northern Spitsbergen. *Nordic Hydrology* **26**, pgs.169-190

Wadham, J.L. Hodson, A.J. Tranter, M. and Dowdeswell, J.A. (1998) The hydrochemistry of meltwaters draining a polythermal-based, high Arctic glacier, south Svalbard: I. The ablation season. *Hydrological Processes* **12,** pgs. 1825-1849

Walder, J.S. and Fowler, A.C. (1994) Channelised subglacial drainage over a deformable bed. *Journal of Glaciology* **40**, pgs.3-15

Appendix 1: Mean supraglacial solute concentration calculations, and subglacial: supraglacial ratio calculations

Sea-salt ions

Julian Day	Nunatak			Ridge			Str.4			Str.1		
	Cl	Na	K	Cl	Na	K	Cl	Na	K	Cl	Na	K
174.667				10.6964	15.2362	2.38258						
178.601	9.73788	13.5435	0.669788	7.55788	10.7013	0.58454						
179.76	9.58418	9.27577	0.556009	8.47375	12.3673	1.37051						
181.542	10.9979	16.3184	0.782544	9.06921	12.7175	0.818168						
185.618	14.0692	21.3515	2.32172	9.42458	15.442	0.843369						
190.854	16.0916	15.1791	1.73331	10.132	23.5149	5.46428						
192.486	11.8926	7.65559	0.489687	9.82924	13.4396	0.708937				10.3015	6.03972	0.18313
195.618	12.2025	17.8324	0.948698	11.9031	18.468	2.48682	10.9757	16.8109	1.40869	10.9244	16.2573	1.31967
196.6875	11.6256	15.9115	0.466459	8.9316	11.8058	0.613524						
197.531	11.4888	16.8009	1.11064	9.59466	13.0249	0.857963	9.3179	12.8356	0.363964			
199.528	10.005	13.2196	0.631201				7.82032	7.17082	0.299281			
201.51	10.5715	13.374	0.460897	8.25908	11.5422	0.597787	8.60076	11.3747	0.357616			
203.622	18.0478	24.5699	7.42842	9.7422	14.4493	1.26566	9.36185	13.8721	1.0264	14.5645	19.6668	4.9659
205.576	28.4248	38.7416	13.5235	15.1049	22.4	3.84677	11.816	17.8609	1.89436			
207.597	10.2512	14.317	0.799478	8.48504	12.1718	0.723779	8.0413	11.5365	0.968315	9.60204	13.3674	
	0.592182											
209.618	17.8995	27.8268	4.83235	10.7988	17.7822	2.2252	8.75537	12.087	0.621306			
211.503	9.27294	13.188	0.681645	8.3198	11.7858	0.7076	7.00684	9.84315	0.461199	7.04079	10.0012	1.12493
213.531	13.2013	17.3123	1.30832	9.56805	12.7759	0.845611	8.88745	11.9885	0.445117			
Mean=	13.25672	17.43634	2.279098	9.758252	14.68381	1.549594	9.058349	12.53802	0.784625	10.48665	13.06648	
	1.637162											

Str.2			mean supra			Subgl.			Sub/Supra ratio		
Cl	Na	K	Cl	Na	K	Cl	Na	K	Cl	Na	K
			10.6964	15.2362	2.38258	57.3983	332.269	44.5368	5.366133	21.80787	18.69268
			8.64788	12.1224	0.627164	12.5582	72.0198	9.35408	1.452171	5.941051	14.91489
			9.028965	10.82154	0.96326	12.8795	78.455	9.9598	1.426465	7.249896	10.33969
			10.03356	14.51795	0.800356	13.3808	75.718	8.32444	1.333605	5.215475	10.40092
			11.74689	18.39675	1.582545	16.2405	82.3578	8.75696	1.382536	4.476758	5.533468
			13.1118	19.347	3.598795	11.682	57.8084	8.10685	0.890953	2.987977	2.252657
9.6142	12.3026	0.458504	10.40939	9.859378	0.460065	15.7067	73.7033	8.20603	1.508898	7.475452	17.83669
			11.50143	17.34215	1.54097	23.2282	130.58	10.7521	2.019593	7.529632	6.97749
			10.2786	13.85865	0.539992	32.2789	155.218	14.4725	3.140398	11.20008	26.80135
			10.13379	14.22047	0.777522	14.4456	47.5707	6.63296	1.425489	3.345228	8.530893
			8.91266	10.19521	0.465241	11.3822	41.8893	8.49808	1.277082	4.108724	18.26597
			9.14378	12.09697	0.4721	17.986	50.7425	12.0195	1.96702	4.194647	25.45965
			12.92909	18.13953	3.671595	12.2976	53.0413	6.06004	0.951158	2.924073	1.65052
			18.44857	26.33417	6.421543	15.1632	62.9927	10.1627	0.821918	2.392052	1.582595
12.232	19.4327	2.79371	9.722316	14.16508	1.175493	26.2654	172.328	14.9173	2.701558	12.16569	12.69025
			12.48456	19.232	2.559619	14.0136	73.7693	9.5789	1.122475	3.835758	3.742315
			7.910093	11.20454	0.743844	14.118	65.9122	16.1479	1.784808	5.882635	21.70873
			10.55227	14.02557	0.866349	13.8535	52.0127	8.22837	1.312846	3.708421	9.497751
10.9231	15.86765	1.626107	10.87178	15.06197	1.647168	18.60434	93.24378	11.92863	**1.771395**	**6.468968**	**12.04881**
	Mean (excl.outburst)		10.88209	15.05173	1.603909	16.32235	79.18347	10.0105	**1.55994**	**5.566679**	**11.65799**

Carbonate ions

Julian Day	Nunatak HCO3	SO4	Ca	Mg	Ridge HCO3	SO4	Ca	Mg	Str.4 HCO3	SO4	Ca	Mg
174.667					82.456	3.28549	55.8202	21.2059				
178.601	267.366	5.55401	219.598	48.5792	484.590	7.28965	420.076	69.0421				
179.76	189.002	5.37736	160.76	33.3719	479.499	8.08002	428.695	54.1844				
181.542	298.552	8.65018	254.086	47.0127	405.791	6.4738	352.972	54.8263				
185.618	229.798	9.24007	190.619	38.8148	418.428	6.93575	361.995	57.3321				
190.854	201.595	11.3555	176.195	38.0046	736.560	4.07919	619.786	95.8997				
192.486	153.103	5.61414	134.429	28.0353	532.684	6.64778	462.907	71.5283				
195.618	315.609	5.21302	252.007	62.2369	545.447	7.49841	460.113	83.7829	212.457	3.83301	172.129	36.9171
196.6875	252.809	6.50961	204.033	50.5334	446.537	5.83084	389.173	59.7075				
197.531	317.287	5.71789	258.991	58.5007	476.906	5.79997	414.732	63.6857	61.93558	3.45088	43.6777	17.8271
199.528	229.698	4.63821	189.488	41.0026					23.35365	3.04081	18.1376	8.60708
201.51	251.862	4.97726	209.442	44.1343	517.682	5.25901	460.18	58.8799	72.17163	3.31333	53.818	18.5354
203.622	327.800	5.86293	258.037	54.6989	445.652	5.44871	380.074	65.8878	218.6325	3.73758	179.213	38.5344
205.576	354.044	6.04505	240.211	51.3291	486.236	6.05221	419.513	62.4696	81.56036	5.19364	59.4979	20.558
207.597	240.601	4.43128	204.251	36.8497	448.535	5.96154	394.27	56.857	40.12575	3.37834	27.0186	12.7466
209.618	289.540	6.14352	235.439	46.7057	493.551	6.46412	442.566	49.6297	52.92836	4.00398	38.7189	14.2605
211.503	281.319	4.58285	240.859	40.8069	513.365	6.10658	469.073	47.1446	126.1553	3.42407	114.59	11.6919
213.531	403.119	18.7545	353.983	63.8052	581.888	8.99103	533.329	54.3176	52.60153	4.56412	39.1764	15.4654
Mean=	270.7709	6.980434	222.4958	46.14246	476.2239	6.2473	415.6044	60.37536	94.19216	3.793976	74.59771	19.51435

Str.1 HCO3	SO4	Ca	Mg	Str.2 HCO3	SO4	Ca	Mg	mean supra HCO3	SO4	Ca	Mg
								69.138	3.28549	55.8202	21.2059
								390.677	6.42183	319.837	58.81065
								365.732	6.72869	294.7275	43.77815
								352.438	7.56199	303.529	50.9195
								336.740	8.08791	276.307	48.07345
								519.314	7.717345	397.9905	66.95215
31.26253	4.56022	29.2987	10.6027	114.1992	4.35326	92.8813	23.4292	315.723	5.29385	179.879	33.39888
82.44158	3.81871	57.8267	22.7337					383.407	5.090788	235.5189	51.41765
								362.840	6.170225	296.603	55.12045
								317.715	4.98958	239.1336	46.67117
								126.526	3.83951	103.8128	24.80484
								325.474	4.516533	241.1467	40.51653
309.4607	5.06621	249.769	55.7535					343.040	5.028858	266.7733	53.71865
								335.338	5.763633	239.7406	44.78557
42.00683	3.80501	28.5444	13.7487	156.8357	4.35599	133.562	18.8278	256.074	4.386432	157.5292	27.80596
								319.646	5.537207	238.908	36.8653
179.2121	3.82077	162.752	17.795					347.478	4.483568	246.8185	29.3596
								392.735	10.76988	308.8295	44.5294
128.8768	4.214184	105.6382	24.12672	135.5174	4.354625	113.2217	21.1285	325.5575	5.87074	244.6058	43.26299
						Mean (excl.outburst)		340.641	6.023	255.711	44.560

Subgl. HCO3	SO4	Ca	Mg	Sub/Supra ratio SO4	HCO3	Ca	Mg	Julian Day
2440.847	2796.09	4122.4	747.29	851.042	35.30394	73.8514	35.23972	174.667
778.481	1161.54	1681.15	173.547	180.8737	1.992645	5.256271	2.950945	178.601
568.569	1394.54	1698.1	170.192	207.2528	1.554606	5.761593	3.887601	179.76
705.274	1215.86	1660.35	171.234	160.7857	2.001128	5.470153	3.362837	181.542
608.032	1150.94	1502.64	166.219	142.3038	1.80564	5.438299	3.457605	185.618
611.495	1120.82	1514.88	146.503	145.2339	1.177506	3.806322	2.188175	190.854
737.008	1034.33	1516.23	172.325	195.3833	2.334348	8.429166	5.159605	192.486
611.508	1085.88	1388.49	171.543	213.303	1.594933	5.89545	3.336267	195.618
623.688	1032.86	1342.76	160.819	167.3942	1.718906	4.527129	2.917592	196.6875
296.433	993.406	1105.03	130.944	199.0961	0.933016	4.620974	2.805672	197.531
575.373	1122.84	1464.73	174.419	292.4436	4.547471	14.10934	7.031652	199.528
533.666	880.79	1207.45	136.413	195.0146	1.639659	5.007119	3.366848	201.51
472.422	879.036	1147.06	141.797	174.7984	1.377164	4.299756	2.639623	203.622
867.474	1056.91	1683.72	156.932	183.3756	2.586863	7.02309	3.504075	205.576
914.964	1843.77	2949.06	214.881	420.3348	3.573051	18.72072	7.727876	207.597
1250.332	1753.41	2724.63	170.2	316.6597	3.911611	11.40452	4.616808	209.618
1544.938	1658.51	2867.5	212.25	369.9086	4.446146	11.61785	7.229322	211.503
811.866	830.765	1445.71	120.37	77.13779	2.067212	4.681257	2.703158	213.531
830.6872	1278.460944	1834.549444	196.5488	**249.5745**	**4.142547**	**11.10669**	**5.784743**	
735.972	1189.189	1699.970	164.152	**214.194**	**2.310**	**7.416**	**4.052**	

Appendix 2: Example of speciation calculations performed by PHREEQC, including description of solution, distribution of species and saturation indices.

Initial solution 2. Outburst water (JD174)

----------Solution composition----------

Elements	Molality	Moles
Alkalinity	2.977e-03	2.977e-03
Ca	2.062e-03	2.062e-03
Cl	5.751e-05	5.751e-05
K	4.457e-05	4.457e-05
Mg	3.738e-04	3.738e-04
Na	3.324e-04	3.324e-04
S(6)	1.398e-03	1.398e-03
Sr	2.540e-05	2.540e-05

----------Description of solution----------

pH	=	8.236
pe	=	4.000
Activity of water	=	1.000
Ionic strength	=	8.542e-03
Mass of water (kg)	=	1.000e+00
Total carbon (mol/kg)	=	2.999e-03
Total CO2 (mol/kg)	=	2.999e-03
Temperature (deg C)	=	0.000
Electrical balance (eq)	=	-5.309e-04
Percent error, 100*(Cat-|An|)/(Cat+|An|)	=	-5.20
Iterations	=	8
Total H	=	1.110153e+02
Total O	=	5.552075e+01

----------Distribution of species----------

Species	Molality	Activity	Log Molality	Log Activity
OH-	2.162e-07	1.967e-07	-6.665	-6.706
H+	6.306e-09	5.808e-09	-8.200	-8.236
H2O	5.551e+01	9.999e-01	-0.000	-0.000
C(4)	2.999e-03			
HCO3-	2.872e-03	2.625e-03	-2.542	-2.581
CO2	5.767e-05	5.778e-05	-4.239	-4.238
CaHCO3+	2.452e-05	2.241e-05	-4.611	-4.650
CaCO3	1.872e-05	1.876e-05	-4.728	-4.727
CO3-2	1.523e-05	1.063e-05	-4.817	-4.973
MgHCO3+	7.757e-06	7.069e-06	-5.110	-5.151
MgCO3	1.650e-06	1.653e-06	-5.783	-5.782

	NaHCO3	4.445e-07	4.454e-07	-6.352	-6.351
	SrHCO3+	3.018e-07	2.759e-07	-6.520	-6.559
	SrCO3	5.233e-08	5.243e-08	-7.281	-7.280
	NaCO3-	1.655e-08	1.508e-08	-7.781	-7.822
Ca		2.062e-03			
	Ca+2	1.852e-03	1.292e-03	-2.732	-2.889
	CaSO4	1.668e-04	1.671e-04	-3.778	-3.777
	CaHCO3+	2.452e-05	2.241e-05	-4.611	-4.650
	CaCO3	1.872e-05	1.876e-05	-4.728	-4.727
	CaOH+	4.049e-08	3.691e-08	-7.393	-7.433
Cl		5.751e-05			
	Cl-	5.751e-05	5.233e-05	-4.240	-4.281
H(0)		5.086e-28			
	H2	2.543e-28	2.548e-28	-27.595	-27.594
K		4.457e-05			
	K+	4.438e-05	4.039e-05	-4.353	-4.394
	KSO4-	1.855e-07	1.690e-07	-6.732	-6.772
	KOH	2.406e-11	2.411e-11	-10.619	-10.618
Mg		3.738e-04			
	Mg+2	3.412e-04	2.392e-04	-3.467	-3.621
	MgSO4	2.319e-05	2.324e-05	-4.635	-4.634
	MgHCO3+	7.757e-06	7.069e-06	-5.110	-5.151
	MgCO3	1.650e-06	1.653e-06	-5.783	-5.782
	MgOH+	1.396e-08	1.272e-08	-7.855	-7.895
Na		3.324e-04			
	Na+	3.307e-04	3.017e-04	-3.481	-3.520
	NaSO4-	1.168e-06	1.064e-06	-5.933	-5.973
	NaHCO3	4.445e-07	4.454e-07	-6.352	-6.351
	NaCO3-	1.655e-08	1.508e-08	-7.781	-7.822
	NaOH	3.425e-10	3.432e-10	-9.465	-9.464
O(0)		0.000e+00			
	O2	0.000e+00	0.000e+00	-46.180	-46.179
S(6)		1.398e-03			
	SO4-2	1.205e-03	8.368e-04	-2.919	-3.077
	CaSO4	1.668e-04	1.671e-04	-3.778	-3.777
	MgSO4	2.319e-05	2.324e-05	-4.635	-4.634
	SrSO4	1.909e-06	1.913e-06	-5.719	-5.718
	NaSO4-	1.168e-06	1.064e-06	-5.933	-5.973
	KSO4-	1.855e-07	1.690e-07	-6.732	-6.772
	HSO4-	3.199e-10	2.916e-10	-9.495	-9.535
Sr		2.540e-05			
	Sr+2	2.314e-05	1.617e-05	-4.636	-4.791
	SrSO4	1.909e-06	1.913e-06	-5.719	-5.718
	SrHCO3+	3.018e-07	2.759e-07	-6.520	-6.559
	SrCO3	5.233e-08	5.243e-08	-7.281	-7.280
	SrOH+	1.563e-10	1.427e-10	-9.806	-9.845

----------Saturation indices----------

Phase	SI	log IAP	log KT	
Anhydrite	-1.60	-5.97	-4.37	CaSO4
Aragonite	0.36	-7.86	-8.22	CaCO3
Calcite	0.52	-7.86	-8.38	CaCO3
Celestite	-1.17	-7.87	-6.70	SrSO4
CO2(g)	-3.13	-21.45	-18.32	CO2
Dolomite	0.00	-16.46	-16.46	CaMg(CO3)2
Gypsum	-1.35	-5.97	-4.62	CaSO4:2H2O
H2(g)	-24.38	-24.47	-0.09	H2
O2(g)	-43.52	48.94	92.46	O2
Strontianite	-0.42	-9.76	-9.34	SrCO3

Appendix 3: Input compositions (in ppm) for PHREEQC modeling of supraglacial waters.

	Snowpack	Stream 1	Stream 2	Ridge Stream (post-outburst)	Ridge Stream (pre-outburst)	Stream 4	Nunatak Stream	Ridge Lake	Nunatak Lake
pH	6.951	67.487	7.383	7.679	6.387	7.201	7.476	7.801	8.312
HCO3	3.847	7.863	8.268	30.790	4.916	5.667	17.052	44.110	36.328
Cl	0.304	0.372	0.388	0.345	0.393	0.321	0.461	0.339	0.331
SO4	0.094	0.202	0.209	0.314	0.186	0.184	0.355	0.771	0.664
Na	0.313	0.300	0.365	0.337	0.355	0.287	0.394	0.323	0.297
K	0.078	0.064	0.064	0.058	0.089	0.029	0.083	0.061	0.065
Mg	0.184	0.293	0.257	0.757	0.262	0.234	0.582	0.982	1.092
Ca	0.871	2.117	2.269	8.882	1.137	1.477	4.678	13.083	10.323

Appendix 4: Input compositions for PHREEQC modeling (in ppm) of subglacial solutions and phases.

	DAY 174	DAY 180	MEAN P2A	MEAN P2B	MEAN P2C	DAY 205	DAY 208	DAY 209
pH	8.236	8.650	8.382	7.763	8.746	9.290	9.825	9.285
HCO3	148.923	43.393	38.336	41.362	35.456	52.844	51.503	76.286
Cl	2.038	0.466	0.512	1.102	0.504	0.538	0.864	0.498
SO4	134.234	57.877	56.432	56.509	54.833	50.740	43.871	84.177
Na	7.638	1.769	1.631	4.026	1.394	1.448	3.910	1.696
K	1.742	0.347	0.362	0.564	0.357	0.397	0.605	0.375
Mg	9.084	2.039	2.091	2.283	2.130	1.908	2.091	2.069
Ca	82.613	33.245	30.694	29.867	29.514	33.742	28.276	54.602
Sr	2.225	0.836	0.862	0.851	0.920	1.133	0.690	1.808